HIGH TEMPERATURE MEASUREMENT
OF
WATER VAPOR ABSORPTION

by

Dennis Keefer, James W. L. Lewis
and
Richard Eskridge

The University of Tennessee Space Institute
Tullahoma, Tennessee 37388

July 1985

ABSTRACT

An investigation was undertaken to measure the absorption coefficient, at a wavelength of 10.6 micrometers, for mixtures of water vapor and a diluent gas at high temperature and pressure. The experimental concept was to create the desired conditions of temperature and pressure in a laser absorption wave, similar to that which would be created in a laser propulsion system. A simplified numerical model was developed to predict the characteristics of the absorption wave and to estimate the laser intensity threshold for initiation. A non-intrusive method for temperature measurement utilizing optical laser-beam deflection (OLD) and optical spark breakdown produced by an excimer laser, was thoroughly investigated and found suitable for the non-equilibrium conditions expected in the wave. Experiments were performed to verify the temperature measurement technique, to screen possible materials for surface initiation of the laser absorption wave and to attempt to initiate an absorption wave using the 1.5 kW carbon dioxide laser at The University of Tennessee Space Institute (UTSI). The OLD technique was proven for air and for argon, but spark breakdown could not be produced in helium. It was not possible to initiate a laser absorption wave in mixtures of water and helium or water and argon using the 1.5 kW laser at UTSI, a result which was consistent with the model predictions.

TABLE OF CONTENTS

LIST OF FIGURES

v

I. INTRODUCTION

Laser energy beamed from a remote laser to an orbital transfer vehicle can provide a propulsion system with an exceptionally high specific impulse [1,2]. Several systems studies [3,4,5] have identified missions for which a beamed laser propulsion system can have significant cost or performance advantages. Several different methods have been proposed to absorb the laser energy [6,7], but molecular absorption and plasma absorption appear to be the most promising.

An ideal absorbing medium is one which can absorb the entire laser beam energy in a relatively small volume, and then be expelled from the vehicle as the propellant. In addition to these essential requirements, the absorber should have a low molecular weight to provide high specific impulse and be relatively easy to store on-board the vehicle. The ideal absorber, from the standpoint of specific impulse, is hydrogen, but it is not absorbing to the visible and infrared radiation characteristic of current high power lasers unless it is heated to temperatures at which it becomes ionized. Since significant levels of ionization are not reached until the temperature has reached approximately 10,000 K, it is attractive to consider the use of mixtures of hydrogen and molecular absorbers, such as water vapor, to reduce the temperature at which the laser beam can be absorbed in the propellent.

Both the required size of the absorbing chamber and the specific impulse of the propulsion device depend critically on the magnitude of the laser absorption coefficient for the mixture at the high temperatures desired for a rocket propellent. Prediction of the laser absorption coefficient is difficult for mixtures of water and hydrogen at high temperature due to dissociation of the water molecule under the influence of laser absorption and the complex chemical interactions involved. For this reason, several previous investigations [8,9,10] have attempted to measure the absorption coefficient of water at the 10.6 micrometer wavelength characteristic of the carbon dioxide laser.

Two methods have been used to obtain the conditions of pressure and temperature required: heating of the mixture in a laser sustained plasma [9], and shock heating of the mixture in a shock tube [8,10].

Fowler [9] obtained measurements of the absorption coefficient at 10.6 micrometers for mixtures containing H_2O, D_2O and NH_3 in hydrogen at pressures to 13 atm. A laser sustained plasma was created in the test chamber using a vertical beam from a cw carbon dioxide laser of 7 kW power. Measurements of both temperature and absorption coefficient were made using Abel inversion of the output

of a Mach-Zehnder interferometer illuminated with a separate carbon dioxide laser. The values of absorption coefficient measured in this experiment (approximately 1 cm^{-1}) exceeded the calculated values by more than a factor of ten for both H_2O and D_2O.

Kemp and Krech [8] made direct absorption measurements in the incident and reflected regions of a shock tube operating in mixtures of H_2O and argon at temperatures to 3064 K and pressures to 49 atm. The maximum value of absorption coefficient measured was 0.45 cm^{-1} ama^{-1}. This is smaller, by a factor of 25, than the comparable value measured by Fowler. Rosen et. al. [10] made additional shock tube measurements in mixtures of CO_2, H_2O and NH_3 with similar differences in measured values compared to those obtained by Fowler.

To avoid the complications associated with the use of laser sustained plasmas, a method utilizing a laser absorption wave has been developed. In this technique a laser beam impinges on a ceramic surface, heating the surface and the cold propellent mixture adjacent to it. When the mixture near the surface has reached a temperature where it becomes absorbing to the incident laser beam (approximately 1000 K), an absorption wave is initiated. This absorption wave propagates through the propellent mixture in the direction of the incident beam at moderate velocities, and simultaneous measurements of temperature and absorption coefficient can be made as the wave passes through a test chamber. For this investigation, non-intrusive optical diagnostic techniques were developed to measure the translational temperature of the propellent mixture, and a test cell was designed and constructed to carry out the measurements.

II. EXPERIMENT DESCRIPTION

A. Absorption Wave Concept

The experimental concept was arrived at jointly by personnel at NASA Marshall Space Flight Center (MSFC) and The University of Tennessee Space Institute (UTSI). It consists of using a laser absorption wave initiated from a plate heated by the impinging laser beam to create the conditions of temperature and pressure required for the absorption measurements. As the absorption wave propagates through a mixture of water vapor and a diluent gas, the mixture is heated to the maximum temperature which can be sustained by the laser absorption. When the wave propagates past observation ports in the test chamber, simultaneous measurements are obtained for the optical transmission of a separate 10.6 micrometer laser

$-2-$

and for the translational temperature of the mixture. Thus, for each occurrence of a wave, a series of transmission measurements are obtained at different values of mixture temperature. A schematic of the experimental apparatus is shown in Figure 1.

Since the mixture will be heated by strong absorption of the laser beam in the rovibrational bands of the H_2O molecule, the temperature within the absorbing beam will not be uniform, and it is likely that the mixture will not be in thermodynamic equilibrium. To obtain accurate measurements of absorption it is necessary that the transmission measurements be made across the entire cross-section of the wave. A pyroelectric array detector was chosen to obtain the required spatially resolved measurements of laser transmission. The transmission data can then be Abel inverted to give spatially resolved measurements of the absorption coefficient. An optical measurement of temperature utilizing the measurement of acoustic wave velocity was chosen to avoid the uncertainties in rotational or vibrational temperature measurements arising from the uncertain state of equilibrium in the mixture. Acoustic wave speed is determined from a time-of-flight measurement of the decaying blast wave produced by an excimer laser induced spark, using helium-neon laser beams of known separation.

A simple one-dimensional model of the initiation and propagation of a laser absorption wave was developed to determine whether this concept was feasible. The primary goals of this analysis were to determine if the wave speed was slow enough that the required measurements could be obtained during wave passage, and to determine the threshold laser beam intensity for the initiation of the laser absorption wave.

B. Numerical Model

A numerical model was constructed in order to study the feasibility of the laser absorption wave technique and to provide a first approximation for the time and spatial characteristics of the phenomenon. The model was based on a one-dimensional, time-dependent algorithm for thermal conduction in the target gas with volumetric absorption of laser beam power governed by Beer's Law.

The derivation of the finite element approximation follows the method given by Patankar [11]. Consider the one-dimensional unsteady heat conduction equation with source term:

$$\rho c \frac{\partial T}{\partial t} = \frac{\partial}{\partial x}\left(\kappa \frac{\partial T}{\partial x}\right) + S \qquad (1)$$

where T is temperature, t is time, x is the spatial coordinate, ρ is the density, c is the specific heat and κ is the thermal conductivity.

For the case of an absorbing gas with emission of radiation, the source term is given by:

$$S = \alpha I - \Phi \qquad (2)$$

where α is the absorption coefficient for laser radiation of intensity I and Φ is the net radiation emission coefficient.

The intensity of incident laser radiation is prescribed by Beer's Law:

$$\frac{dI}{dx} = \alpha I \qquad (3)$$

for a laser beam propagating in the negative x direction.

For a gaseous medium the properties are related by the equation of state:

$$P = \rho R T \qquad (4)$$

where P is pressure and R is the gas constant.

The heat conduction equation may be discretized by integration over a finite time interval and over the control volume of Figure 2,

$$\int_t^{t+\Delta t} \int_w^e \rho c \frac{\partial T}{\partial t} dx dt = \int_t^{t+\Delta t} \int_w^e \left[\frac{\partial}{\partial x} \left(\kappa \frac{\partial T}{\partial x} \right) + S \right] dx dt. \tag{5}$$

In the equations below, denote the state at time t by the superscript 0, and at time, $t + \Delta t$ by the superscript 1. Assume the quantity ρc is constant over the time interval Δt. Then equation (5) may be written as:

$$\rho c (T_p^1 - T_p^0) \Delta x = \int_t^{t+\Delta t} \int_w^e \left[\frac{\partial}{\partial x} \left(\kappa \frac{\partial T}{\partial x} \right) + S \right] dx dt. \tag{6}$$

The integral over x in (6) may be evaluated and separated into terms to yield:

$$\rho c \Delta x (T_p^1 - T_p^0) = \int_t^{t+\Delta t} \left[\kappa_e \frac{(T_E^1 - T_p^1)}{\delta x_e} - \kappa_w \frac{(T_p^1 - T_w^1)}{\delta x_w} + \bar{S} \Delta X \right] dt \tag{7}$$

Here, the partial derivatives have been replaced by the difference approximation, and the source term has been replaced by the mean value over the cell, $\bar{S}$. If it is assumed that all properties except the grid temperature T_p are constant over the time interval Δt then Eq. (7) may be integrated over time to obtain the fully implicit difference equation:

$$\frac{\rho c \Delta x}{\Delta t} (T_p^1 - T_p^0) = \bar{S} \Delta x \Delta t + \kappa_e \frac{(T_E^1 - T_p^1)}{\delta x_e} - \kappa_w \frac{(T_p^1 - T_w^1)}{\delta x_w} \tag{8}$$

Approximate the source term $\bar{S}$ by the sum of a constant and linear term as follows:

$$\bar{S} = S_c + S_p T_p \tag{9}$$

Equation (8) may now be rewritten by the collection of terms into a new form as follows by the definition of a series of grid coefficients:

$$A_p T_p = A_E T_E + A_w T_w + b \qquad (10)$$

where

$$A_E = \kappa_e / \delta x_e$$

$$A_W = \kappa_w / \delta x_w$$

$$A_p^0 = \frac{\rho c \Delta x}{\Delta t}$$

$$A_p = A_p^0 + A_E + A_W - S_p \Delta x$$

and

$$b = A_p^0 T_p^0 + S c \Delta x.$$

This new formulation simplifies the numerical solution of the problem as it allows the matrix formulation of the equation set to be cast into a tri-diagonal matrix form. Note that the behavior of temperature at the given point depends only on the values to the left and right in the spatial grid. This formulation will create a "banded" matrix of coefficients. The solution algorithm proceeds at each time step by the solution of a spatially coupled, steady-state problem using a tri-diagonal matrix algorithm. The parameters and properties used in the formulation of each steady-state problem are the results of the solution from the previous time step. In this manner, the temporal dependence is determined. Note, however, that the properties "lag behind" the solution by one time step. This requires the use of very small time steps for the solution to accurately track the true time behavior.

The source term has also been linearized by the assumption that the temperature dependent part S is zero. Instead, the constant portion of the source term, S is calculated from the properties belonging to the previous time step.

The spatial grid was divided into two principle regions: one of an absorbing gas and the second of a ceramic target as shown in Figure 3. The boundary conditions were chosen so that the temperatures on either end of the grid were prescribed for all times t. The initial conditions were those of uniform temperature equal to the temperature prescribed on either end for all points in both regions. The laser beam is assumed to proceed from right to left in the solution grid as shown in Figure 3. The source term S may be written in discrete form by an approximation to Eq. (2). The energy absorbed into the nth volume element is given by:

$$P_n = \frac{I_{N+1} - I_N}{\Delta x_N} \tag{11}$$

The laser intensity I is determined by integration of the Beer's law equation at the end of each time step. The absorption coefficient for 10.6 micrometer radiation used in the model was curve fitted to shock tube data from Kemp and Krech [8] for the $P(20)$ CO_2 laser line.

The net source term is the difference of the energy absorbed and the energy lost due to radiation Φ. The total radiation from the nth volume element is given by:

$$\Phi_N = 4 < K_\nu > \sigma T_N^4 \tag{12}$$

Here $< K_\nu >$ is the spectrally averaged absorption coefficient . The absorption coefficient is related to the optical cross section $< \sigma_\nu >$ by:

$$< K_\nu >= N_s < \sigma_\nu > \tag{13}$$

where N_s is the number density of the absorbing species.

Radiation from both H_2O and OH were considered in the program in order to calculate the net source term. The cross-sections were calculated from experimental

data obtained by Kemp and Krech [8] who give values for the emissivity of these species for various values of pressure-length product, ps. The cross section $< \sigma_\nu >$ is then related to the emissivities by:

$$< \sigma_\nu > \cong \frac{\varepsilon K_b T}{ps}. \tag{14}$$

The thermal conductivities and specific heats for the gaseous H_2/H_2O mixture were taken to be equal to those of the major constituent H_2. These data were taken from Patch [12] who calculated properties for spin-equilibrated H_2 for a range of pressures and temperatures.

The properties were treated differently in the ceramic region of the solution grid. This was accomplished by the use of steering logic in the property subroutines . The solution algorithm is not disturbed by discontinuity in properties along the solution grid as long as the grid is sufficiently fine in the region of the discontinuity. The "fineness" of the grid at the discontinuity was chosen by trial and error to achieve stability in the solution without incurring excessive memory requirements.

The source terms for this region of the solution were set to zero except for the first ceramic cell at the solid-gas interface. This cell absorbed all of the remaining laser power and emitted radiation given by the Stefan-Boltzmann relation for solid body radiation from a surface. The emissivity of the ceramic was chosen to correspond to 100% dense polycrystalline Al_2O_3 at elevated temperatures, as were the specific heats and thermal conductivities in this region of the grid. None of the re-radiated power from the ceramic surface was considered to be re-absorbed in the adjoining gas mixture.

The mole-fraction of each constituent of the gaseous mixture will change as the temperature is elevated. This is due to the dissociation of the water vapor and diatomic hydrogen to produce other species such as OH, O_2, H, H^+, etc... . This effect was included in the program by curve fitting the output of the NASA code ODE which was run for each case to be considered. It is the inclusion of these effects which limits the maximum temperature of the thermal wave since the number density of absorbing molecules is reduced by the onset of dissociation at higher temperatures. In this model, only H_2O is considered as an absorber, hence the maximum temperature is limited to approximately 4000 K for the cases considered.

Two major cases were considered for use of the model. These were for a mixture of H_2 and H_2O, with 20 percent H_2O by volume initially at ambient temperature for pressures of 1 and 10 atm. These cases represented extremes readily accessible to laboratory apparatus and encompassed regimes of interest to propulsion. Two major sets of property subroutines were built for these cases, primarily by simple curve fits to available data. Conservative estimates were used where data were sketchy or unavailable.

The results of the two major cases are shown plotted in Figures 4 and 5. The assumed incident laser intensity was 375 W/cm^2 for both of these cases. The time steps were .01 sec for the 10 atm case and .05 sec for the 1 atm case. The temperature profiles are plotted every 2 sec up to a maximum of 20 sec, in order to show the progression of the wave with time. For the 1 atm case shown in Figure 4, the wave velocity reaches a constant velocity of 7.5 cm/sec after 10 sec. The maximum temperature in the wave is about 3600 K and the maximum temperature on the ceramic wall reaches 1800 K. For the 10 atm case, the wave velocity reaches 3 cm/sec after 10 sec. The maximum temperature in the thermal wave approaches 4000 K and the maximum wall temperature is about 1600 K. The higher wave velocity for the 1 atm case is a result of the lower thermal conductivity which leads to steeper thermal gradients at the leading edge. The higher wall temperature for the 1 atm case is also due to the lower thermal conductivity which reduces heat transfer from the wall surface.

The laser intensity has a major effect on the behavior of the solution. Several alternate cases were examined to investigate the solution for lower intensities. One of these cases is shown plotted in Figure 5. No persistent wave is launched from the wall for this case. Instead, a heated zone is established away from the wall which converges to a steady-state profile. This behavior is due to a lack of incident power necessary to overcome the radiative and conduction losses.

The conclusions drawn from this study were that it was possible to create a laser absorption wave and that it might provide a viable means for the creation of the conditions necessary for the study of H_2/H_2O mixture properties at high temperatures. The study did demonstrate a sensitivity to laser power levels, although the predicted power levels were within the reach of available high energy lasers.

It is important to note that several important loss mechanisms were not included in the model. The major factor not included in the study was that of the convective term in the energy equation. The exact effect of the convective terms have not been determined due to the difficult nature of such a solution. Unfortu-

nately, time did not permit a more complete analysis of the convective flow through the wave. It was anticipated that this effect would raise the laser power threshold for the initiation of the wave due to the losses incurred and the subsequent reduction in thermal gradients. Another important effect not included in the model was that of radial conduction in the thermal wave and the ceramic end-wall. This effect would also raise the necessary laser power threshold but it was felt that this effect would be minimal because of the size of the beam and the nature of its unstable resonator beam pattern.

Complete Fortran 77 program listings for the computer program are included in Appendix A. This program was executed on a VAX 11/780 machine at the University of Tennessee Space Institute. Property subroutines are also included in the listings for the 1 and 10 atm cases.

C. Temperature Measurement

The measurement of local, time-resolved gas temperatures was essential for the prediction of the varying constituency of the high-temperature, subsonic, gas sample. Since the laser absorption measurements were to be performed in the comparatively slowly varying trailing-edge of the thermal wave, the gas mixture parameters and their gradients in this trailing-edge region are of fundamental importance in determining the criteria that must be satisfied by the temperature measurement method. Figure 7 shows a sample result for the space-time variation of the thermal wave for a $20\%H_2O/80\%He$ volume mixture at 10 atm total pressure for $I_o = 375\ w/cm^2$. At a sample axial location, say $x = 50\ cm$, from Figure 7 it is seen that an axial spatial resolution of approximately 5-10 mm will yield an uncertainty of less than $pm \pm 5\%$ in T, which is an acceptable measurement error. Further, from Figure 7 it can be estimated that the axial flow speed is less than 10 cm/sec. Consequently, the temporal resolution necessary to determine accurately the thermal wave profile in the trailing-edge region is seen to be on the order of 10 $msec$ or less. An additional criterion that should be satisfied for measurement of the temperature of the reacting gas sample is an insensitivity to the gas sample's local, instantaneous constituency, which should be considered as an *a priori* unknown for the experimental measurements.

A variety of methods of temperature measurement exists; most of these methods, however, fail to satisfy the desired criteria. For example, since local thermal equilibrium cannot be ensured and the spectral broadening parameters are poorly known for the high-temperature region of this study, emission-absorption techniques cannot be used. Spontaneous Raman scattering (SpRS) is attractive, but the SpRS

cross section and scattering signal are so low that adequate time resoltuion cannot be achieved for a single thermal wave; i.e., multiple thermal waves would be required to map the spatial profile of an "average thermal wave" profile. Coherent Anti-Stokes Raman scattering (CARS) is known to be capable of temperature measurements with good signal-to-noise (S/N) ratios for combustion sources. However, for this study, the pressure-temperature region is such that significant thermal dissociation occurs, resulting in a substantial decrease in all initial molecular species. The OH radical species will, however, increase during the disociation processes, but its concentration is too small for its use for a CARS temperature measurement with large values of S/N. Furthermore, LTE may be a questionable assumption for OH radicals produced by thermal dissociation of H_2O that has been vibrationally excited by absorption of CO_2 laser radiation. As a result, CARS was rejected as a practical approach for the temperature measurement. Laser-induced fluorescence (LIF) satisfies all criteria but the last; the results may be sensitive to the instantaneous mixture constituency. Before embarking on a study related to quenching cross sections of various molecular species and the effects of such cross sections on temperature measurements, other possible methods were sought.

The method of Zapka et al [14] was chosen for the temperature measurement of and is designated the optoacoustic laser-beam deflection (OLD) method. As sketched in Figure 8, OLD consists of using a high-power laser which is focused to a small volume in the gas sample. The excitation laser irradiance exceeds the gas breakdown threshold, and a plasma spark and cylindrical blast-wave are produced. The blast-wave propagates outward and, after a distance x_D, it decays into an acoustic wave. Two probe-laser beams, separated by a distance Δx, detect the passage of the acoustic wave with a passage time difference Δt, which corresponds to the separation distance Δx. If the gas sample possesses a flow speed v_F and a_o is the sample's sound speed, then

$$a_o + v_F = \Delta x_d / \Delta t_d \qquad (15)$$

and

$$a_o - v_F = \Delta x_u / \Delta t_u \qquad (16)$$

where the subscripts d and u denote the downstream and upstream directions,

respectively.

For an assessment of the order of magnitudes (O),

$$O(a_o) > \sim 10^4 \ cm/sec,$$

$$O(v_F) << \sim 10^2 \ cm/sec,$$

so that

$$O(v_F/a_o) < \sim 10^{-2},$$

and now

$$a_o \cong \Delta x_{d,u}/\Delta t_{d,u}. \tag{17}$$

For the subsonic flow of assumed one-dimensional speed v_F, note that Eqs. (15 and 16) indicate a method of measurement of V_F:

$$v_F = (1/2)[(\Delta x_d/\Delta t_d) - (\Delta x_u/\Delta t_u)]. \tag{18}$$

Consequently, probe beam-pair detectors located both downstream and upstream of the excitation beam can be used to infer values of v_F.

Now, returning to Eq. (17), it is recalled that for a perfect gas of specific heat ratio γ, molecular weight M and temperature T,

$$a_o^2 = (\partial p/\partial \rho)S = \gamma RT/M \tag{19}$$

$- 12 -$

where p and ρ denote, respectively, the gas pressure and density, and subscript S denotes an isentropic derivative and R is the universal gas constant. Therefore, if γ and M of the ideal gas are known, measurement of a_o yields a measurement of T.

Several features of the gas sample require much closer scrutiny before declaring as feasible the use of OLD for measurement of temperature in this study. First, the gas sample is reacting, and an initial assessment of OLD would indicate the likelihood of dependence of a_o on the sample's constituency. Second, the use of a pulsed excitation source of short-duration ($\cong nsec$) will produce a short-duration acoustic pulse, and the Fourier transform of this pulse will exhibit a range of frequencies. Since the sample consists of molecular species and acoustical dispersion will exist, the validity of describing the sound speed by an isentropic (and dispersion-free) relation (Eq. (19)) must be determined. Third, the question of the effect of refraction on the excitation and probe beams must be considered, and, fourth, the magnitude of Δx_D and the limiting spatial resolution that is set by $(\Delta x_{d,u})_{max}$ and $(\Delta t_{d,u})_{min}$ are of interest.

To determine the sensitivity of a_o on constituency, it was necessary to calculate the equilibrium concentrations of the dissociating, reactive samples as a function of temperature. For this purpose and subsequent rate kinetics calculations, the reaction rate data of Refs. [15] and [16] were used. Since $H_2O/He, H_2O/Ar$ and H_2O/H_2 mixtures were all of interest, equilibrium concentration and sound speed calculations were performed for all three mixtures for a range of initial concentrations and pressures for $1000 \sim< T <\sim 5000\ K$. Figures 9 through 12 show sample concentration results for Ar and H_2 mixtures. Specifically, for the initial mixture (by volume) of $20\%H_2O$ and $80\%Ar$ at $P = 1\ atm$. Figure 9 shows the variation of the concentrations of H_2O, H_2, H, and OH, $[H_2O]$, $[H_2]$, $[H]$ and $[OH]$, respectively, as a function of T. Figure 10 shows similar variations for $P = 10\ atm$. Several features of Figure 9 and 10 are of interest. First, note the small concentrations of H_2O for both $P = 1$ and $10\ atm$ at $T = 4000\ K$. Second, at $T \cong 4000\ K, [H_2] <\sim .03$ and note the increasing concentration of $H([H] >\sim ,0.1)$ for $T \cong 4000\ K$. Finally, the peak in $[H]$ at a value of approximately 0.04 is of interest and justifies the rejection of CARS as a candidate measurement method. Further, a comparison of Figures 9 and 10 shows clearly the suppression of the dissociation reactions that results from the incresae of pressure from 1 to 10 atm. Figures 11 and 12 show similar variations for a $20\%H_2O/80\%H_2$ initial concentration mixture at $P = 1$ and 10 atm, respectively. Relative to the Ar mixtures, a significant increase in $[H_2O]$, $[H_2]$, $[OH]$ and $[H]$ understandably results. Further, the peak in $[OH]$ is shifted to $T/4000\ K$ for $P = 1\ atm$ and significantly beyond $4000\ K$ for $P = 10\ atm$. Finally, from such results, the equilibrium sound speed $a o$

was computed, and, as examples, Figures 13 and 14 show the variation of ao with T for $20\%H_2O/80\%He$ at $P = 5$ and $10\ atm$, and Figure 15 shows ao versus T for a $20\%H_2O/80\%H_2$ mixture at $P = 1\ atm$. From Figures 13 and 14, it can be seen that a measurement of the equilibrium sound speed provides a unique value of temperature for an equilibrium reacting mixture. Further, note that little difference in a_o versus T results from the change of pressure from 5 to 10 atm for H_2O/He mixtures. As expected, however, significant variations result for ao versus T as one changes the non-absorbing gas from He to H_2. Results similar to Figures 13 and 14 were found for H_2O/Ar mixtures.

The calculation of the equilibrium, isentropic sound speeds relied upon the validity of Eq. (18) which presumes the absence of dispersion effects. Specifically, Eq. (18) assumes the absence of relaxation processes and be categorized as a zero-frequency speed of sound. As the sound wave frequency (ν) increases, relaxation processes result and the internal modes of molecular motion fail to maintain equilibrium with the translational mode. For an example of order of magnitude relations, suppose the molecular species is characterized by an equilibrium value of $\gamma = 1.2$. As ν increases, γ increases from 1.2 to 1.667, the monatomic gas value, and the speed of sound increases according to Eq. (18). The inferred values of corresponding to this range of γ and a_o^2 differ by almost forty percent. Therefore, it is necessary to determine the Fourier frequency spectra expected for a laser excitation pulse-width on the order of $1 - 10\ nsec$.

Assume the laser ρ-induced, time-dependent pulse amplitude can be described by the functional form

$$E_L = E_o cos(\pi t/t_L). \qquad (20)$$

The Fourier transform $\bar{E}_L(\omega)$ is easily found to be

$$\bar{E}_L(\omega) = 2\tau_L E_o - cos(\omega t_L/2)/[1 - \omega^2 t_L^2/\pi^2)] \qquad (21)$$

where $\omega = 2\pi\nu$ and $T_L = 2t_L/\pi$.

From Eq. (21), it is seen that the predominant Fourier amplitude occurs at $\nu = \omega = 0$ and that the first and largest "secondary maximum", which occurs

at $\nu_1 t_L \cong 5\pi/8$, has an amplitude less than 10^{-1} times the zero frequency amplitude. Since $t_L \sim 10$ $nsec = 10^{-8}$ $sec, \nu_1 \cong 200MHz$. For $P \cong 10$ atm and $T > \sim 3000$ K, at $\nu_1 \cong 200MHz$, all vibrational modes can be considered frozen and rotational relaxation will have become significant. [15]. As a result, at $\nu_1 \cong 200MHz, \gamma(200MHz) > \sim 1.4$ and vibrational dispersion would result in an increase in a_o^2 (and inferred (and incorrect)) T of approximately twenty percent. Therefore, in summary, for a temporally symmetric 10 $nsec$ laser excitation pulse and blast wave, the acoustic pulse can be expected to exhibit detectable dispersion. However, the predominant (and slowest) component of the anticipated asymmetric acoustic wave will be the zero-frequency component that is predicted by Eq. (18) and shown in the previous figures.

The preceding conclusions were formed on the basis of the assumption of chemical equilibrium. Since, as Figure 7 shows, a laser absorption wave processes the initial mixture sample, time-dependent reactions result and the chemical constituency will vary with time. The evaluation of the effect of such finite-rate chemical kinetics on the previous conclusion required an assessment of the time required to achieve a condition approximately that of local thermal equilibrium. To do this, differential equations corresponding to the reaction processes of Refs. [16] and [17] were solved numerically as a function of time to yield the time-dependent concentrations of the mixture. To describe approximately the passage of the laser absorption wave, the gas temperature of the initial mixture was assumed to be subjected to a step-function increase which corresponded to the arrival of the leading-edge of the wave. Recall that from Figure 7 and the estimated value of $v_F (\sim 10$ $cm/sec)$, one expects characteristic times of significant change of parameters (τ_p) in the thermal wave pulse to be no less than 10 $msec$. Therefore, if one finds the (maximum) time to approach chemical equilibrium $(\tau_c([x])_{max})$ for the slowest-varying major specie x to satisfy the inequality

$$\tau_c([x])_{max} \ll \tau_p,$$

the assumption of LTE and the previous conclusions are valid for measurements made with data acquisition and resolution times τ_M on the order of, or slightly less than τ_p.

Figures 16 through 34 show sample results for the variation with time of the mole fractions of the mixture species for H_2O/H_e and H_2O/H_2 mixtures.

Figures 16 and 17 show the $20\% H_2O/80\% H_e$ results for a step-function increase

in T from 300 K to 2000 K for $P = 10$ atm. It is seen that all species except H_2O and O_2 attain a steady-state, and LTE, in times on the order of 100 μsec; 1 $msec$, however, is required for H_2O and O_2. Even so, $\tau_c([H_2O]$ or $[O_2])_{max} = 1$ $msec \ll 10$ $msec$, and LTE can be assumed and the desired temporal resolution achieved if

$$1 \ msec < \tau_M < \tau_p = 10 \ msec.$$

Figures 18 and 19 show the results at $P = 5$ atm and $T = 3000$ K, and Figures 20 and 21 present the $P = 10$ atm and $T = 3000$ K case. For $P = 5$ atm, $\tau_c([x])_{max} \cong 1$ $msec$ but for $P = 10$ atm, where the dissociation reactions are retarded, or slowed, $\tau_c([x])_{max} > 1$ $msec$. Therefore, for $P = 10$ atm and $T = 3000$ K, more and careful analysis would have been required for accurate analysis of the data. Similar results are shown for $T = 4000$ K in Figures 22 through 26 as P increases from 1 to 10 atm. The increase in the rates of the reaction kinetics at 4000 K results in $\tau_c([x])_{max} < 1$ $msec$. Therefore,

$$1 \ msec \ < \tau_M < \tau_p = 10 \ msec.$$

The results for mixtures of H_2O and H_2 are shown in Figures 27 through 34 and inequalities similar to the immediately preceding value result.

Finally, for the condition represented by Figure 34, the time-dependent sound speed was computed throughout the reaction processes. Figure 35 shows the sound speed versus time for a step-function temperature change. From Figure 35, it is to be noted that, following the step-function increase in T and initial, rapid change in constituency, neglect of the time-dependent chemical kinetics could result in an error in the sound speed of about 8%, which translates into an error of 16% in temperature. Consequently, for the range of conditions that were anticipated for this study, it is essential to perform such time-dependent kinetics calculations to either avoid or correct for finite-rate chemical kinetics effects on the sound speed and temperature measurements.

On the basis of the preceding studies and calculations, the OLD technique was adjudged to be feasible for determination of temperature for the dissociating, reacting sample of H_2O/He, H_2O/Ar and H_2O/H_2 mixtures at the composition and pressure conditions anticipated for use.

The final major concern regarding application of the OLD method, as well

as other optical techniques, is the effect of the gas dynamic parameters on the quality of the pump and especially the probe beams. Of particular concern, of course, is the effect of refraction and resulting deviation of the pump and probe beams that result from the gradient of the index of refraction of a laminar flow-field as well as the refraction and beam spreading encountered in a turbulent flow-field. For the conditions anticipated for this study, it is seen that $O(Re_L) = 10^2$, where Re_L is the unit length Reynolds number of the gas. Therefore, since a characteristic length L is on the order of 10 cm, it is quite possible that the flow-field is laminar. If so, for a cylindrically symmetric CO_2 laser beam injected along the centerline of the gas sample, a detailed analysis of the experimental results requires the use of the eikonal equation for determination of the refractive displacement of the beams. The approach used by Lewis and Selman [18] provides a prediction of the refractive displacement of the irradiance centroid of the probe beams for specified refractive index (or gas density) gradients. From the expected geometry of the experi mental configuration, it is readily seen that diametral injection of the probe beams of minimal or very small diameters minimizes beam refraction effects. Further, quantitative evaluation of such refraction effects is easily accomplished by observing probe beam deflections without the use of the excitation pump beam.

D. Absorption Measurement

Measurement of the absorption coefficient at a particular point in a volume having axial symmetry can be accomplished if a transverse scan of transmission can be obtained. If the measured transmission transverse to the axis is given by T(x), then the absorption at the radial distance, r, from the axis is given by the Abel inversion,

$$k(r) = \frac{1}{\pi} \int_r^{r_o} \frac{ln[T(x)]}{(x^2 - r^2)^{1/2}} dx \tag{23}$$

where r_0 is the distance from the axis where the absorption coefficient k(r) vanishes. Evaluation of this expression for experimentally measured transmission scans can be performed using a technique developed by Shelby and Limbaugh [19].

The transverse scan of transmission was obtained using a linear pyroelectric array having 32 separate elements. A stabilized, continuous, 6 W carbon dioxide laser beam passed through a variable attenuator, then it was expanded and colli-mated before passing across the test chamber through zinc selenide windows. After

it exited the chamber, the beam passed through a rotating chopper wheel and was imaged onto the detector array so that the elements of the array spanned the region of interest. The output beam from the laser could be directed to a small grating monochrometer to determine the particular rotational transition which was lasing.

The output of the detector array was sampled at a frequency of 5 Hz and read into an LSI-11 data acquisition system which was also used to acquire the data from the temperature measurement. Timing for the experiment was controlled by the computer using the trigger signal from the rotating chopper, to insure that the temperature and transmission measurements coincided in time.

E. Test Chamber

The test chamber and the associated boiler designed to supply the chamber with a known mixture of water vapor and diluent gas was designed and fabricated at MSFC and provided to UTSI for the preliminary experiments performed there. The chamber was constructed from two existing sections of flanged aluminum pipe which were attached to a machined aluminum hexagonal section fitted with six windows to allow optical access. Four of the windows were quartz to permit access for the excimer laser and for the helium-neon laser beams used for the temperature measurement. The other two windows were made of zinc selenide to permit access for the 10.6 micrometer carbon dioxide laser used for the transmission measurement. A third zinc selenide window was fitted to the flanged cylindrical section to permit access for the high power 10.6 micrometer laser beam used to create the laser absorption wave. The test chamber is shown schematically in Figure 1.

A boiler system was designed to supply the test chamber with a known mixture of water vapor and diluent gas. This system was composed of a spherical stainless steel tank of approximately 10 gallons internal volume wrapped with heating coils and heavily insulated. Fittings were installed in the top and bottom of the tank to allow for injection of the diluent gas. The tank was operated approximately half full of water and the diluent gas was introduced through a 1/4 inch stainless steel standpipe and bubbled through the water in the tank. The resulting water-saturated vapor was extracted from the top of the tank through a glass-wool filter to eliminate any water droplets. The pressure in the entire system was controlled by throttling the flow at the outlet of the test chamber.

The temperature of the boiler was controlled to an accuracy of 0.5C using a platinum RTD thermocouple and controller. The partial pressure of water vapor at the boiler operating temperature was determined from the equilibrium steam tables. The pressure of the diluent gas on the water was increased to provide the

desired partial pressure ratio (mole fraction) of diluent gas to water vapor. Using this procedure, the mole fraction of diluent gas exiting the boiler was always known during the test. The boiler typically was operated at a temperature of 120 C and a pressure of 75 psig. This condition corresponds to a water vapor mole fraction of 0.33.

The test chamber was connected to the boiler by a 6 ft length of 1/2 inch diameter stainless steel tubing. The pressure drop through this length of connecting tubing at the relatively low flow rates (approximately 2 liters/min) was negligible. All tubing, fittings and test chamber surfaces were heated to a temperature 30 C higher than the boiler temperature in order to eliminate any possibility of vapor loss due to condensation. Initial testing of the system revealed that thermal stratification was a problem in the boiler. This problem was eliminated by the addition of a closed-loop pumping system which removed water from the bottom of the tank (past the RTD probe) and replaced it at the top. The pumping rate was 4 gpm so that the volume of the water was circulated approximately once every minute. The pumping loop was insulated in order to avoid cooling of the water during circulation. The state of equilibrium in the tank was assured by the installation of a bare wire thermocouple in the top of the tank to measure the temperature of the gas/water vapor mixture. When the gas temperature and the water temperature agreed to within the accuracy of the temperature probes, the state of equilibrium was assumed to exist. This state of equilibrium was normally reached within a period of 4 hours from initial startup of the boiler/test chamber system.

F. Data Acquisition and System Integration

Successful measurement of the absorption coefficient as a function of temperature relies on the simultaneous acquisition of the transmission data from the probe laser and the time-of-flight measurement for the acoustical wave. This requires synchronization between the firing of the excimer laser and the chopper wheel used for the transmission measurement, using the data acquisition computer to control the timing for the acquisition of the pyroelectric array scans and the initiation of the counters used for the time-of-flight measurement. The trigger pulse from the rotating chopper wheel was used to initiate the timing sequence within the LSI-11 computer which delivered the firing pulse to the excimer laser, started the start and stop counters for the time-of-flight measurement and acquired the scan from the pyroelectric array. When one measurement sequence was complete, the counters were reset and a new sequence initiated at the next trigger pulse from the chopper.

A measurement begins when the high power laser is turned on and begins

heating the ceramic end-wall of the chamber. All of the scans from the pyroelectric array are recorded by the computer, but prior to the time that the wave is launched from the wall the absorption across the chamber is negligible, and these early scans are averaged and used to normalize the later scans to obtain the transmission. Since the temperature is measured at only a single point within the wave, the transmission must be Abel inverted using the method described in section II-D to relate the absorption coefficient to the measured temperature.

III. EXPERIMENTAL RESULTS

An experimental study was performed at UTSI to verify the proposed method of temperature measurement, to evaluate the utility of some candidate materials for the end wall and to attempt to launch a laser absorption wave using the small (1.5 kW) laser at UTSI.

An experimental study of the temperature measurement technique was initiated to determine if the excimer laser was an acceptable source for the breakdown spark, and to determine the suitability of the available instrumentation for measurement of the time-of-flight of the resulting acoustic wave. For the initial investigation, the experiment was set up in ambient air using a boxcar integrator to measure the passage of the wave through two helium-neon laser beams which were separated by approximately 2 mm. It was found that the excimer was effective at producing the laser sparks with repetition rates to 200 Hz, and that the measured temperature agreed with the known temperature of the ambient air to within 1%.

Following the initial experiments in air, a small (10 cm diameter, 30 cm long) chamber was constructed to contain an atmosphere of argon or helium, two of the proposed diluent gases for the absorption measurement. For these experiments the time-of-flight of the wave was measured both by the boxcar integrator and by using time-to-digital counters integrated into the LSI-11 computer. In order to insure reliable triggering of the counters by the deflection of the helium-neon beams, the beams had to be accurately focused on the detector pinholes. The chamber could be heated by use of a portable, hand-held, heat gun and the chamber temperature measured with a thermocouple. In argon, the experiments verified that temperatures could be determined to approximately 1%, and were independent of chamber pressure over the range from one to five atmospheres. However, when helium was used as the test gas, the excimer laser failed to produce a spark breakdown, even at helium pressures up to five atmospheres. Addition of water to the cell was found ineffective in promoting breakdown in helium.

An ideal material for the end wall would have the following characteristics: it would absorb all of the incident laser energy, have low thermal conduction to reduce the energy conducted away from the surface, withstand thermal shock without fracturing, and not melt at the temperatures required for initiation of the absorption wave. Experiments were conducted at UTSI using the 1.5 kW carbon dioxide laser to screen some possible candidate materials.

Alumina (Al_2O_3) has a high absorptivity at 10.6 micrometers, but thin sections were found to shatter when subjected to the laser beam, and thicker sections were found to melt and drip. Several varieties were tested and none were found suitable. Tungsten had too great a reflectivity at 10.6 micrometers to be effectively heated by the incident power available from the 1.5 kW laser, and it did not get sufficiently hot to obtain an optical pyrometer measurement of surface temperature. Graphite absorbs the laser beam efficiently, but the energy was carried away rapidly by thermal conduction and, again, it was not possible to obtain a measurement of surface temperature using the optical pyrometer. A ceramic material of unknown composition, Norton Magnorite [R], was found to have the properties required. In a section of 1/2 inch thickness it was possible to obtain surface temperatures of 1850 C, as measured with the optical pyrometer, and it was possible to heat it for as long as six minutes without melting or thermal fracture. After repeated heating cycles the surface appearance changed from the initial brown color to a crystalline white, and some cracking was noted after cooling. Since the measured surface temperature of this material was sufficiently high, according to the model predictions, to initiate a laser absorption wave, it was chosen as the end wall material for the absorption wave experiments.

The model predictions indicated that approximately 375 W/cm^2 would be required to initiate a laser absorption wave, and the 1.5 kW laser at UTSI was unable to produce this flux over a spot size sufficient to obtain a reliable measurement of transmission. However, the high power laser at MSFC was under repair and not available, and it was decided to attempt to initiate a laser absorption wave using the UTSI laser. This would provide an integrated test of the data acquisition system and the test chamber, even if wave initiation was not achieved.

The beam from the 1.5 kW laser was focused by a spherical mirror having a focal length of 10 m to a spot approximately 2 cm diameter. Burn patterns in plastic showed that the beam was fairly uniform in intensity across the spot, due to the effects of spherical aberration and coma, but showed some striations due to diffraction. The power of the beam after passing through the optical train, including a wedge beamsplitter used to monitor the power during the experiment,

was measured by a Scientech calorimeter and found to be 750 W. Thus, the incident laser intensity on the ceramic end-wall was approximately 240 W/cm_2, which was marginal according to the model predictions. For this spot size, using the maximum absorption coefficient reported in Reference [8], the minimum transmission would always exceed 92%, but that value of transmission was thought to be detectable.

When the experiment was first attempted, it was found that the laser beam used for the transmission measurement was not uniform after passing through the test cell. This proved to be due to the effect of interference of the coherent laser beam passing through the nearly-plane zinc selenide windows. To alleviate this problem, new windows having a wedge angle of 1 degree were obtained. The interference fringes from the wedged windows were sufficiently close together that approximately three fringes fell on each of the detector elements of the array, effectively smoothing the beam profile.

Two attempts were made to initiate the laser absorption wave: one in a mixture of 0.33 mole fraction of water in argon at a total pressure of 6 atm, and one in a mixture of 0.33 mole fraction of water in helium at a total pressure of 6 atm. During these experiments, scans from the array detector were obtained at a rate of 5 Hz for approximately 1.5 min. Prior to a test, 1000 scans of the array was recorded to provide a background profile of the laser beam used in the transmission measurement.

Figure 37 shows an average of these 1000 scans where the abcissa is analog-to-digital converter counts. The laser beam intensity was set to provide a maximum signal level of approximately 90% of full scale. The beam profile is fairly uniform in the region of the incident laser beam where the absorption is expected. The probe beam was focused on the array with a magnification chosen so the full array covered a distance in the test cell of 4 cm. Figures 38 and 39 show comparable array scans taken during the argon and helium tests, respectively. The scans appear nearly identical to the background, indicating little absorption during the tests. In Figures 40 and 41 the background scan in Figure 37 has been subtracted from the scans taken during the test. The variations of approximately 20 counts represent only approximately 1% of the signal level. In Figures 42 and 43 the background scan was subtracted from the average of the five scans taken at one second intervals and plotted in a three-dimensional representation to show the difference in transmitted intensity as a function of time and position. There was no evidence from the intensity scans that a laser absorption wave had been initiated, and there was no visual evidence from a closed circuit video camera that visible emission from a "water flame" had occurred.

IV. DISCUSSION AND RECOMMENDATIONS

The concept of using a laser absorption wave initiated at a ceramic end-wall as a means to measure the laser absorption coefficient at high temperatures appears feasible, but was not proved in this investigation.

Failure to initiate a laser absorption wave using the 1.5 kW laser available at UTSI is not surprising, since the model prediction which neglected energy losses due to radial conduction and convection indicated that a higher intensity would be needed. The experiment should be attempted again using the MSFC laser which should be capable of an order of magnitude greater power. Alternate methods of initiating the laser absorption wave might also be considered, such as interrupting the beam sustaining a plasma. In this case the hot decaying plasma might provide the initiation for a laser absorption wave.

The use of time-of-flight measurements of the decaying blast wave from a laser induced spark was verified, and should provide a non-intrusive technique for measurement of translational temperature in molecular gases for which equilibrium between the translational and internal degrees of freedom is not *a priori* insured. Use of an excimer laser having high repetition rates to produce the spark breakdown insures reasonable temporal resolution for transient experiments.

The one-dimensional model employed in this investigation should be modified to include two effects which are likely to be important in the initiation of a laser absorption wave: radial conduction in the ceramic end-wall and in the wave itself, and convection through the wave due to buoyancy and the expansion of the wave material due to heating. Both of these effects represent energy loss mechanisims, and would likely result in larger predicted intensity thresholds for wave initiation.

REFERENCES

1. Kantrowitz, A. R., "The Relevance of Space", Astronatutics and Aeronautics, Vol. 9, No. 3, pp 34-35, March 1971.

2. Minovitch, M. A., "Reactorless Nuclear Propulsion - The Laser Rocket", AIAA Paper No. 72-1095, December 1972.

3. Jones, W. S., Forsyth, J. B., and Skratt, J. P., Final Report: Laser Rocket System Analysis, NASA CR-15921, prepared under contract No. NAS3-20372, Sept. 1978.

4. Keefer, D., Elkins, R., Peters, C., and Jones, L., "Laser Thermal Propulsion", in *Orbit-Raising and Maneuvering Propulsion: Research Status and Needs*, L. H. Caveny, ed., Vol. 89 of Progress in Astronautics and Aeronautics, pp 129-148, 1984.

5. Horvatch, J. C. and Frisbee, R. H., "Laser Propulsion for Orbital Transfer: Laser Technology Issues", AIAA Paper No. 85-1550, July, 1985, and Frisbee, R. H., Horvath, J. C. and Sercel, J. C., "Laser Propulsion for the Orbital Transfer Mission", AIAA Paper No. 85-1224, July 1985.

6. Simons, G. A. and Pirri, A. N., "The Fluid Mechanics of Pulsed Laser Propulsion", AIAA Paper No. 77-699, 10th Fluid and Plasmadynamics Conference, Albuquerque, NM, June 1977.

7. Chapman, P. K., Douglas-Hamilton, D. H., and Reilly, D. A., Investigation of Laser Propulsion, Vols. I and II, Final Technical Report Contract No. N00014-76-0646, Office of Naval Research, Washington, D.C., Nov. 1977.

8. Kemp, N. H., and Krech, R. H., "Laser Heated Thruster", Final Report Contract NAS8-33097, Physical Sciences, Inc., Worcester, Massachusetts, PSI TR-220, Sept. 1980.

9. Fowler, M. C., "Measured Molecular Absorptivities for a Laser Thruster", AIAA Journal, Vol 19, pp 1009-1014, 1981.

10. Rosen, D., Weyl, G., Kemp, N., Ham, D. Cowles, L., and Schertzer, S., <u>Experimental and Theoretical Studies of Laser Propulsion Phenomenology</u>, Interim Scientific Report, Contract F49620-83-C-0039, PSI TR-371, March 1984.

11. Patankar, S. V., <u>Numerical Transfer and Fluid Flow</u>, McGraw-Hill, New York, p. 54, 1980.

12. Grier, N. T., <u>Calculation of Transport Properties and Heat-Transfer Parameters of Dissociating Hydrogen</u>, NASA TN D-1406, October 1962.

13. Patch, R. W., <u>Thermodynamic Properties and Theoretical Rocket Performance of Hydrogen to 100000 K and 1.01325 x $10^8 N/m^2$</u>, NASA SP-3069, 1971.

14. Zapka, W., Pokrowsky, P., and Tam, A.C., "Noncontact Optoacoustic Monitoring of Flame Temperature Profiles", <u>Optics Letters</u>, 7, 477-479, 1982.

15. Herzfeld, K. F., and Litovitz, T. A., <u>Absorption and Dispersion of Ultrasonic Waves</u>, Academic Press, New York, 1959.

16. Rogers, R. C. and Schexnayder, C. J., "Chemical Kinetic Analysis of Hydrogen - Air Ignition and Reaction Times", NASA Technical Paper 1856, July 1981.

17. Duff, R. E., "Calculation of Reaction Profiles Behind Steady-State Shock Waves. I. Application to Detonation Waves", <u>Jour. Chem. Phys.</u>, Vol. 28, pp. 1193-1197, 1958.

18. Lewis, J.W.L., and Selman, J. R., "The Laser-Induced Schlieren Effect in Sodium-Nitrogen Mixtures", <u>Combustion Diagnostics by Nonintrusive Methods</u>, T. D. McCay and J. A. Roux, eds., Vol. 92 of Progress in Astronautics and Aeronautics, pp 132-146, 1984.

19. Shelby, R. T. and Limbaugh, C. C., <u>Smoothing Technique and Variance Propagation for Abel Inversion of Scattered Data</u>, AEDC-TR-76-163, Arnold Engineering Development Center, Tennessee, 1977.
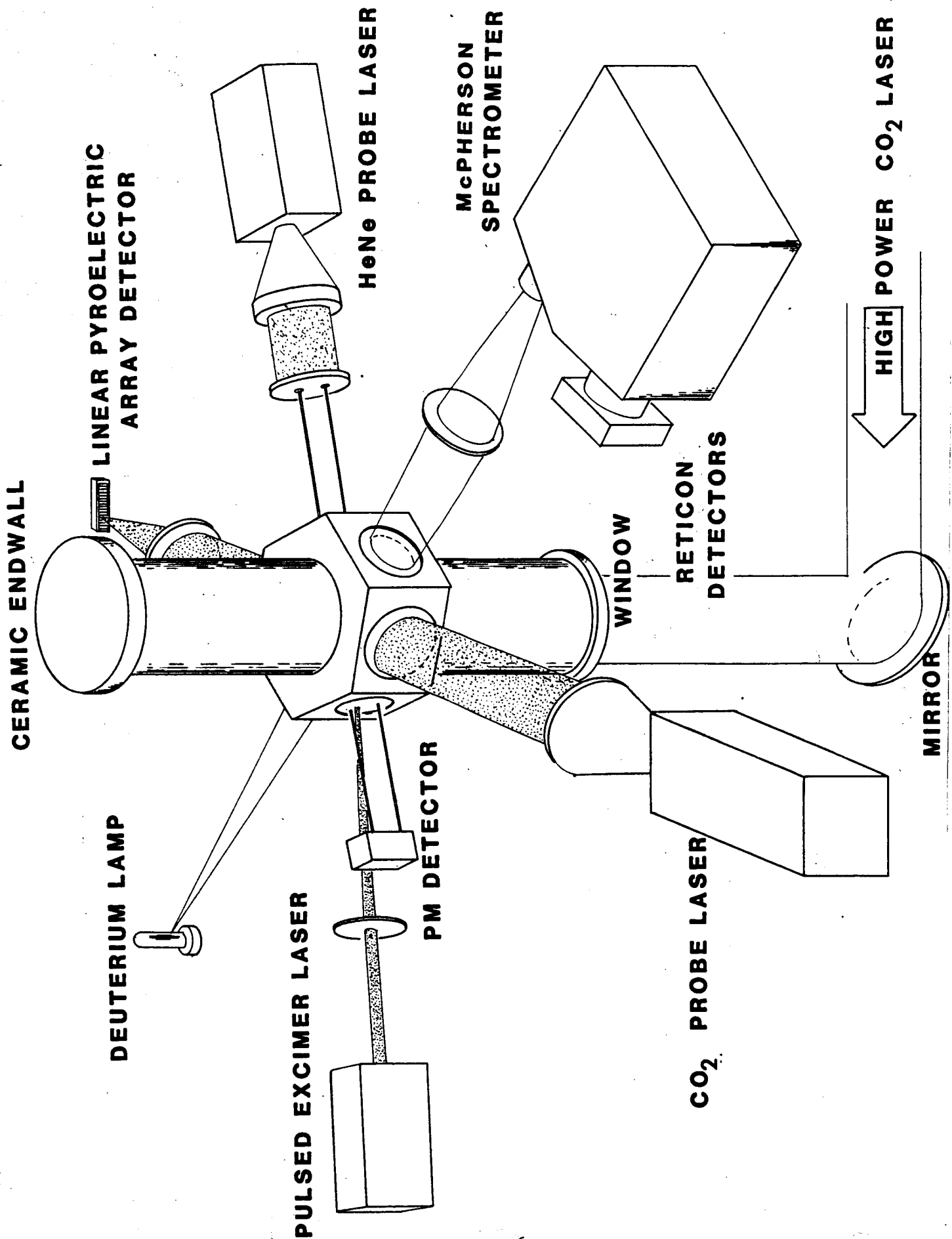
FIGURE 1 Vertical Test Cell and Diagnostics.

LINEAR PYROELECTRIC
ARRAY DETECTOR

HeNe PROBE LASER

McPHERSON
SPECTROMETER

HIGH POWER CO₂ LASER

CERAMIC ENDWALL

WINDOW

RETICON
DETECTORS

MIRROR

DEUTERIUM LAMP

PULSED EXCIMER LASER

PM DETECTOR

CO₂ PROBE LASER
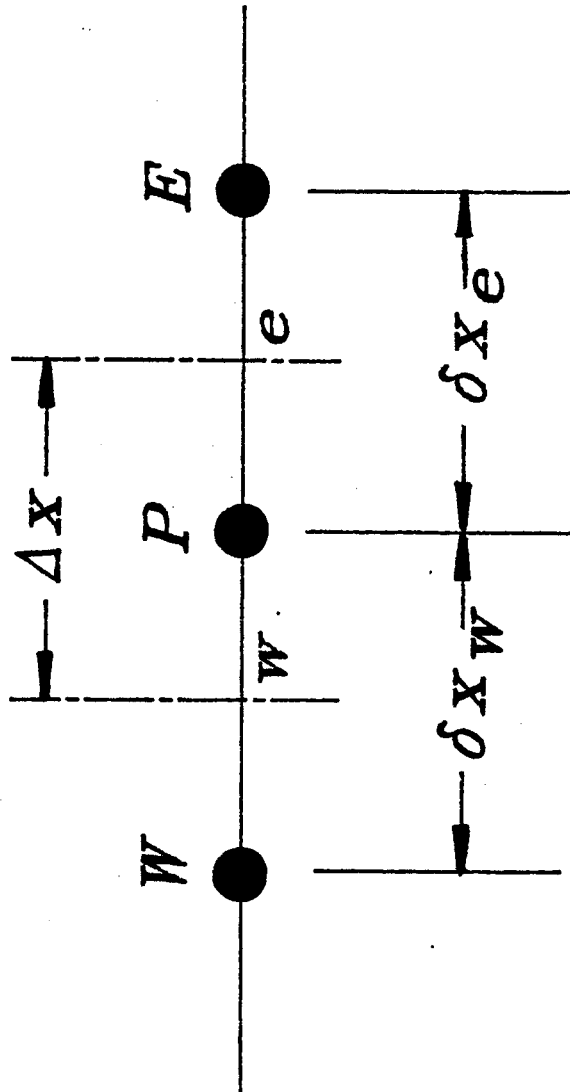
FIGURE 2 Control volume for the finite element approximations.
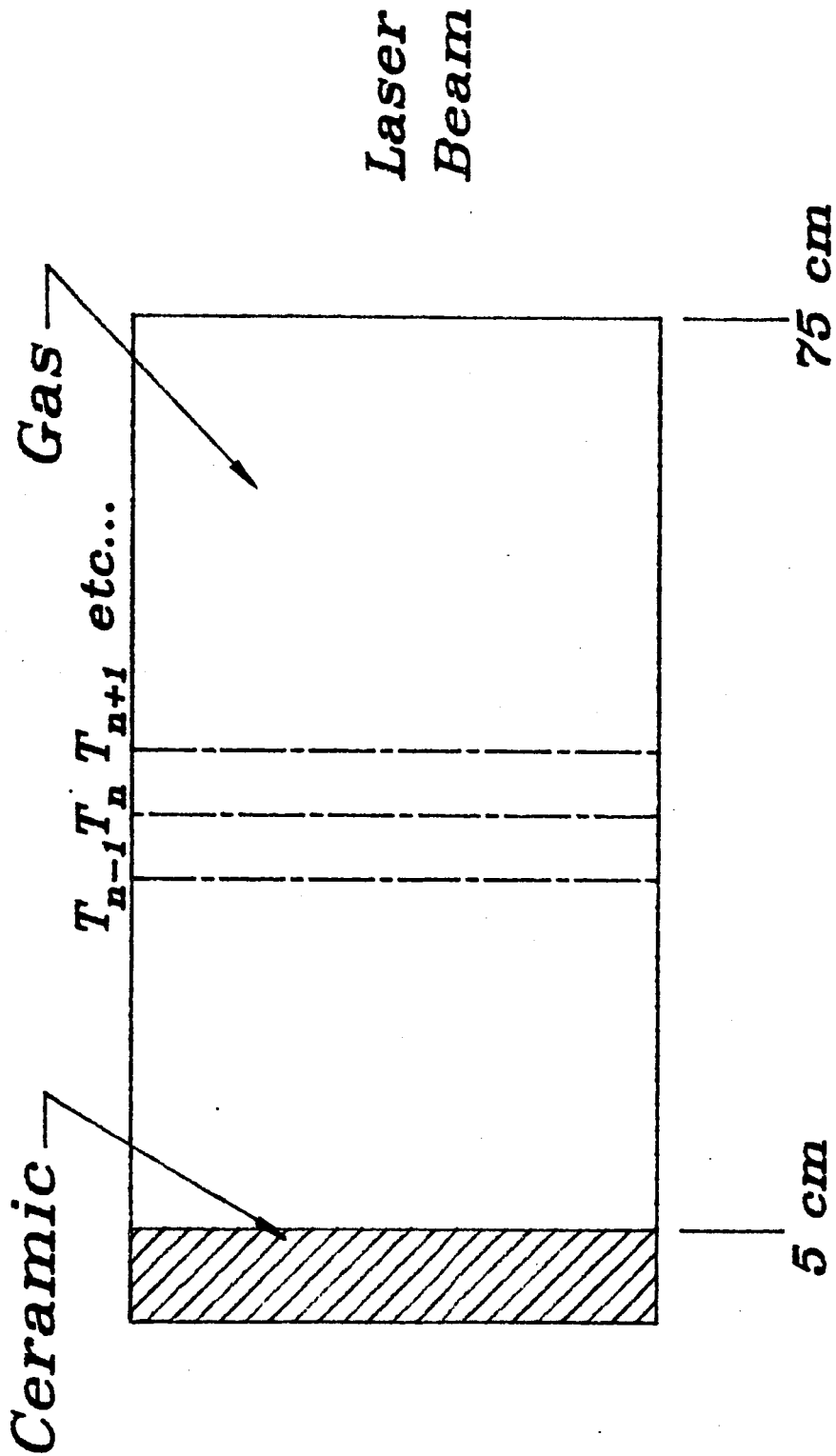
FIGURE 3 Solution space for the laser absorption wave problem. Note that the space is divided into two regions, target and gaseous medium.
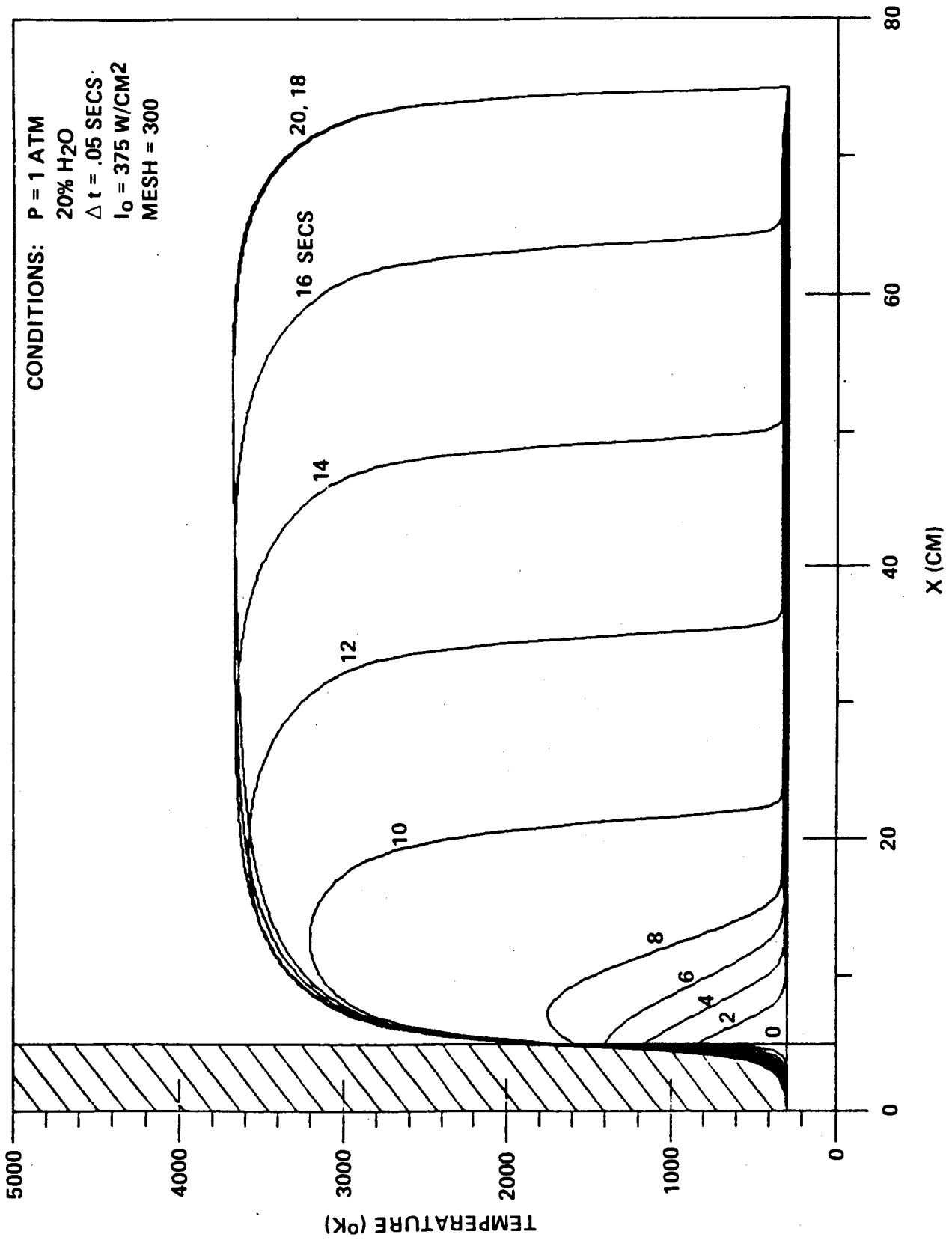
FIGURE 4 <u>Laser absorption wave for the 20%, 1 *atm* Case.</u>
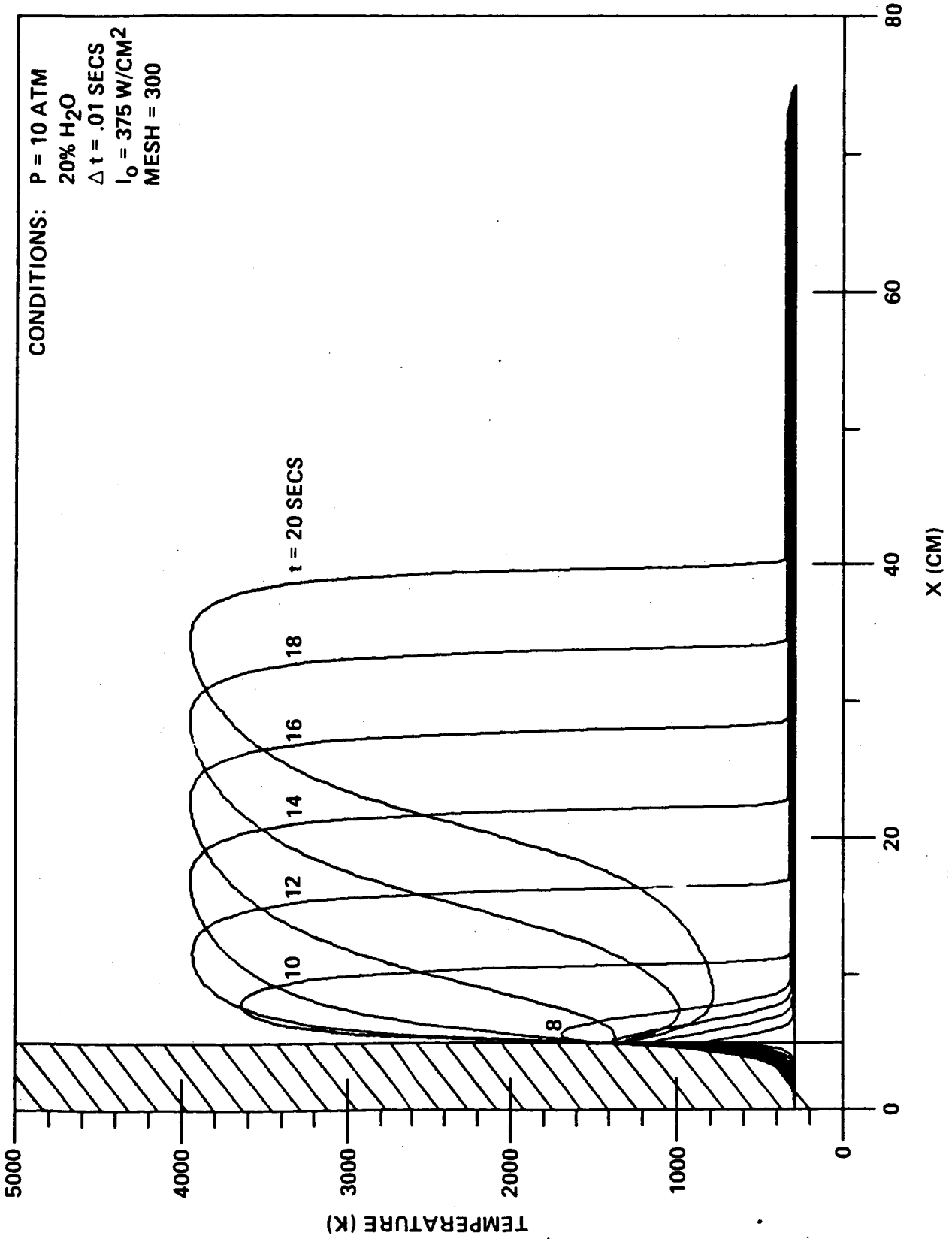
FIGURE 5   Calculated laser absorption wave for the case 20% H_2O in hydrogen at 10 atmospheres pressure. The incident laser intensity is 375 W/cm^2.
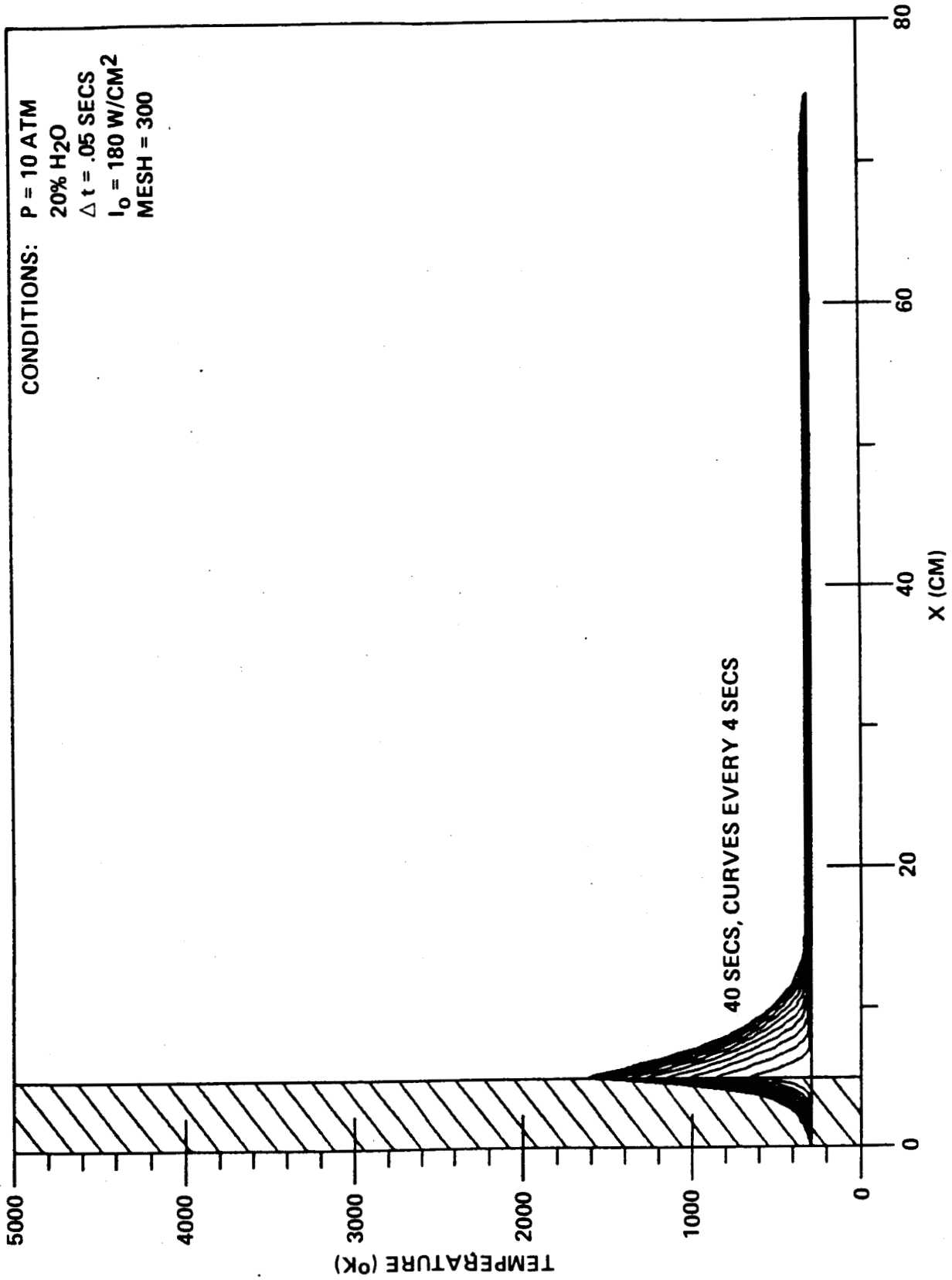
FIGURE 6 Solution for the case 20% H_2O in hydrogen at 10 atmospheres pressure. The incident laser intensity is $180\ W\ cm^2$.

CONDITIONS:
P = 10 ATM
20% H2O
Δ t = .05 SECS
I_o = 180 W/CM^2
MESH = 300

40 SECS, CURVES EVERY 4 SECS

TEMPERATURE (°K)

X (CM)

EP11213
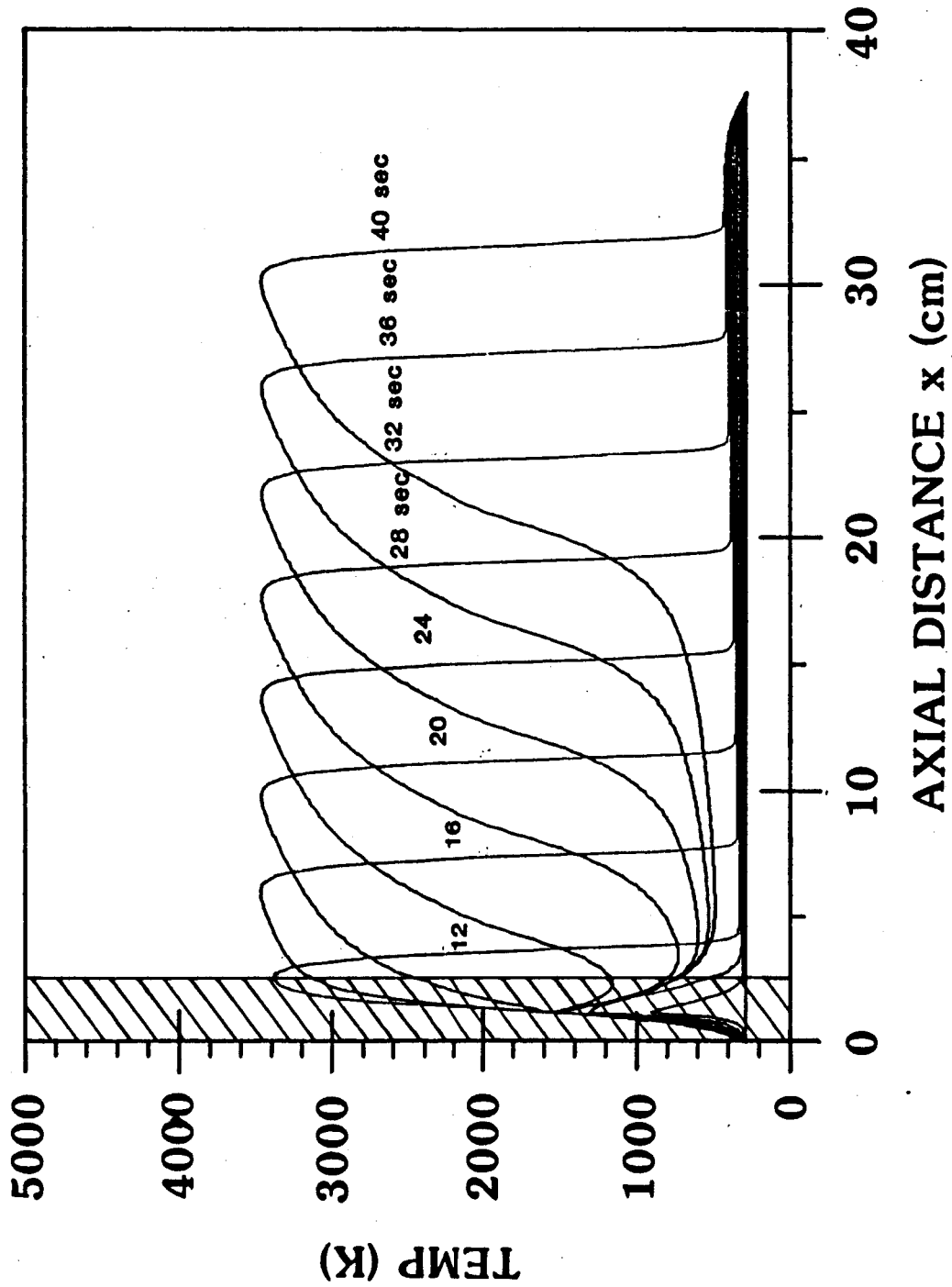
FIGURE 7 Model prediction for a mixture of 20% H_2O and 80% He at a total pressure of 10 *atm* with incident laser beam intensity of 375 W/cm^2.
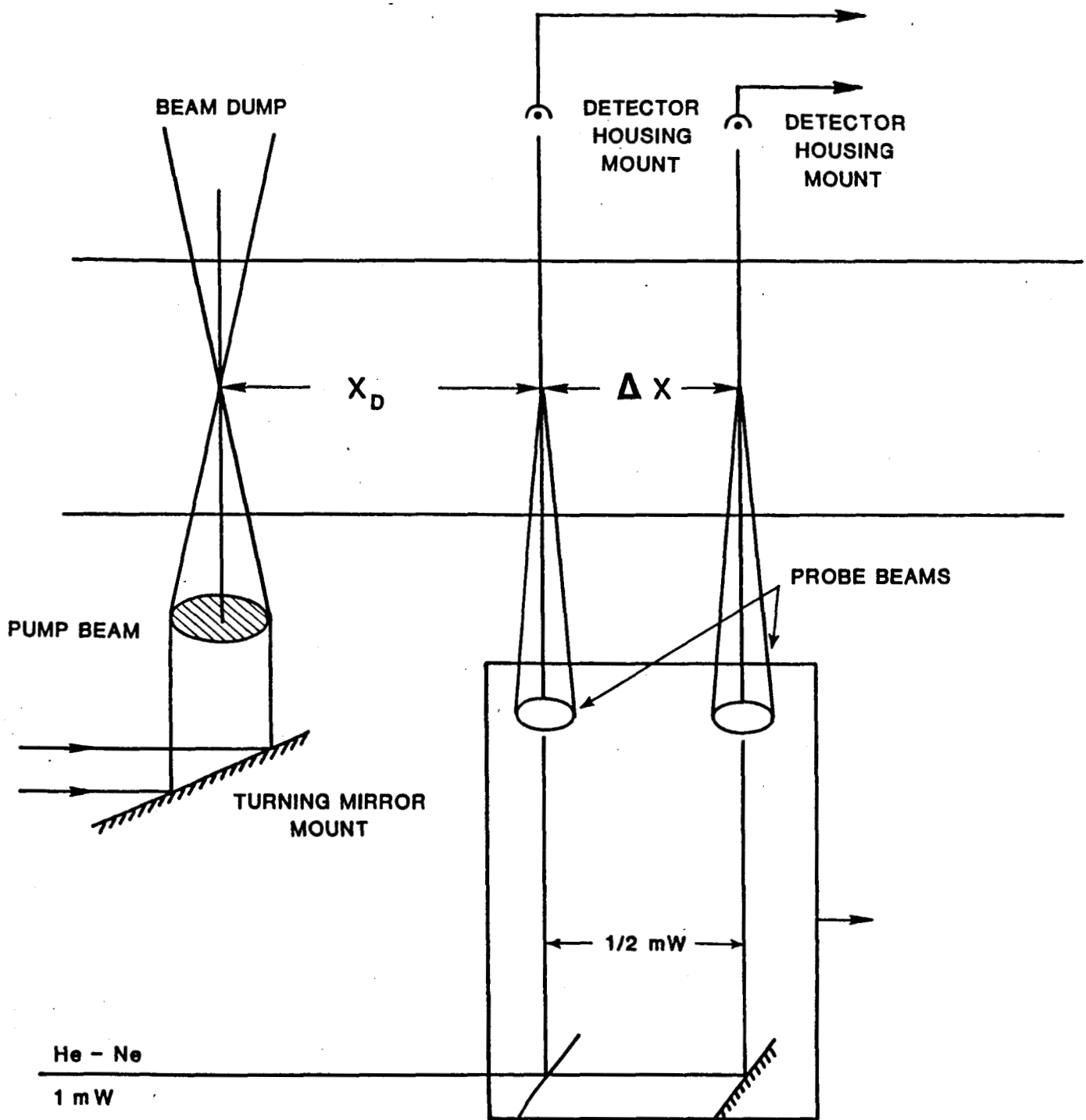
**FIGURE 8** Schematic of the experimental arrangement for the Optoacoustic laser-beam deflection (OLD) technique.
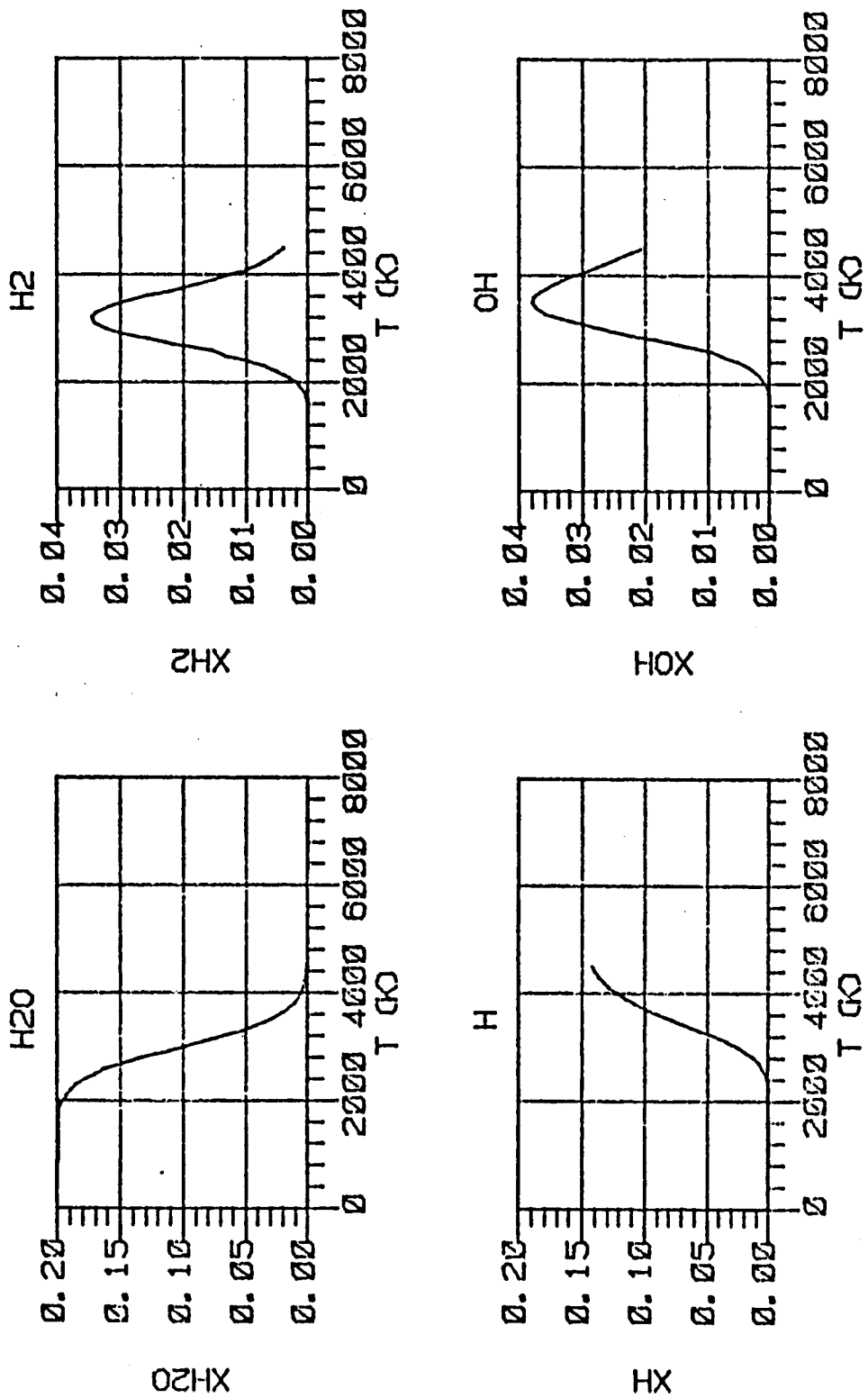
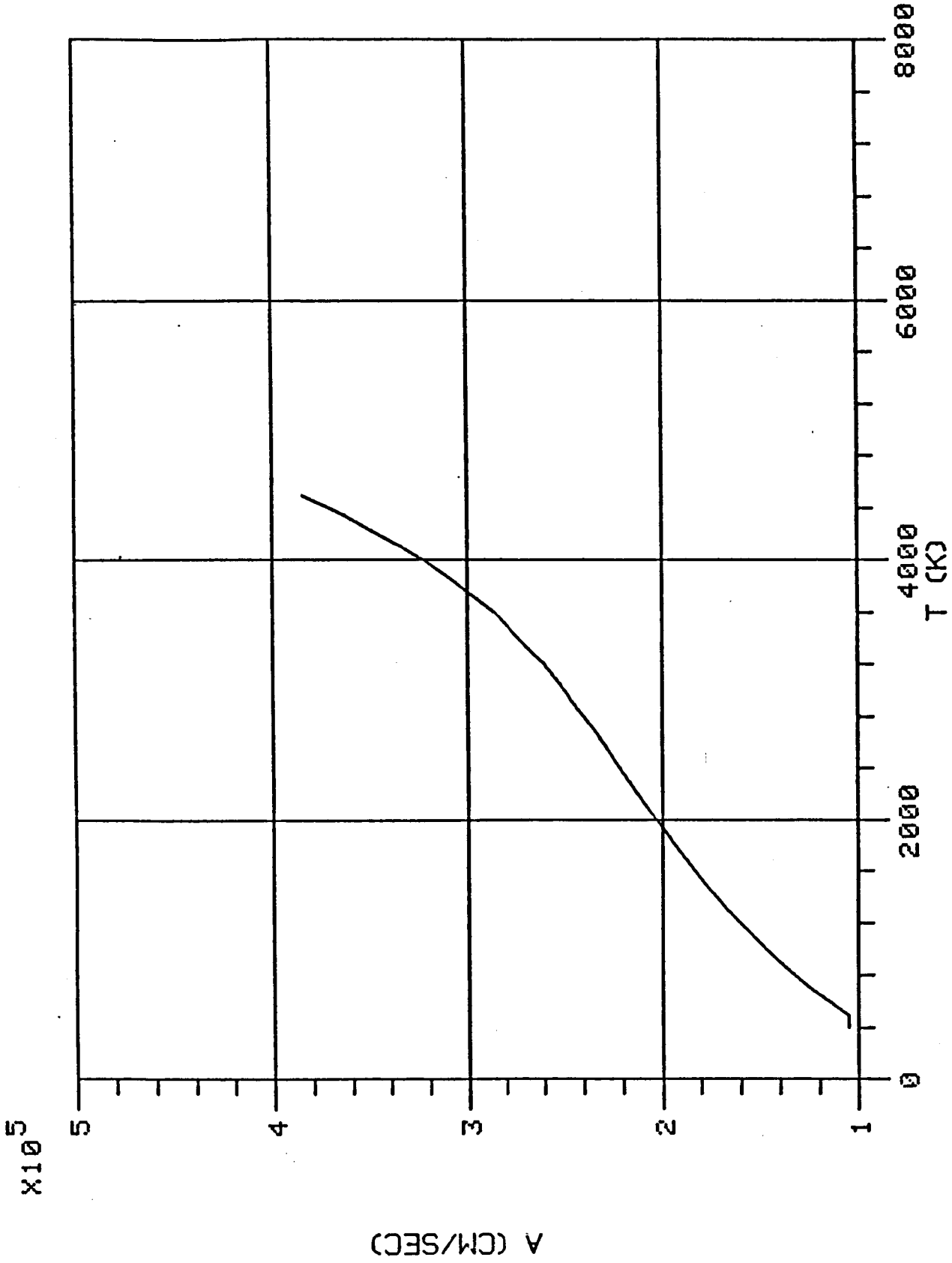**FIGURE 9** Calculated equilibrium concentrations for a mixture of 20% H_2O and 80% Ar at a total pressure of 1 atm.
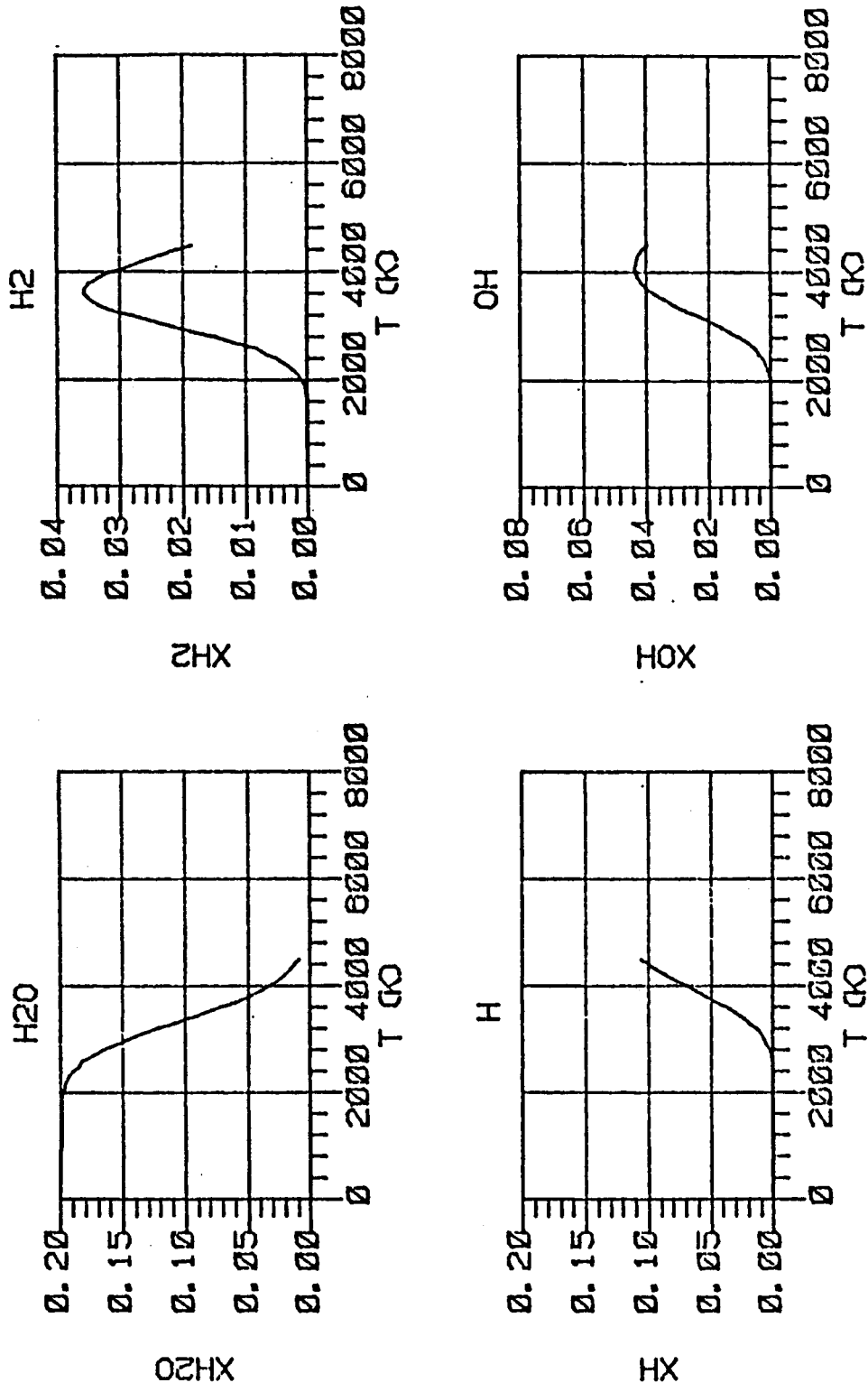
FIGURE 10 Calculated equilibrium concentrations for a mixture of 20% H_2O and 80% Ar at a total pressure of 10 atm.
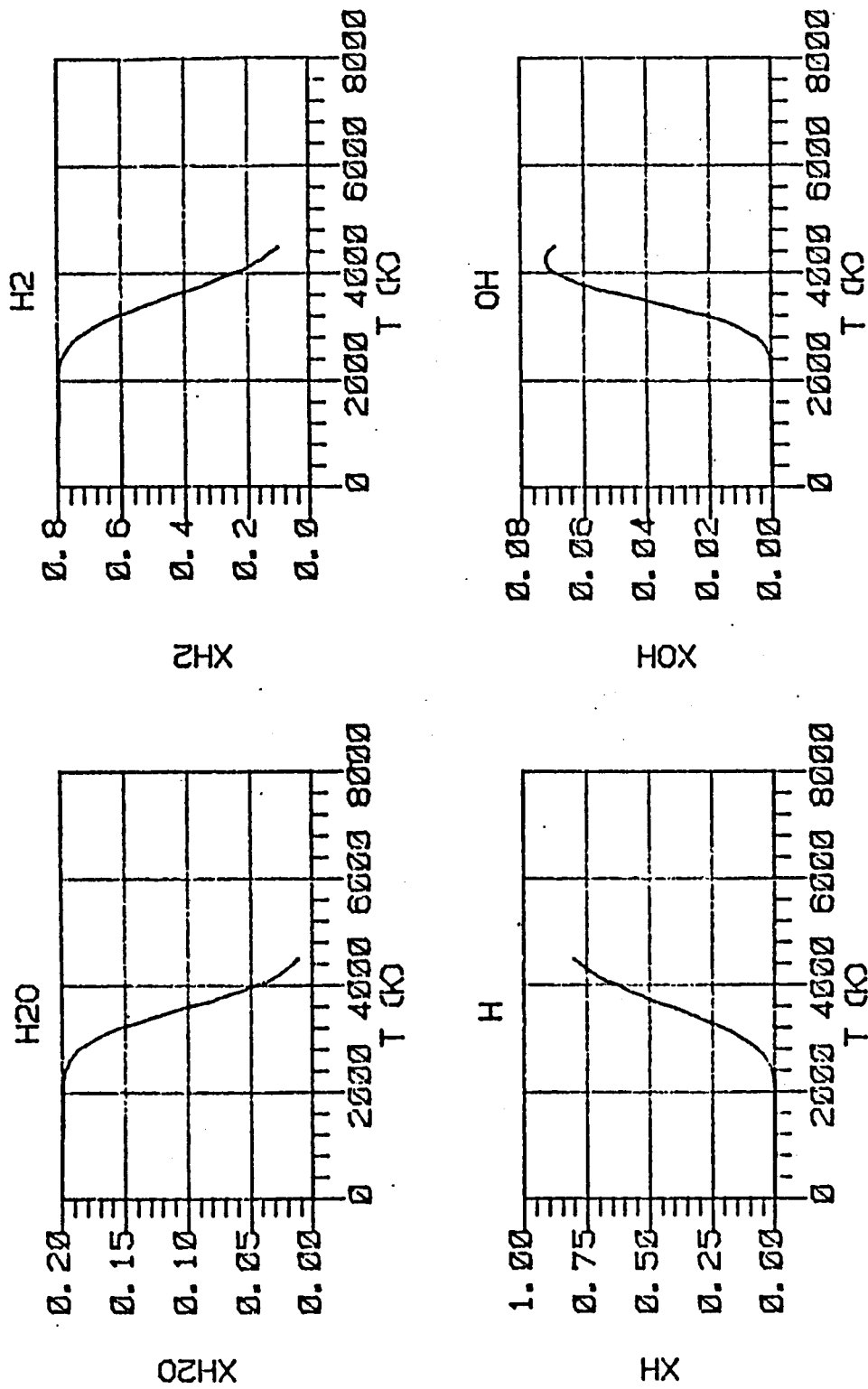
FIGURE 11 Calculated equilibrium concentrations for a mixture of 20% H_2O and 80% H_2 at a total pressure of 1 atm.
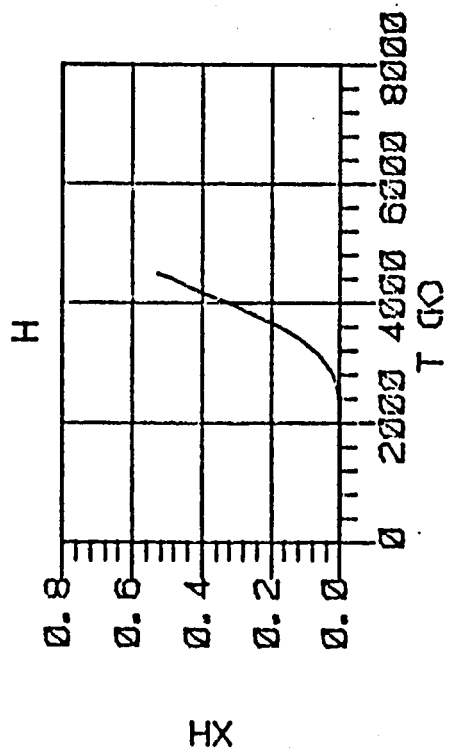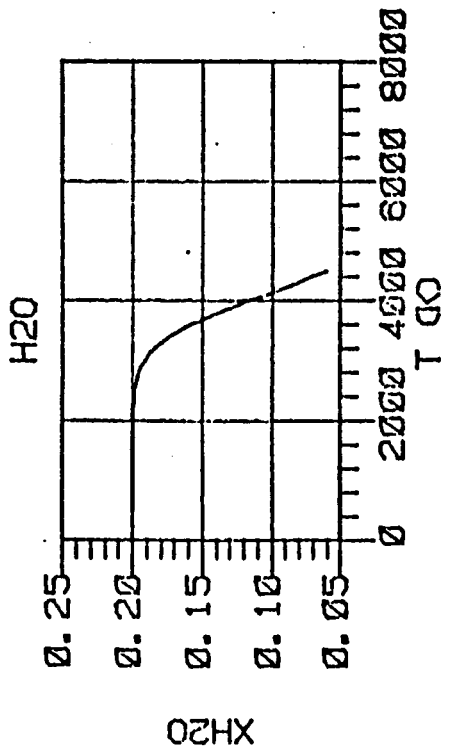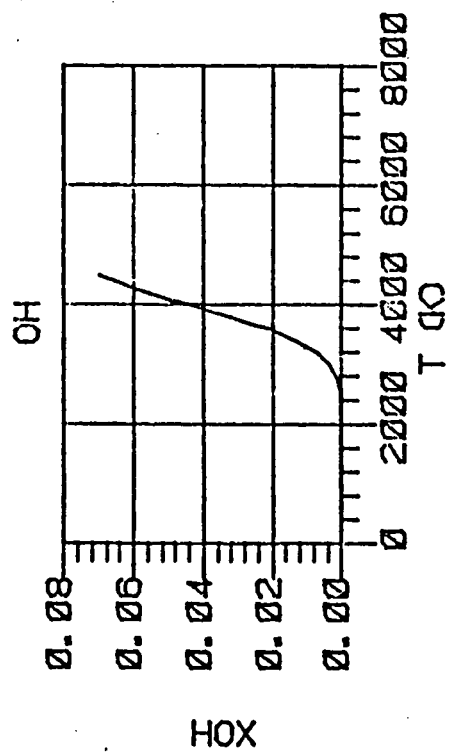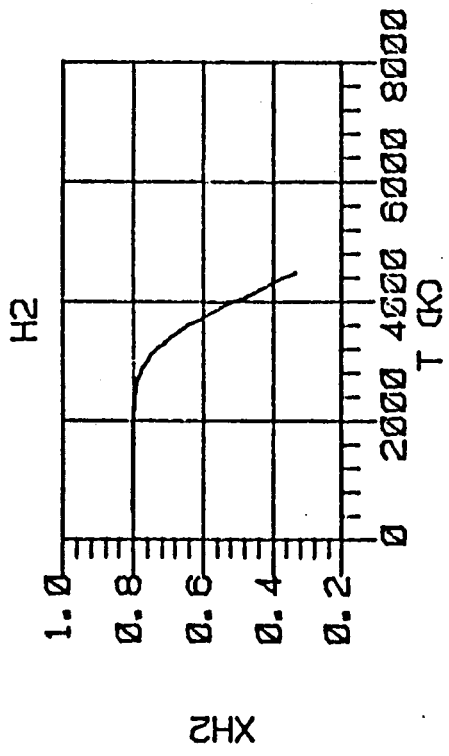
FIGURE 12 Calculated equilibrium concentrations for a mixture of 20% H_2O and 80% H_2 at a total pressure of 10 *atm*.
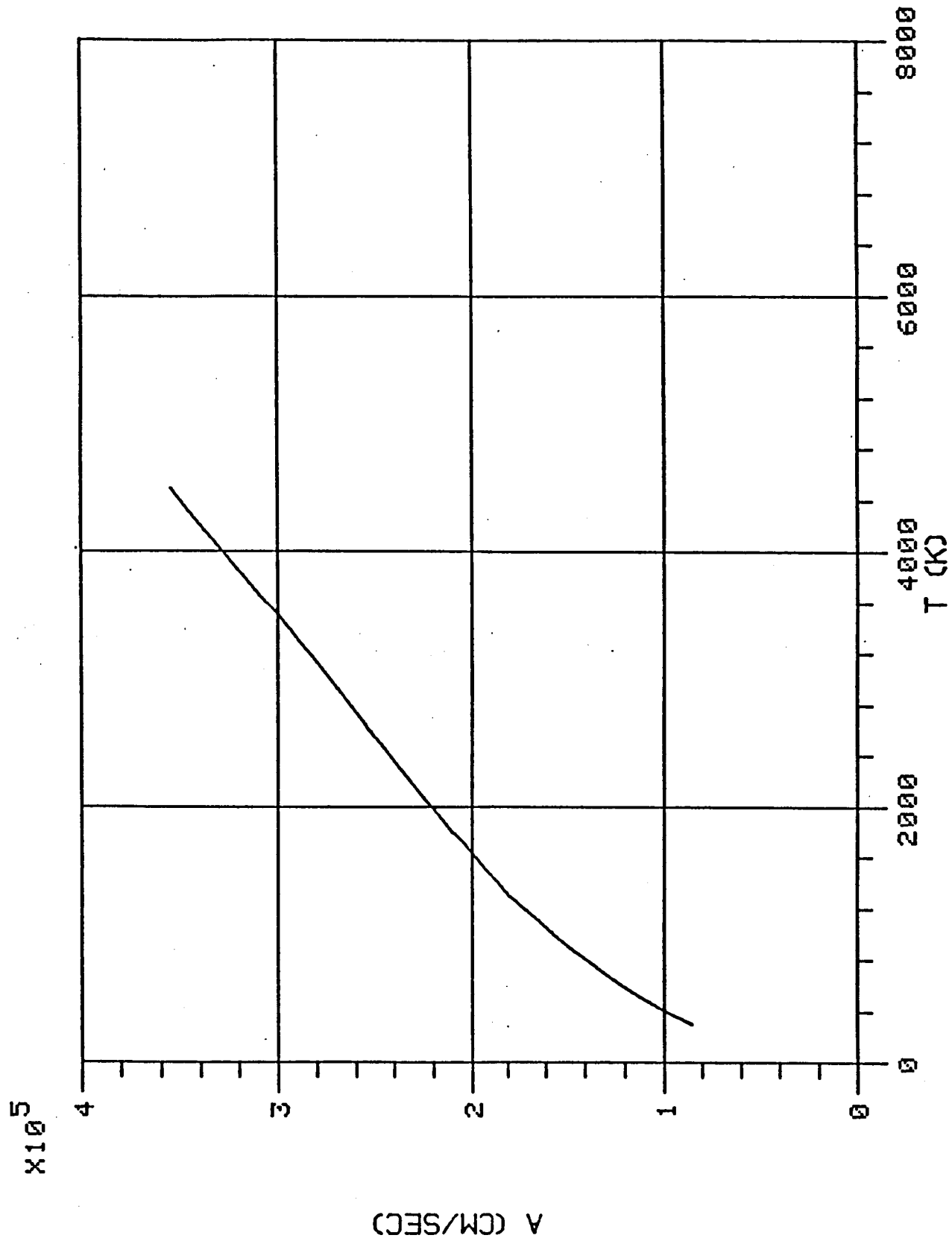
FIGURE 13 Calculated sound speed based on equilibrium concentrations for a mixture of 20% H_2O and 80% He at a total pressure of $5atm$.
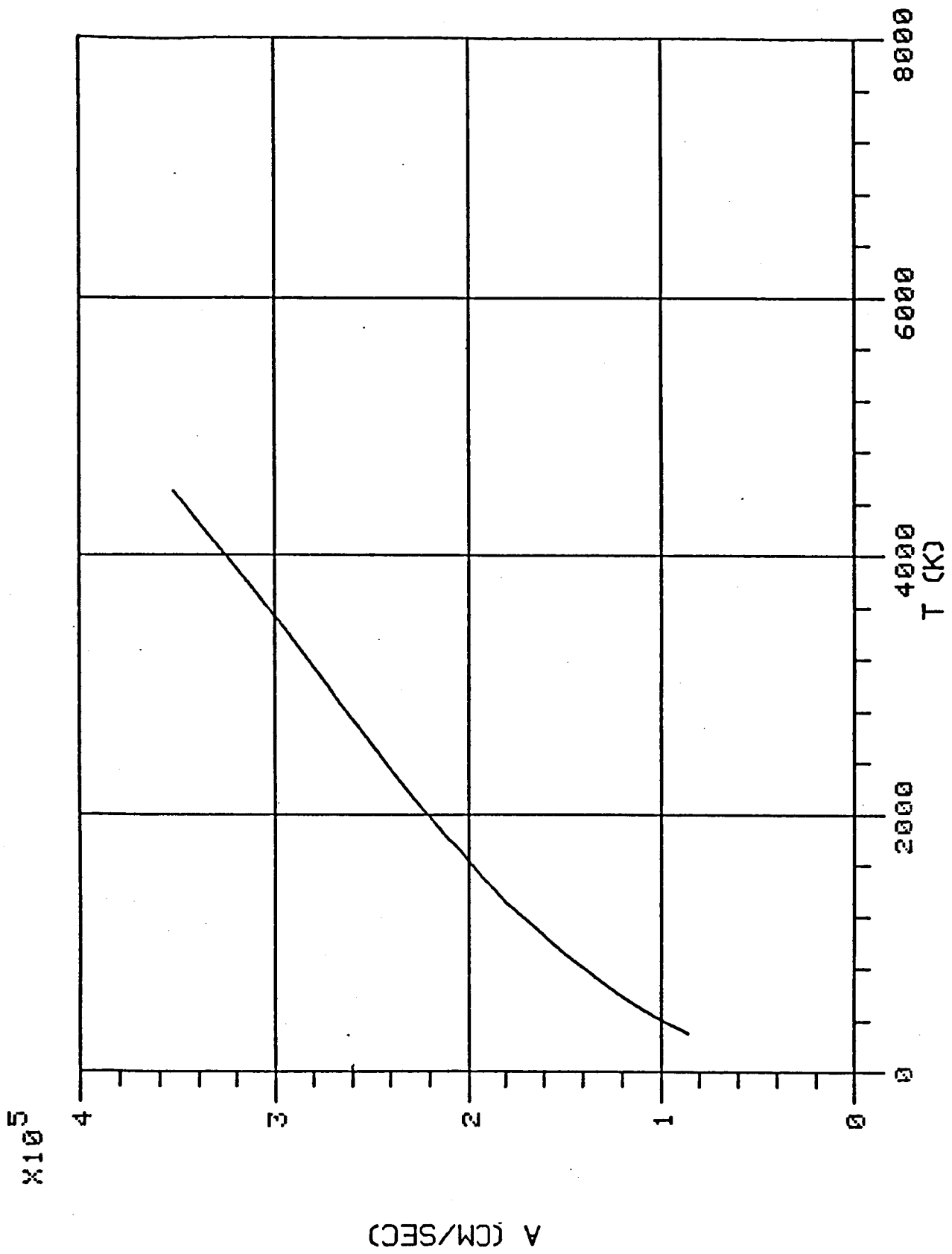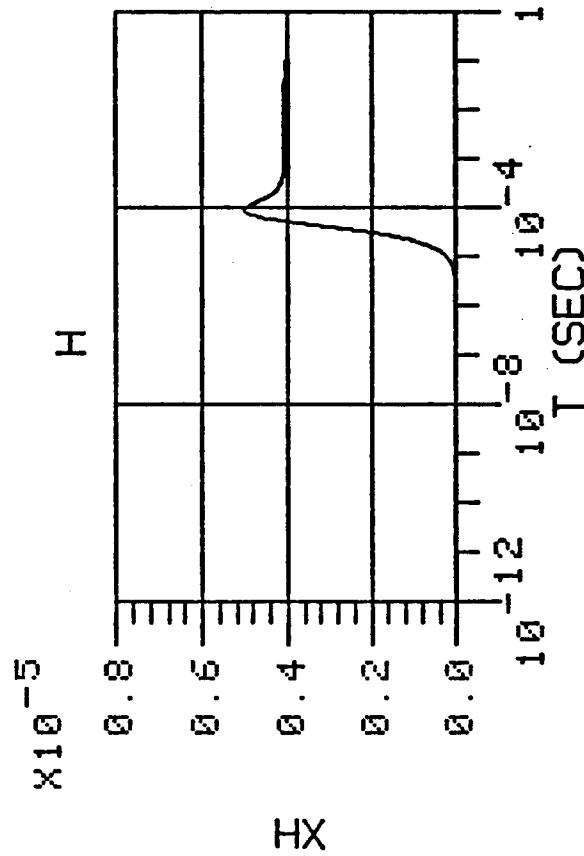
FIGURE 14 Calculated sound speed based on equilibrium concentrations for a mixture of 20% H_2O and 80% He at a total pressure of 10 atm.
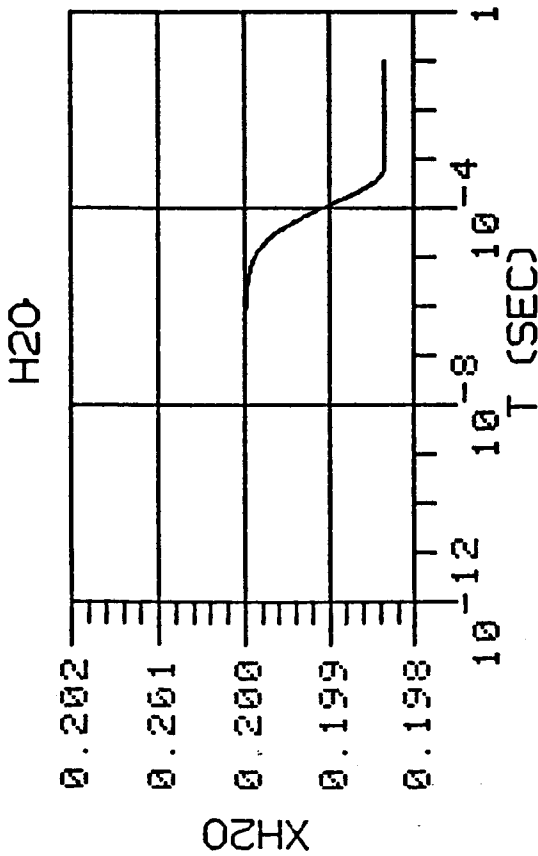
FIGURE 15 Calculated sound speed based on equilibrium concentrations for a mixture of 20% H_2O and 80% H_2, at a total pressure of 1 atm.
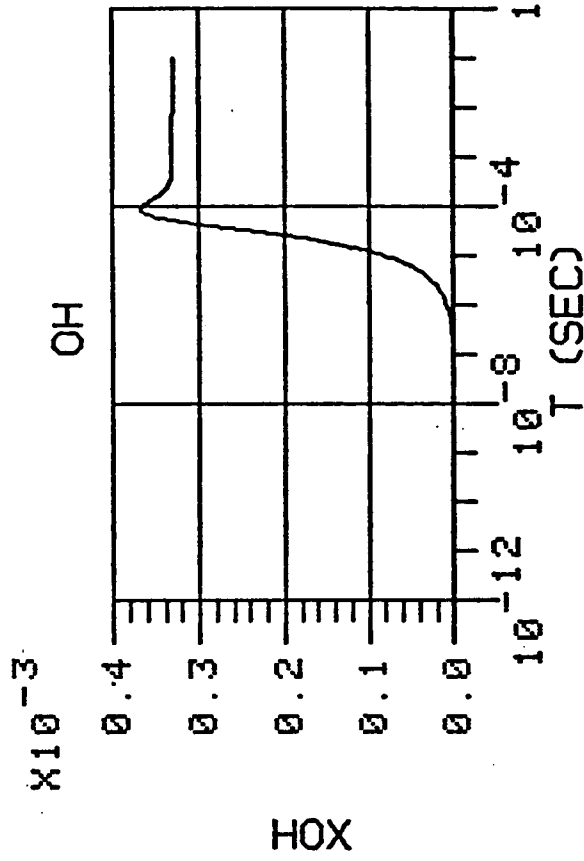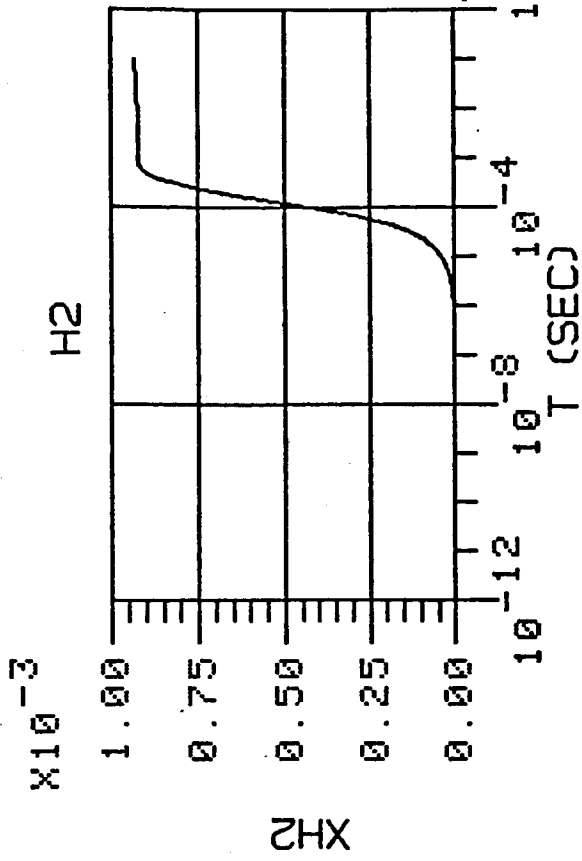
FIGURE 16 Species concentrations resulting from a non-equilibrium calculation for a mixture of 20% H_2O and 80% He at a temperature of 2000 K and a total pressure of 10 atm.
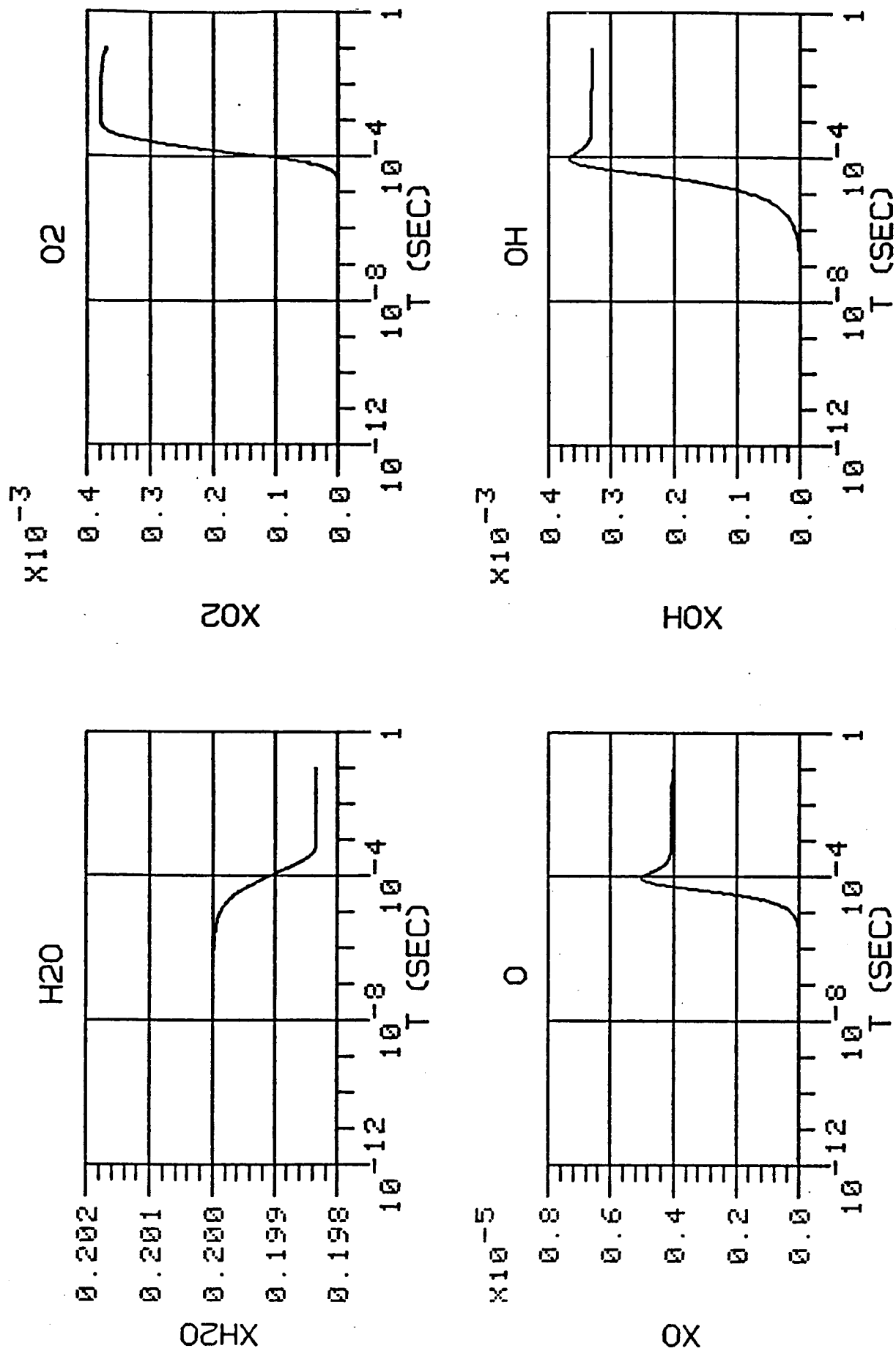
-41-

FIGURE 17 Species concentrations resulting from a non-equilibrium calculation for a mixture of 20% H_2O and 80% He at a temperature of 2000 K and a total pressure of 10 atm.
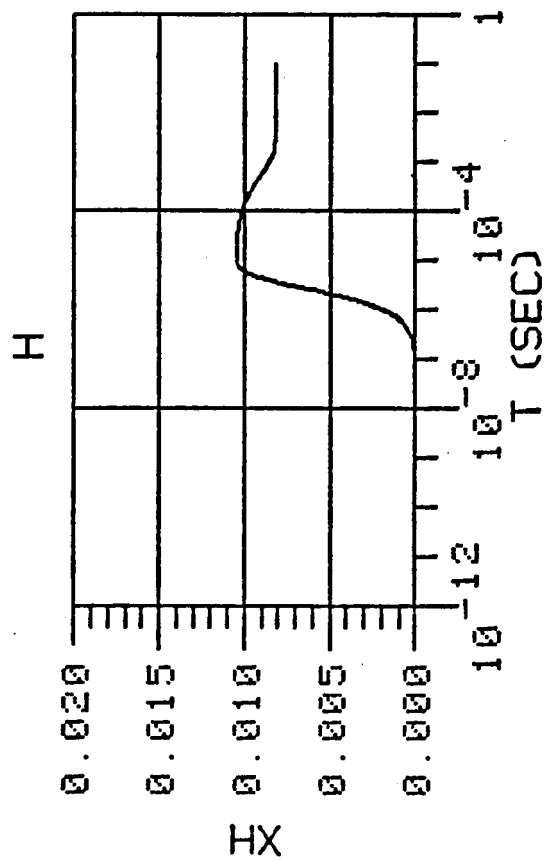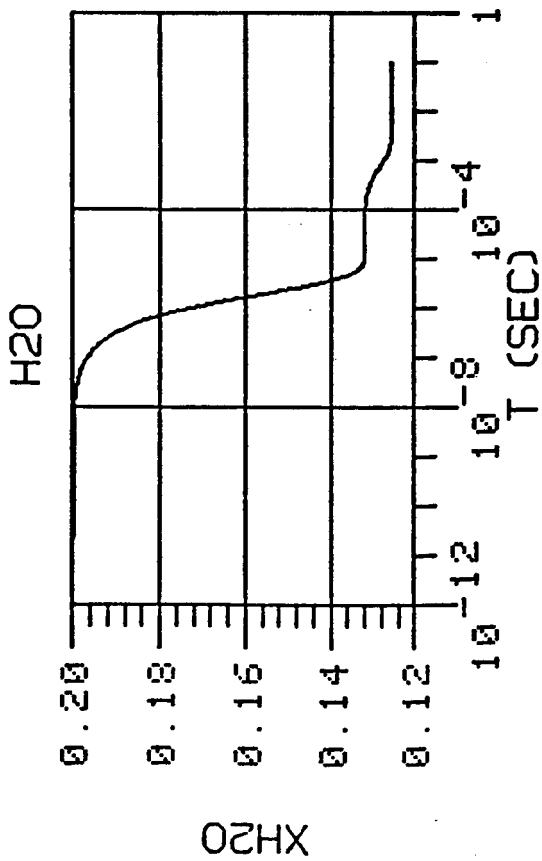
FIGURE 18 Species concentrations resulting from a non-equilibrium calculation for a mixture of 20% H_2O and 80% He at a temperature of 3000 K and a total pressure of 5 atm.

-43-

FIGURE 19 Species concentrations resulting from a non-equilibrium calculation for a mixture of 20% H_2O and 80% He at a temperature of 3000 K and a total pressure of 5 atm.

FIGURE 20 Species concentrations resulting from a non-equilibrium calculation for a mixture of 20% H_2O and 80% He at a temperature of 3000 K and a total pressure of 10 *atm.*
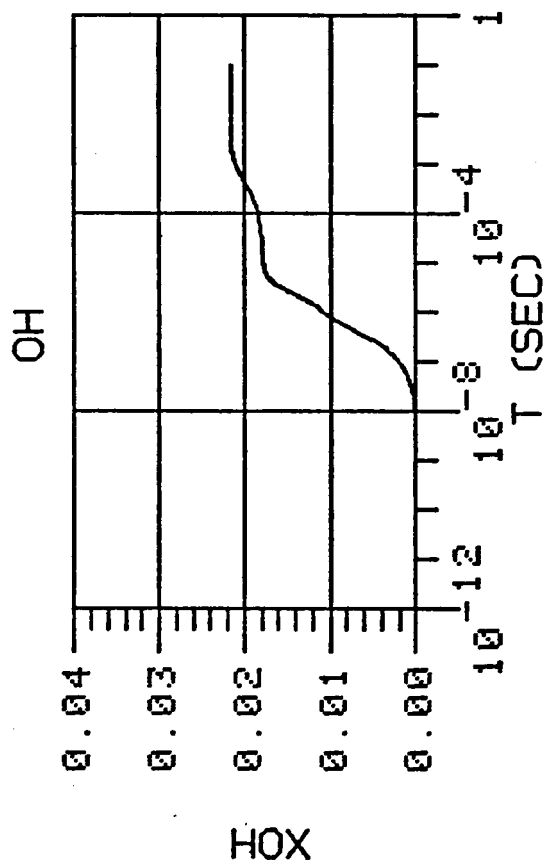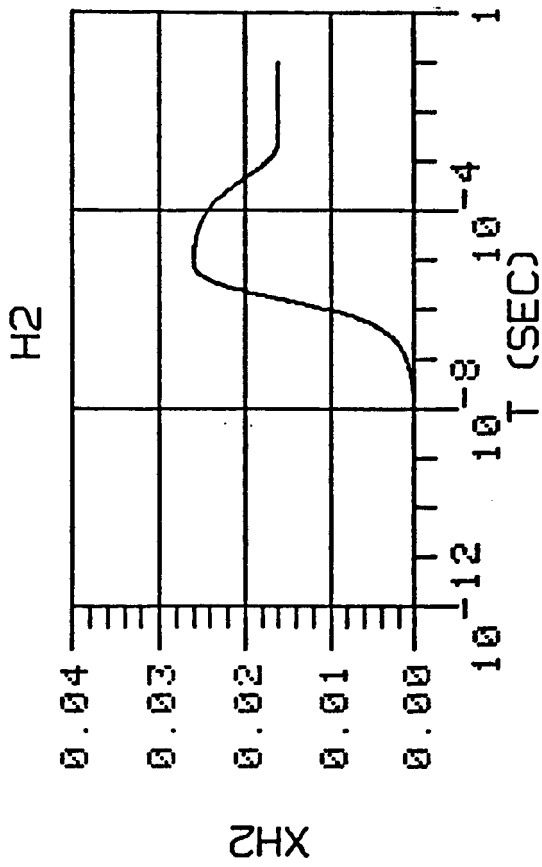
FIGURE 21 Species concentrations resulting from a non-equilibrium calculation for a mixture of 20% H_2O and 80% He at a temperature of 3000 K and a total pressure of 10 atm.

FIGURE 22 Species concentrations resulting from a non-equilibrium calculation for a mixture of 20% H_2O and 80% He at a temperature of 4000 K and a total pressure of 1 atm.
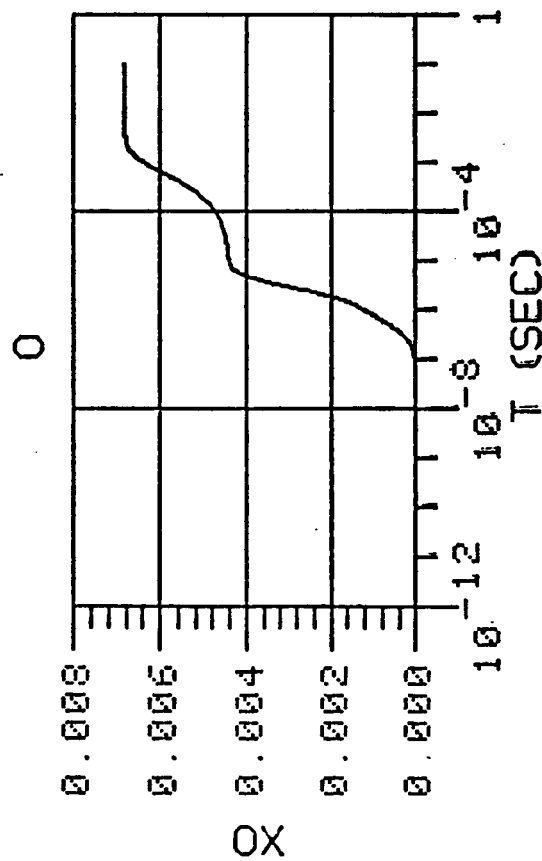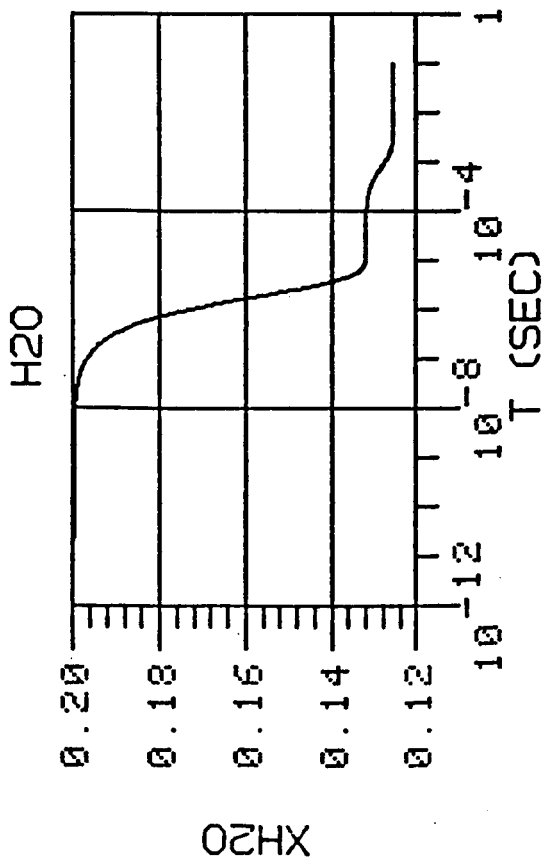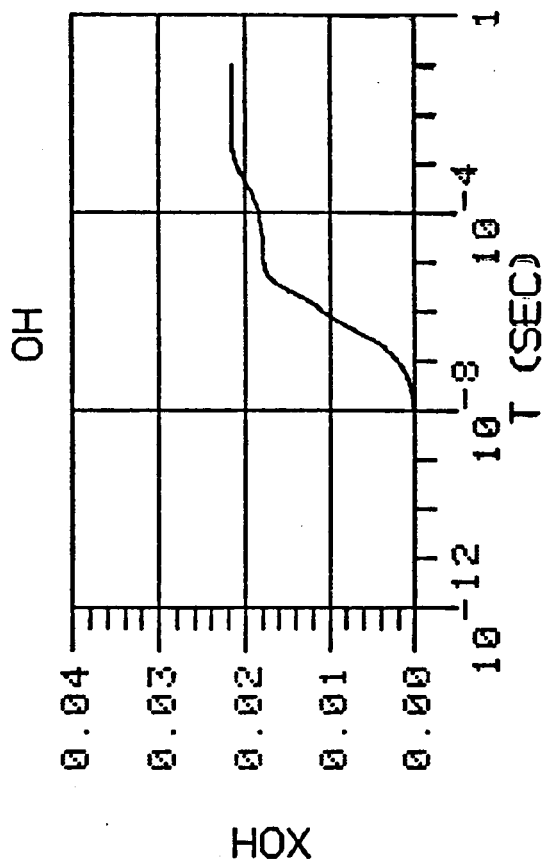
FIGURE 23 Species concentrations resulting from a non-equilibrium calculation for a mixture of 20% H_2O and 80% He at a temperature of 4000 K and a total pressure of 1 atm.

-48-
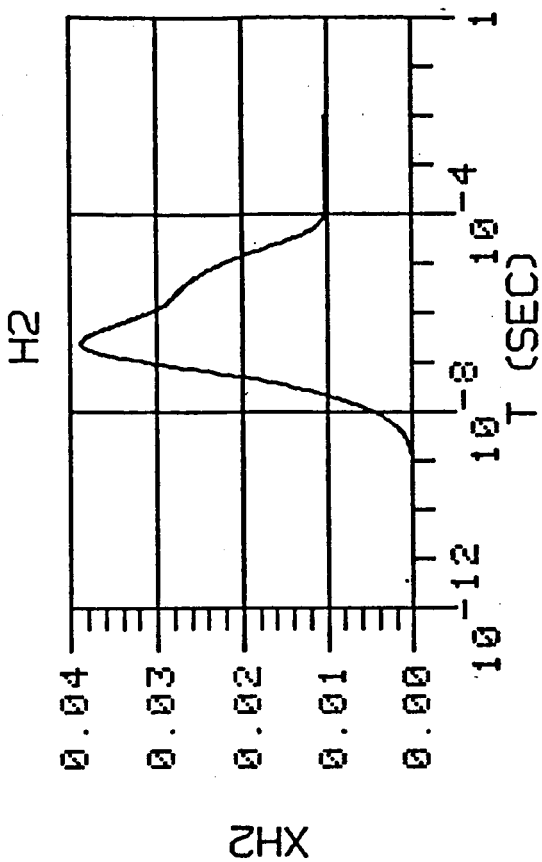
FIGURE 24 Species concentrations resulting from a non-equilibrium calculation for a mixture of 20% H_2O and 80% He at a temperature of 4000 K and a total pressure of 5 atm.
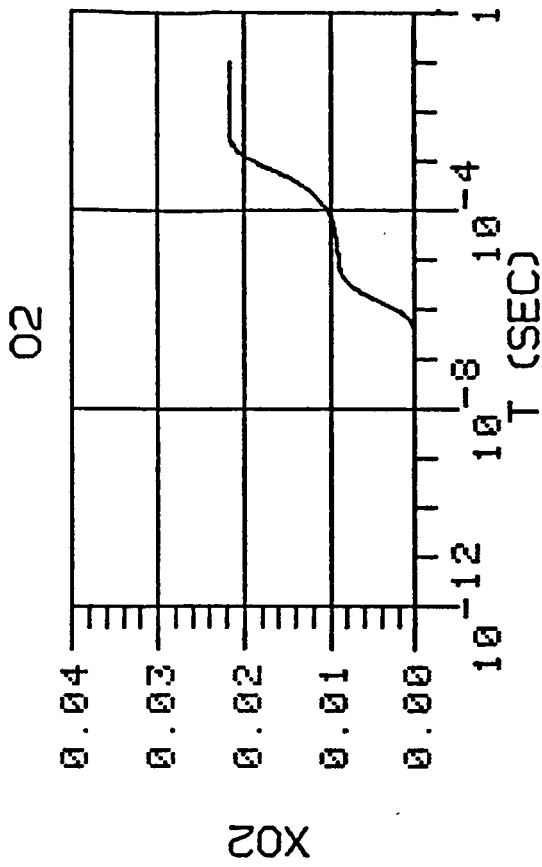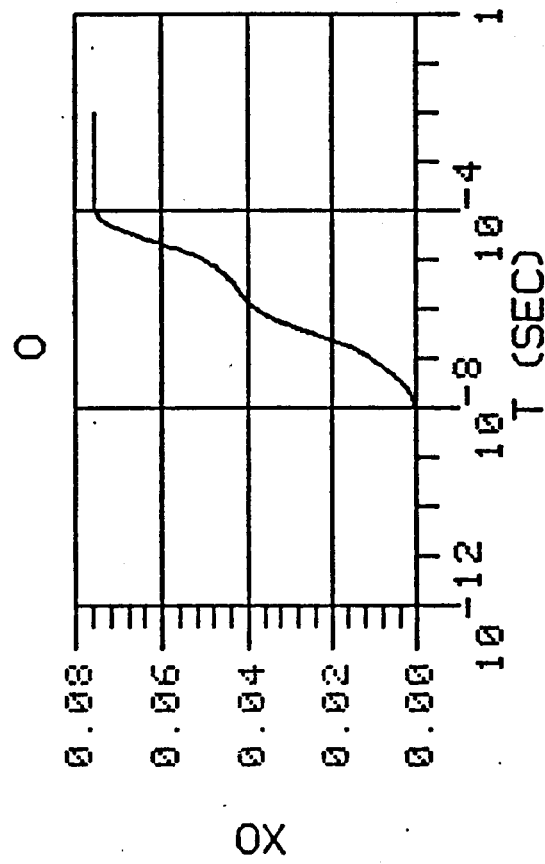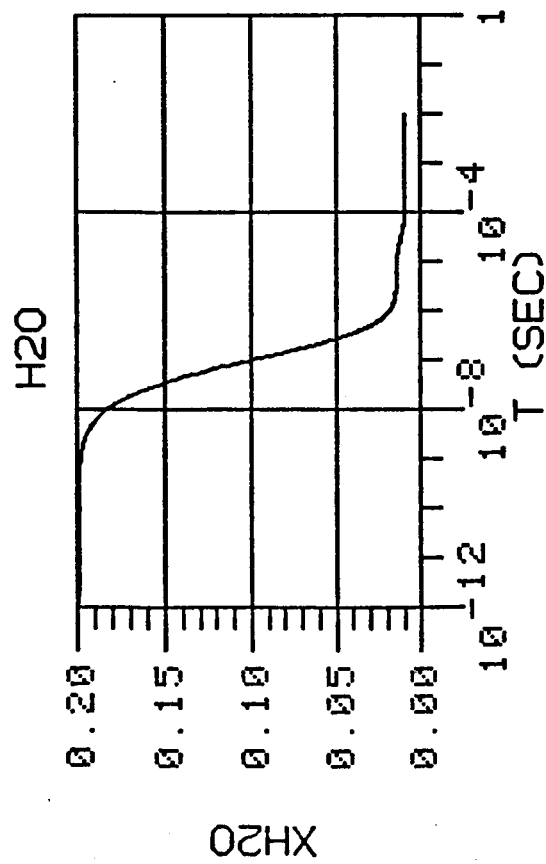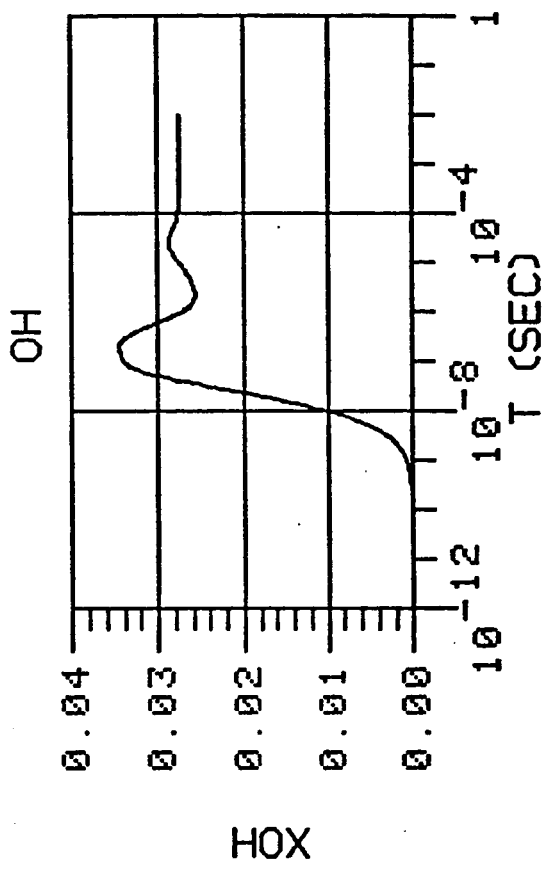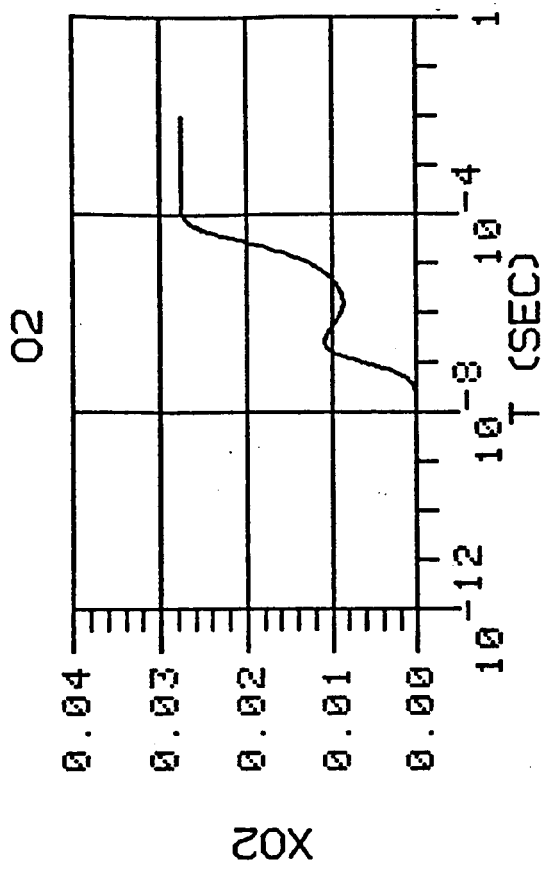
FIGURE 25 Species concentrations resulting from a non-equilibrium calculation for a mixture of 20% H_2O and 80% He at a temperature of 4000 K and a total pressure of 5 atm.
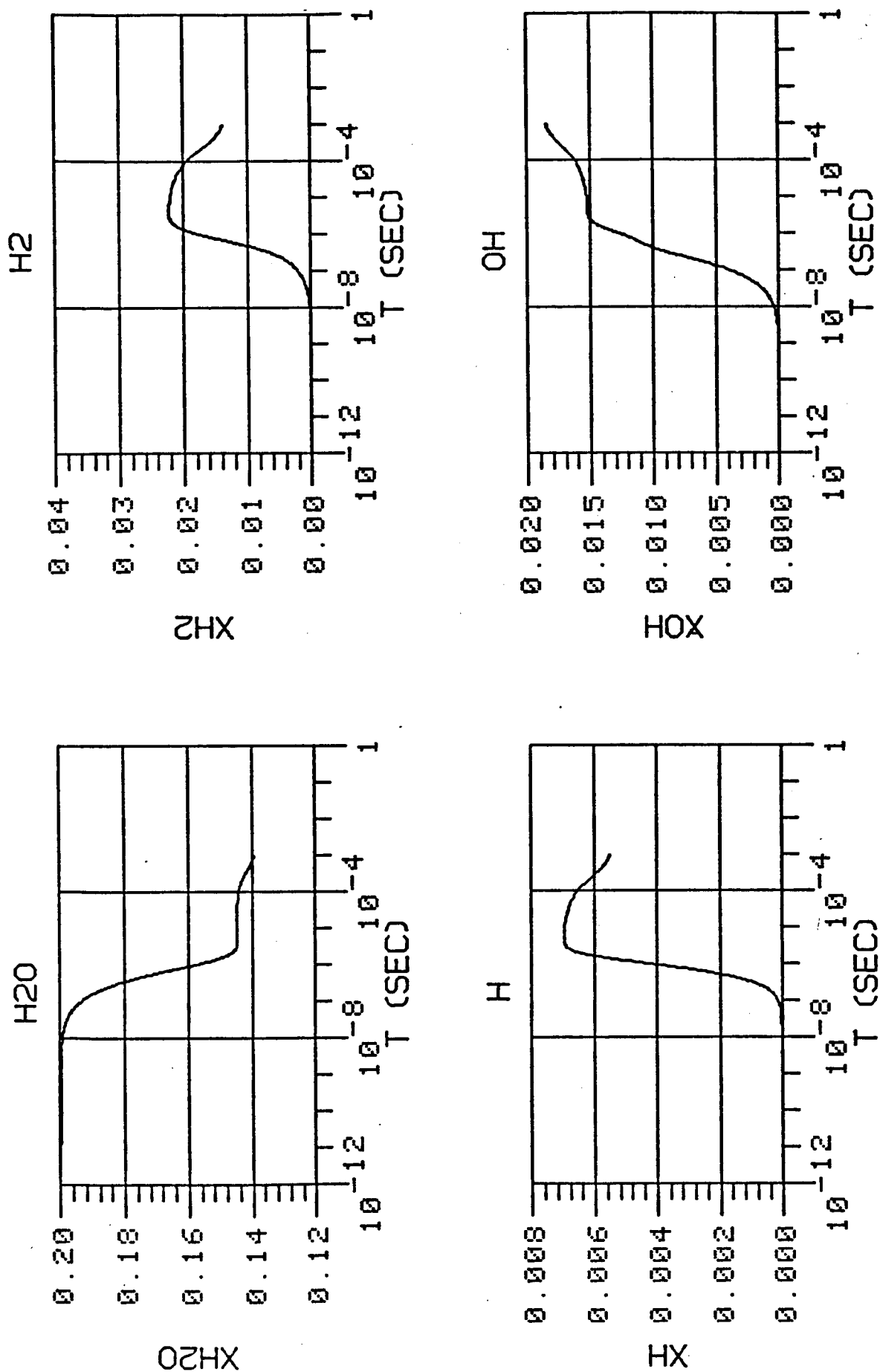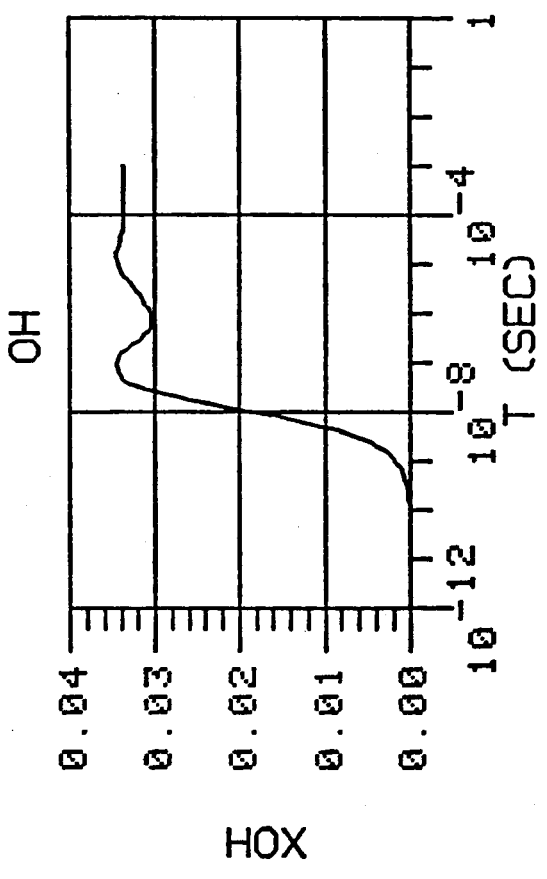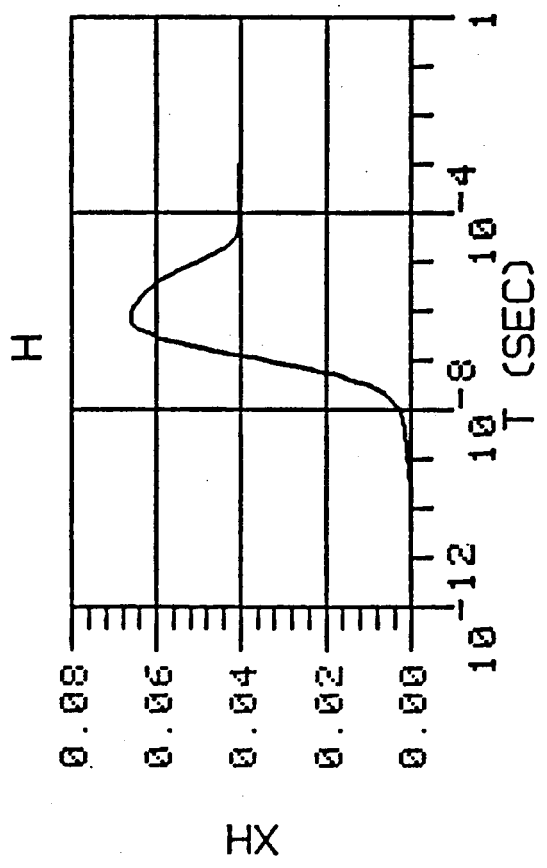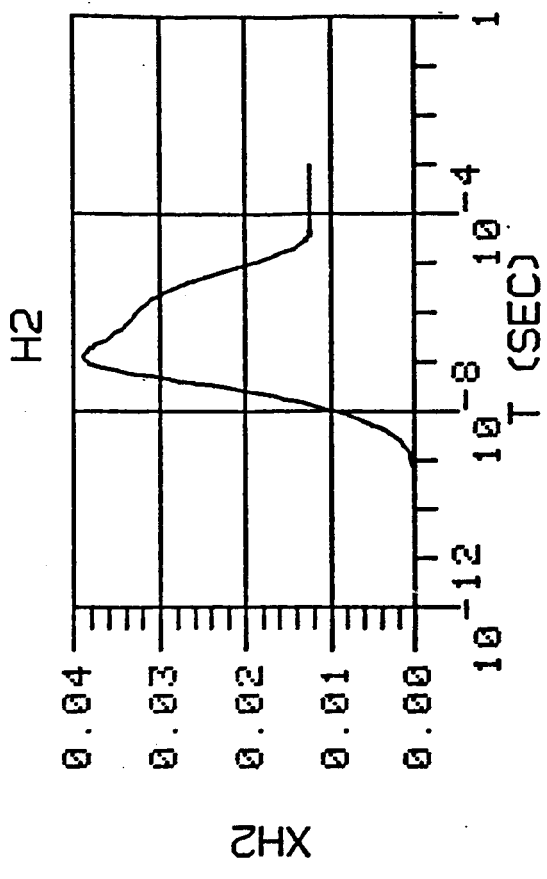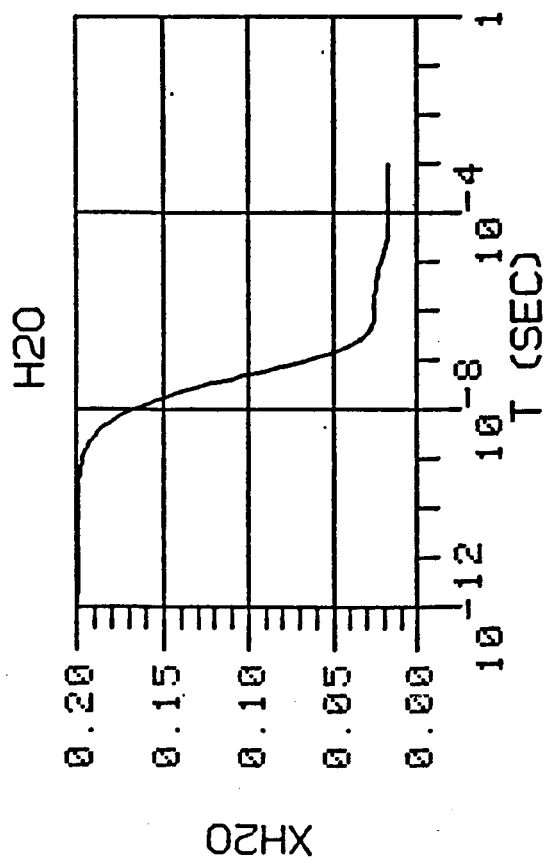
FIGURE 26 Species concentrations resulting from a non-equilibrium calculation for a mixture of 20% H_2O and 80% He at a temperature of 4000 K and a total pressure of 10 atm.
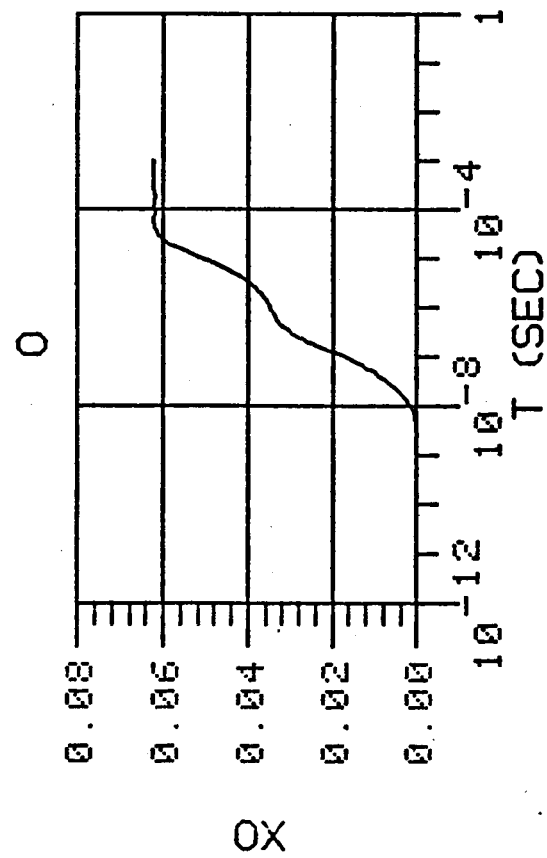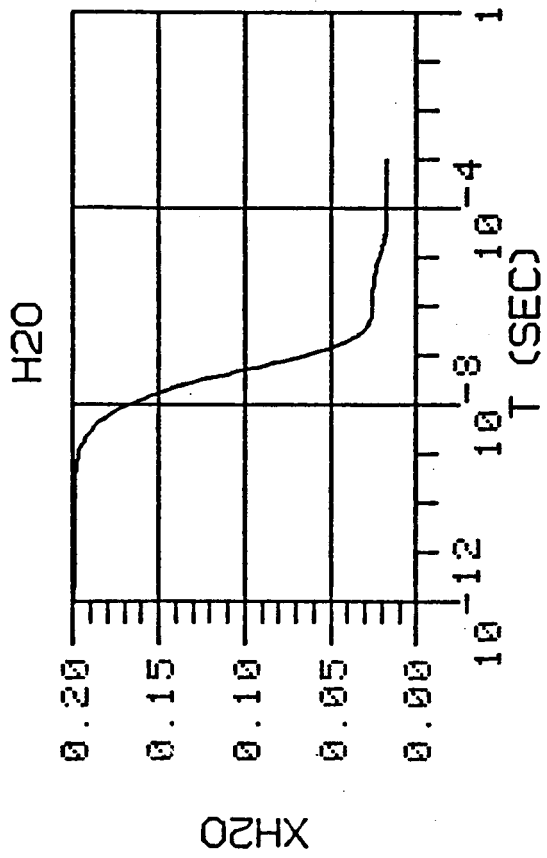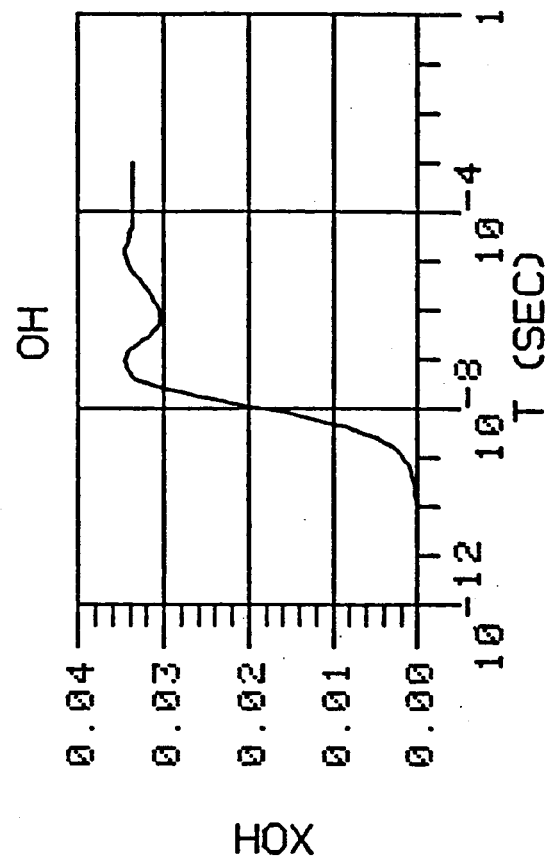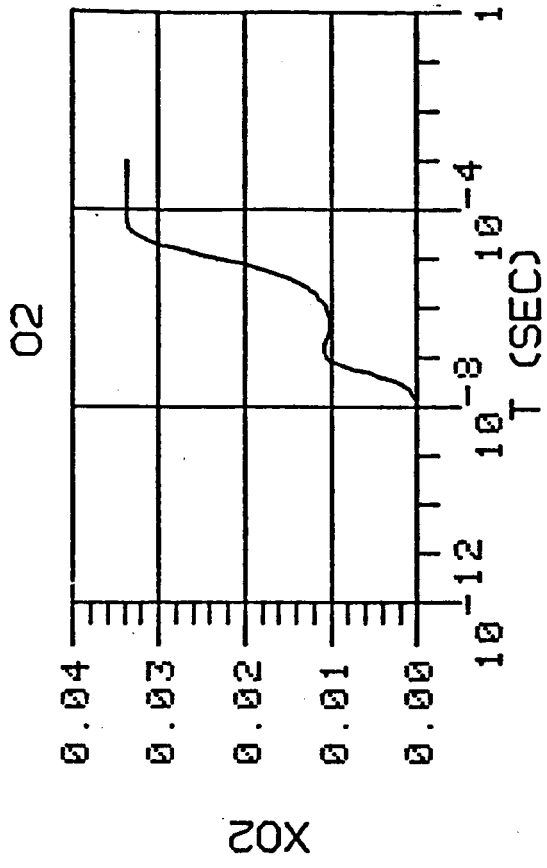
FIGURE 27 Species concentrations resulting from a non-equilibrium calculation for a mixture of 20% H_2O and 80% He at a temperature of 4000 K and a total pressure of 10 atm.
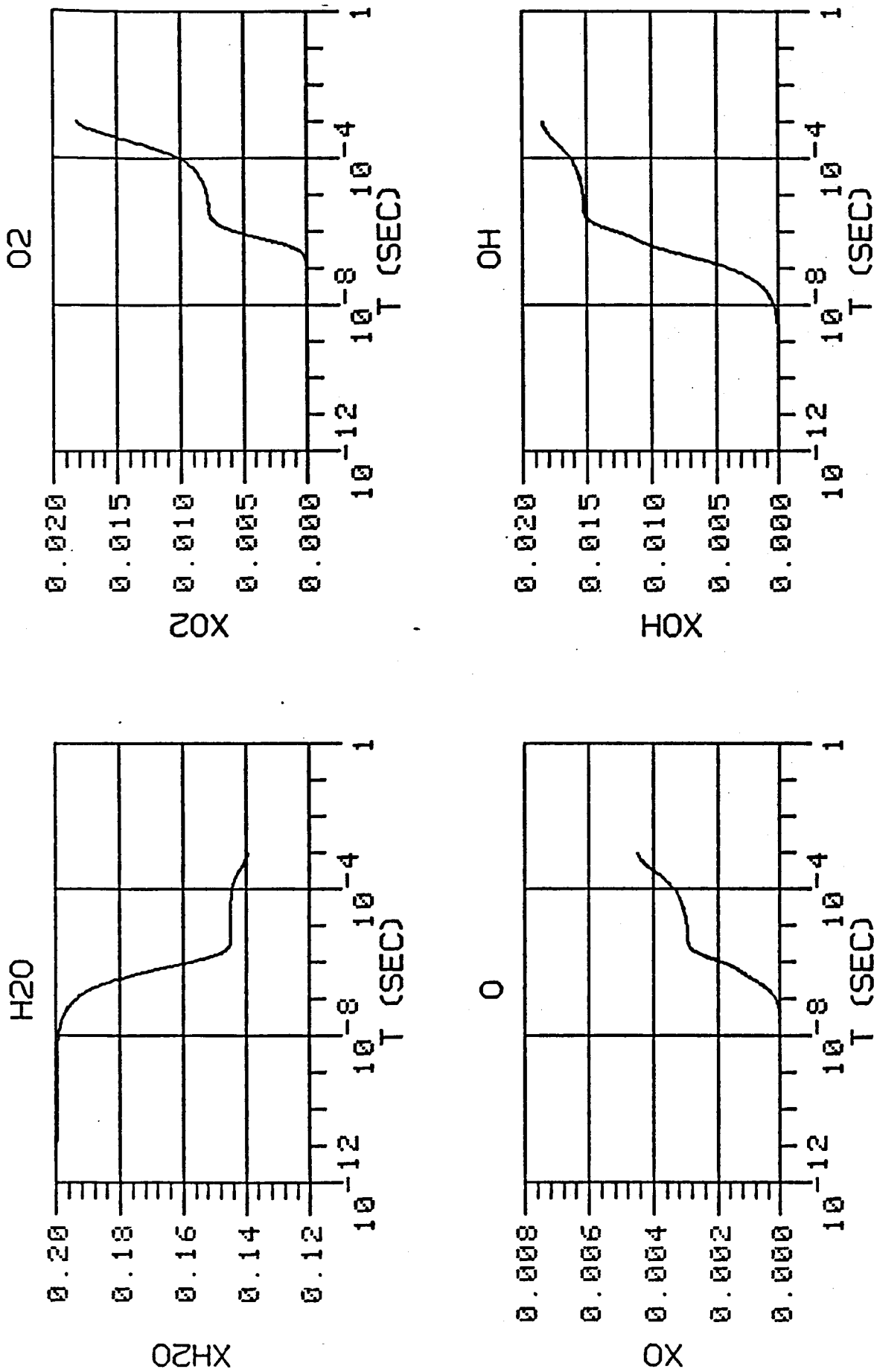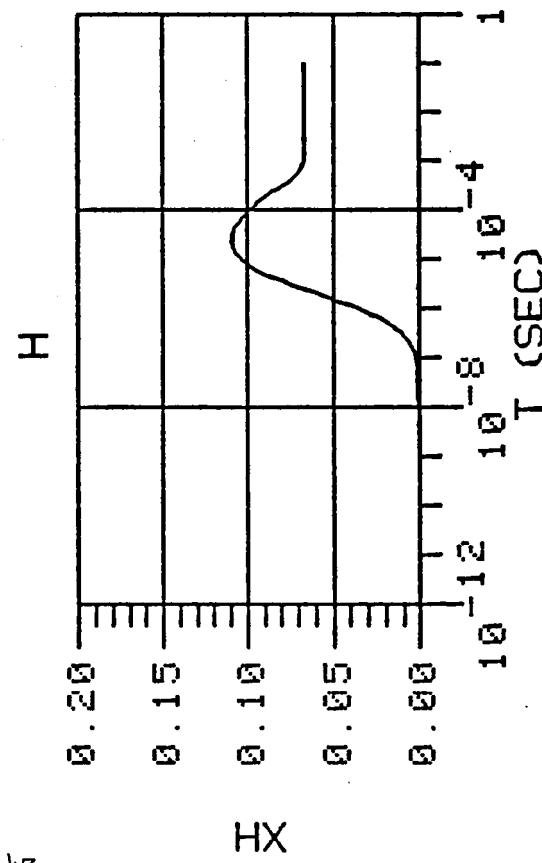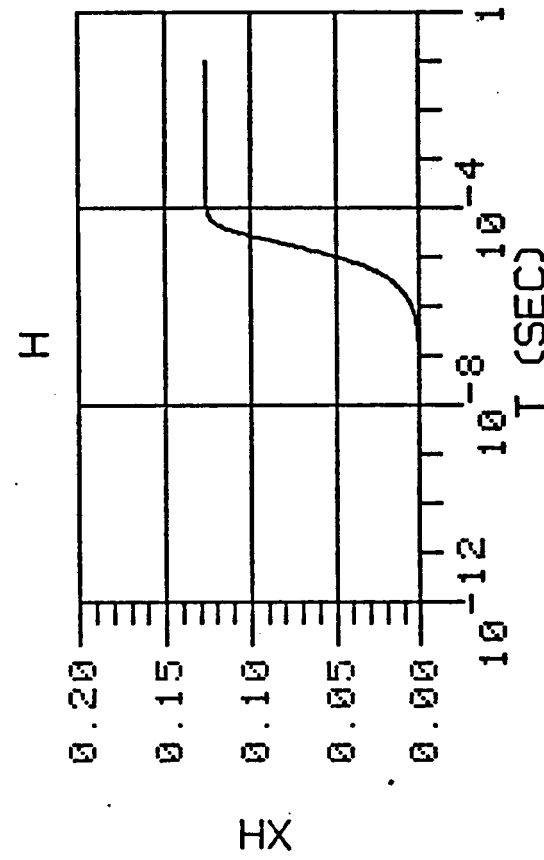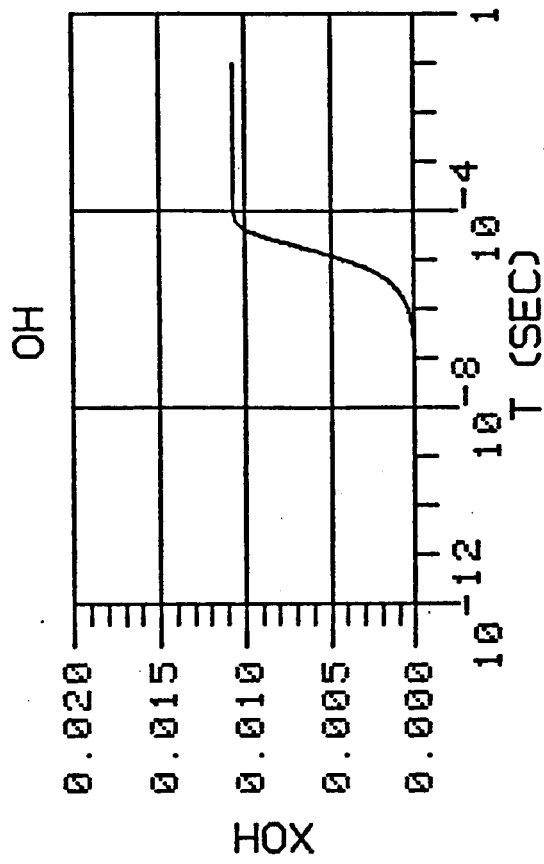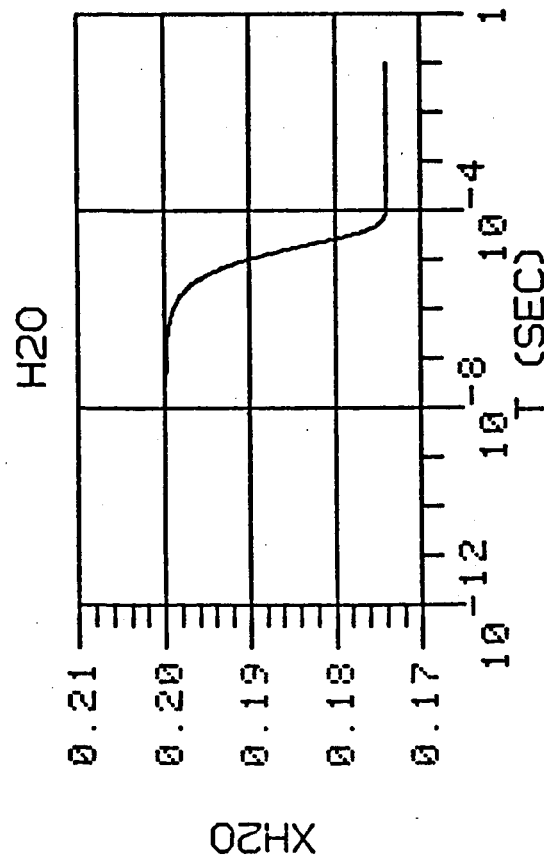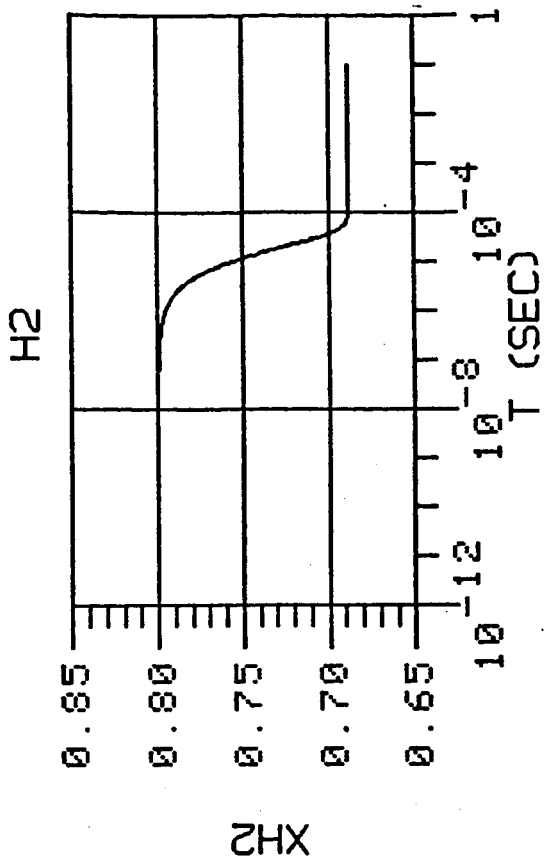
FIGURE 28 Species concentrations resulting from a non-equilibrium calculation for a mixture of 20% H_2O and 80% H_2 at a temperature of 3000 K and a total pressure of 1 atm.
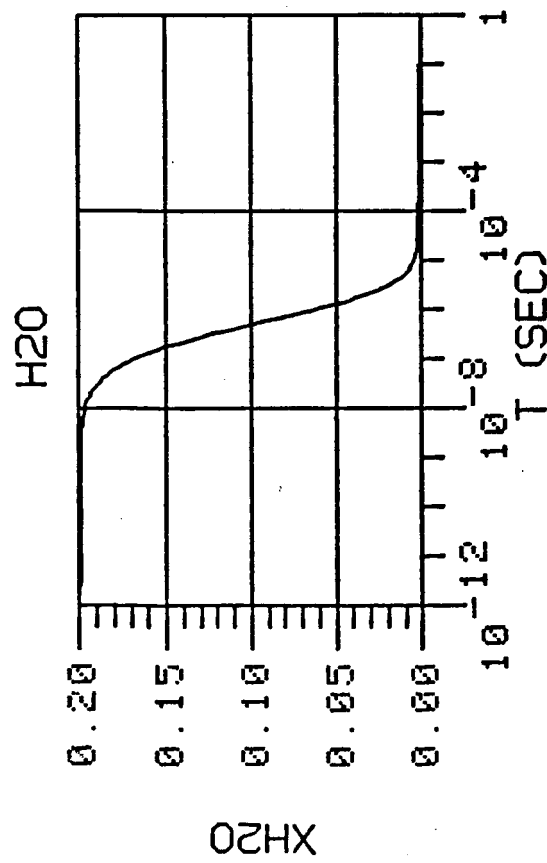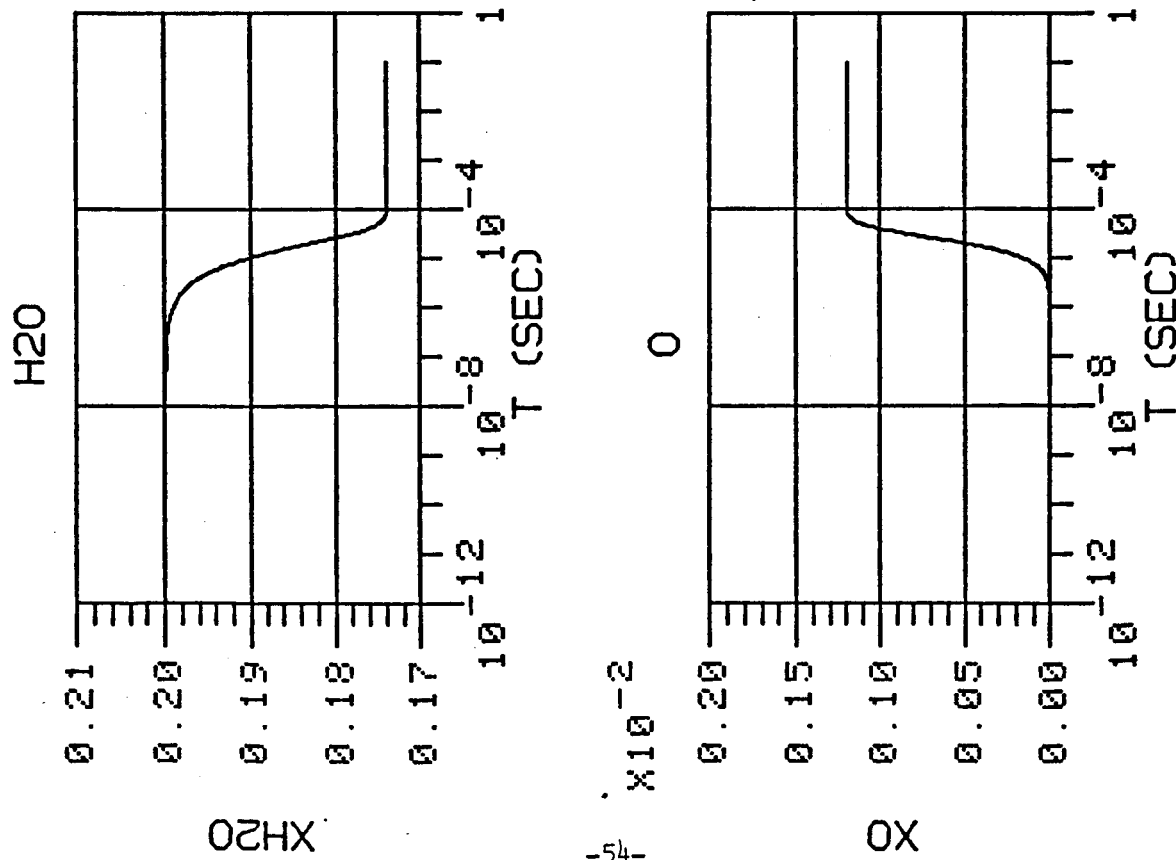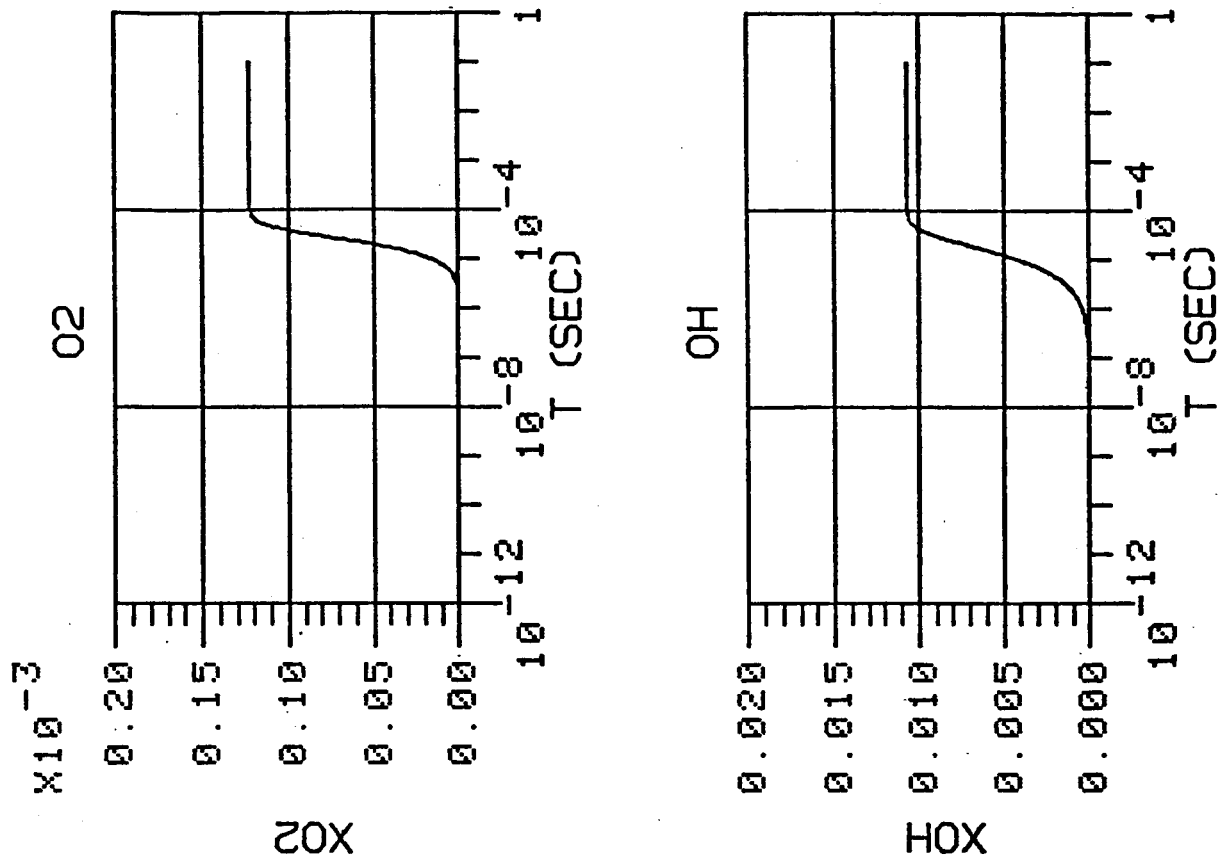
FIGURE 29 Species concentrations resulting from a non-equilibrium calculation for a mixture of 20% H_2O and 80% H_2 at a temperature of 3000 K and a total pressure of 1 atm.
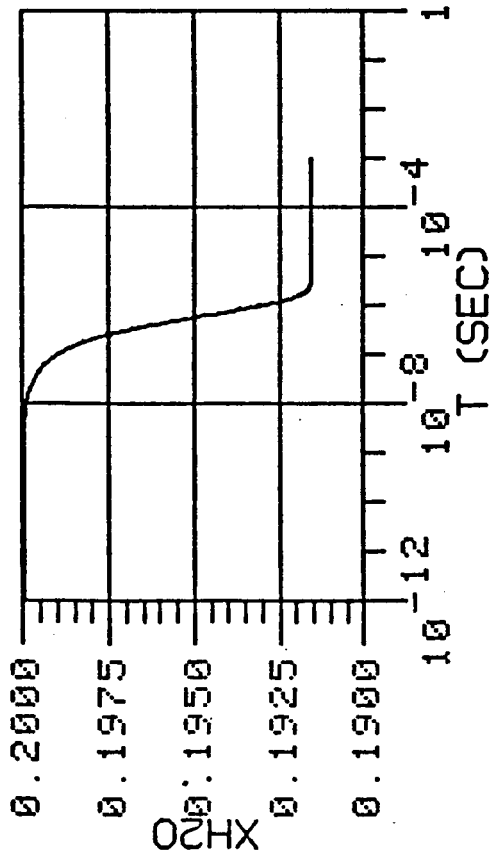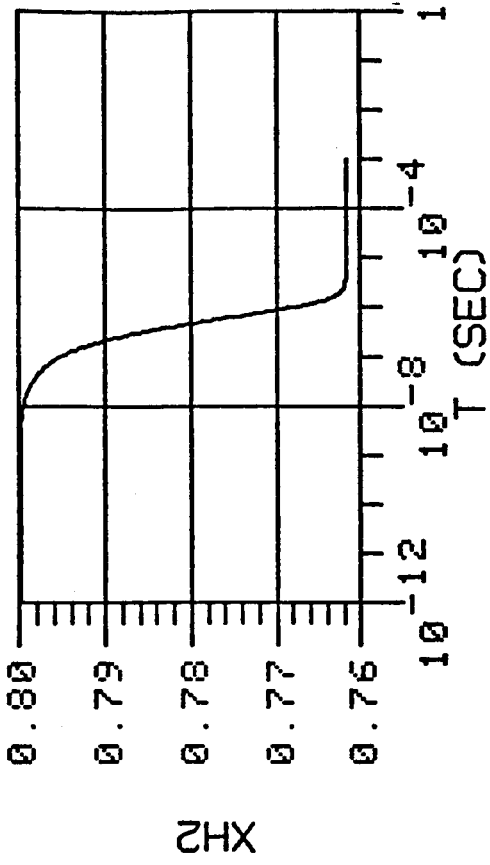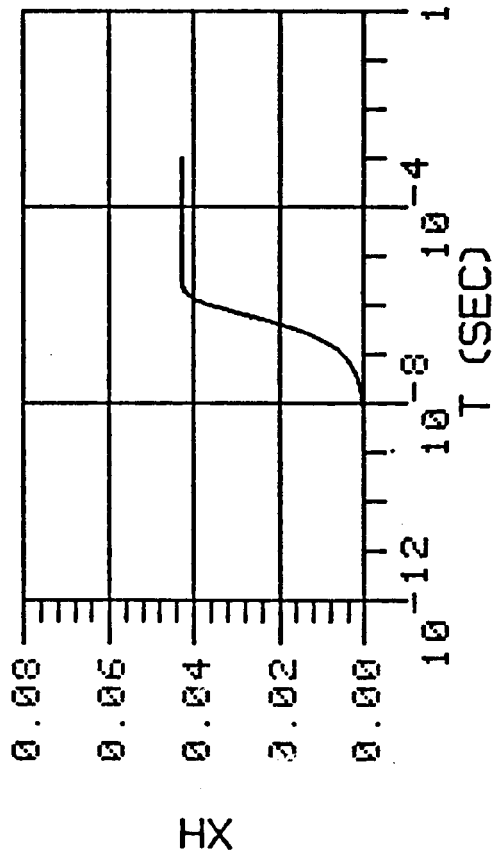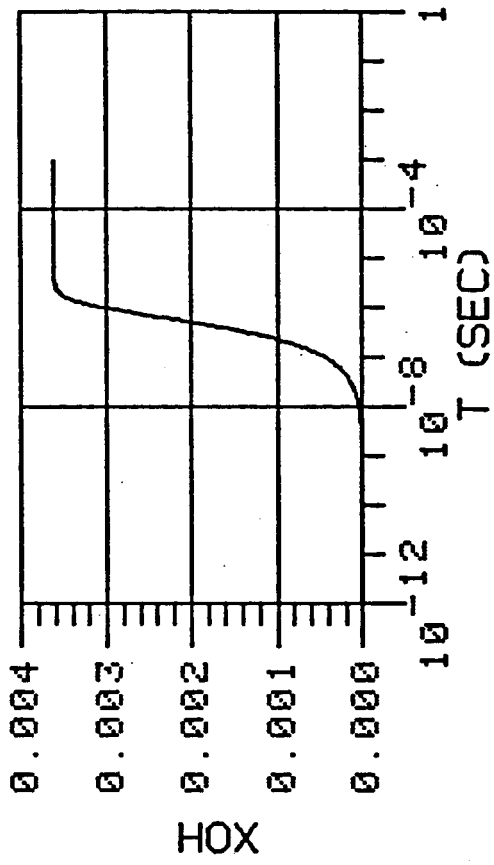
FIGURE 30 Species concentrations resulting from a non-equilibrium calculation for a mixture of 20% H_2O and 80% H_2 at a temperature of 3000 K and a total pressure of 10 atm.
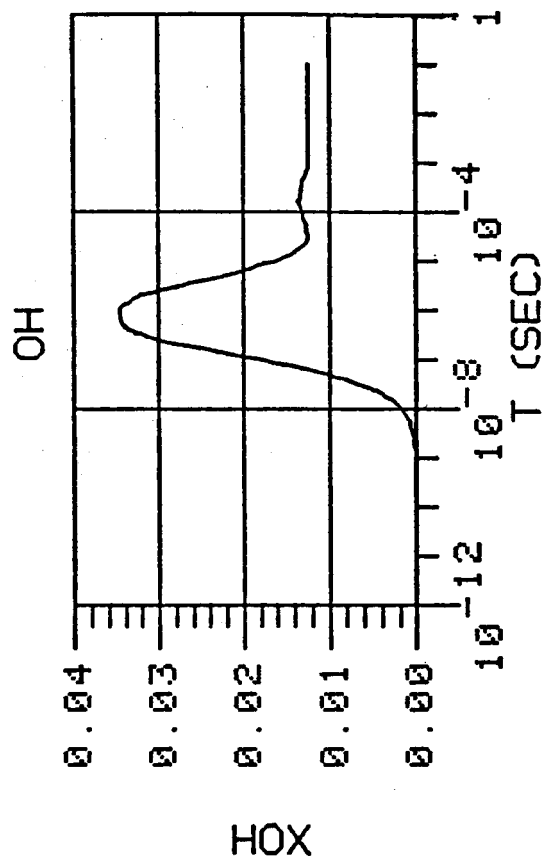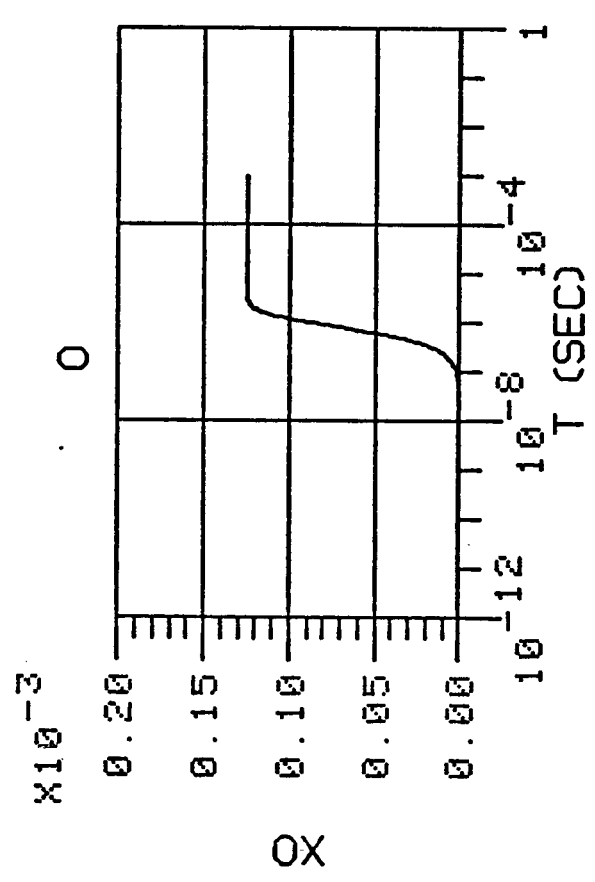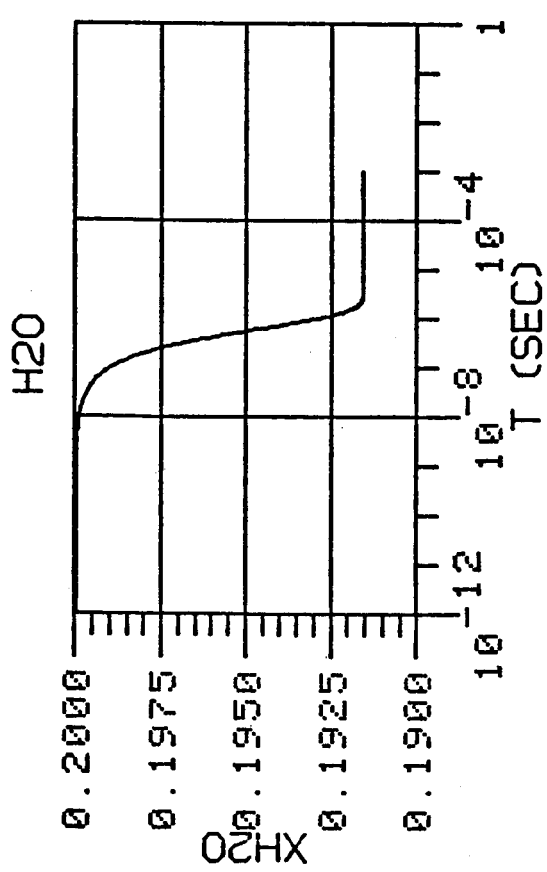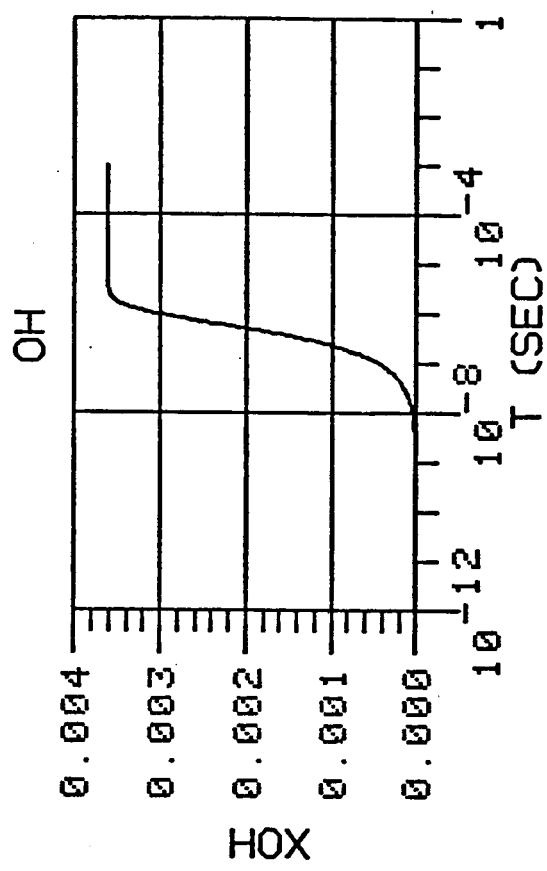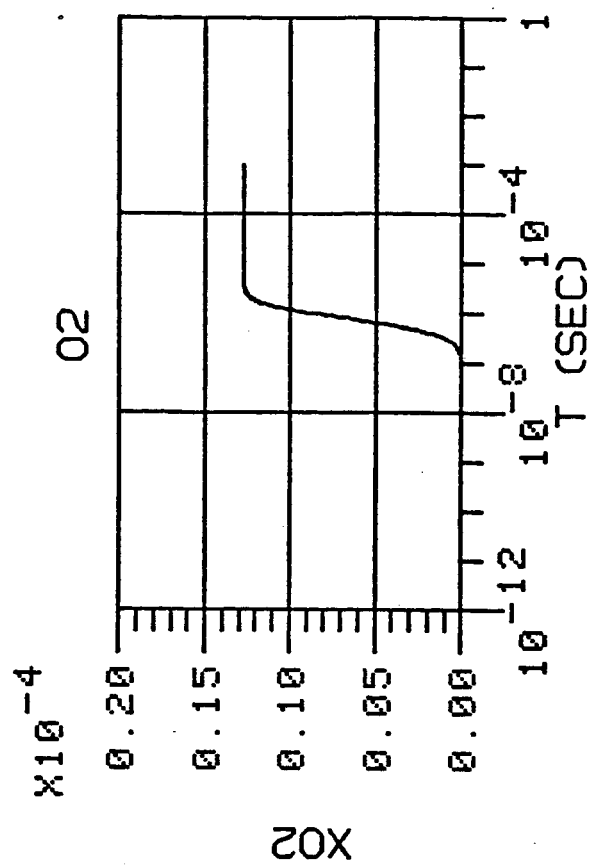
FIGURE 31 Species concentrations resulting from a non-equilibrium calculation for a mixture of 20% H_2O and 80% H_2 at a temperature of 3000 K and a total pressure of 10 *atm*.
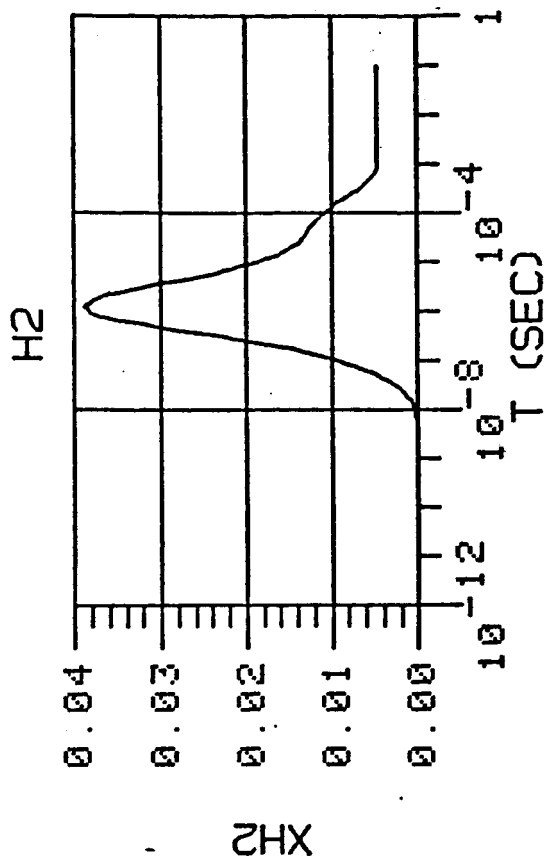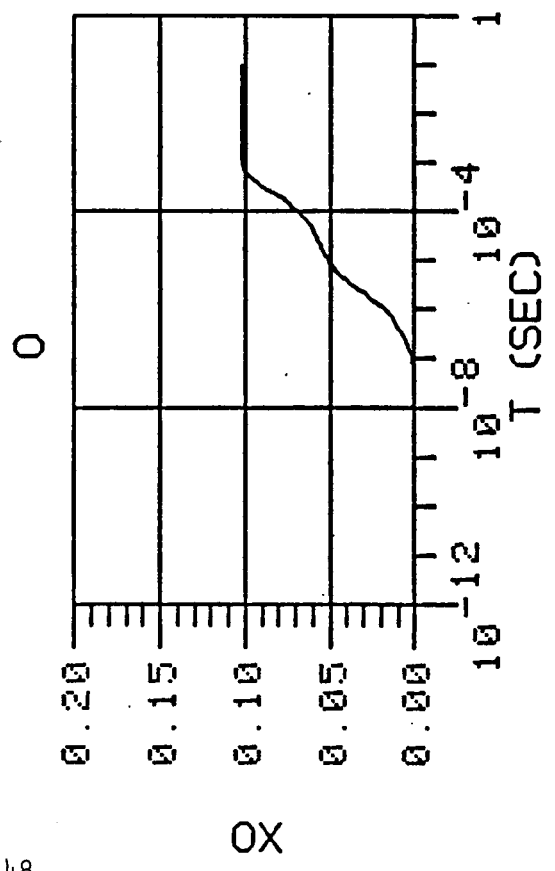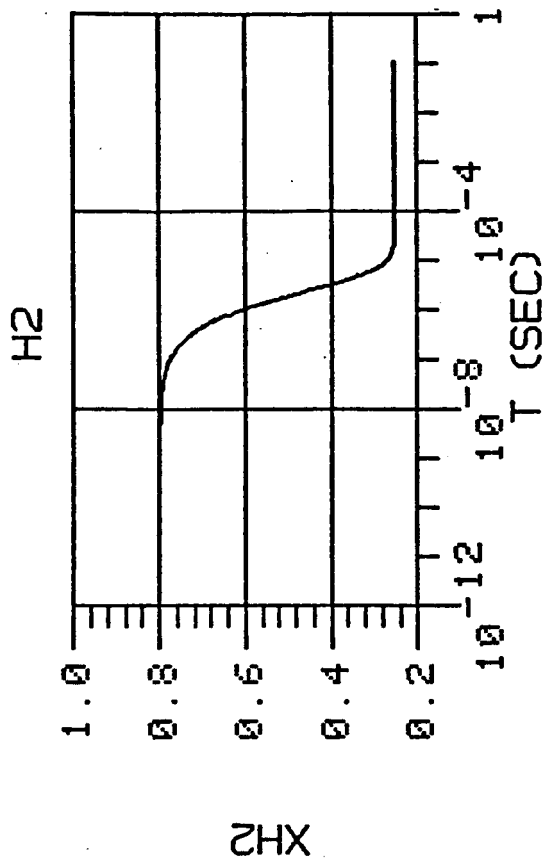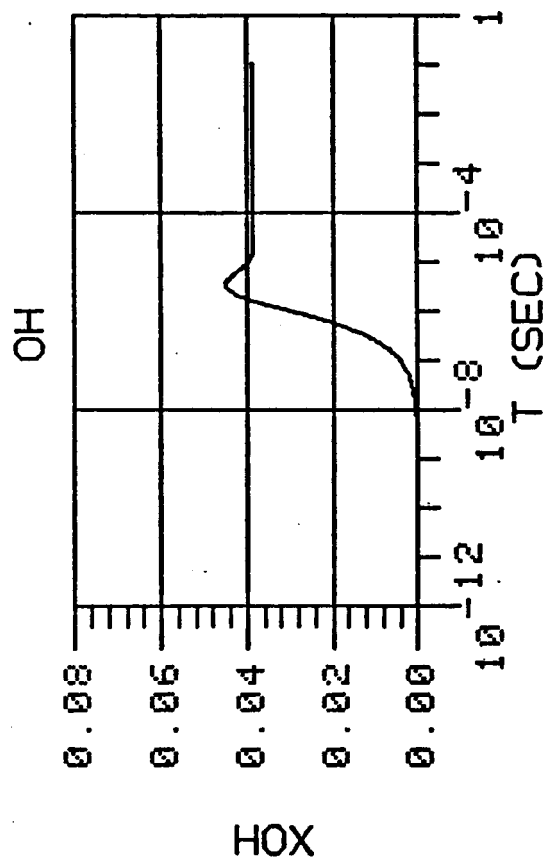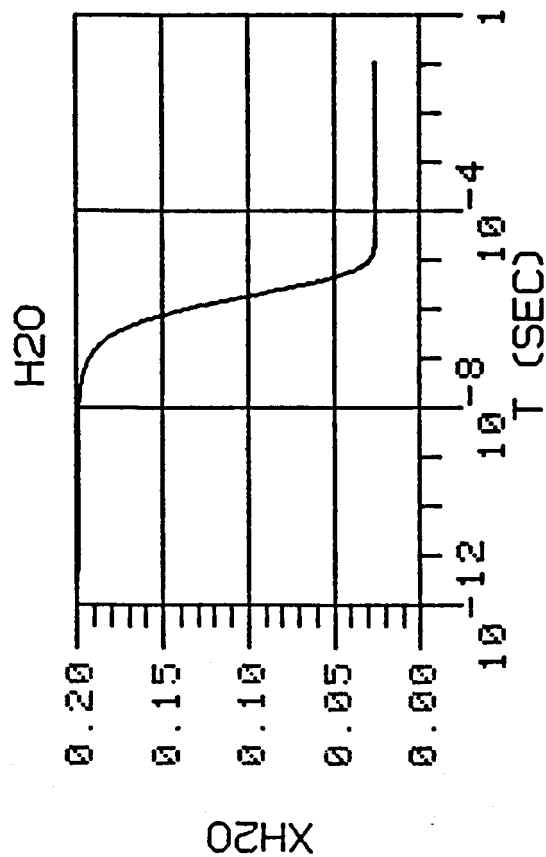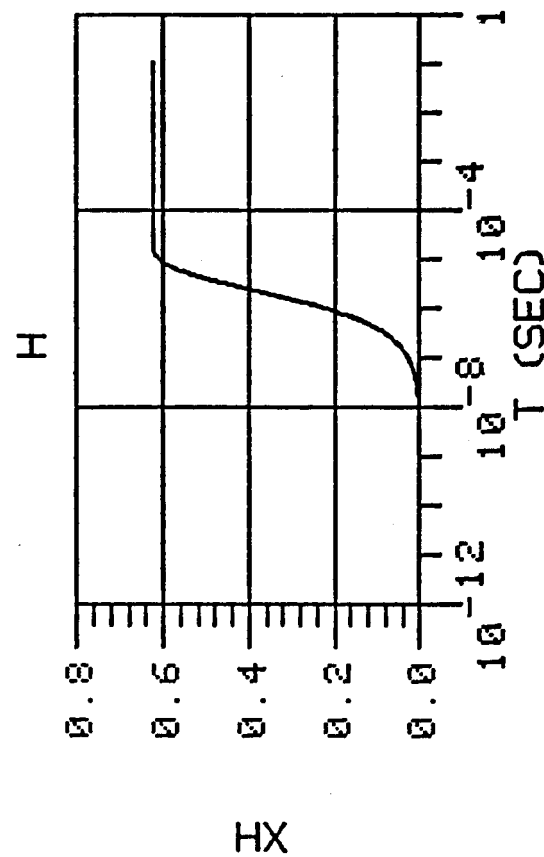
FIGURE 32 Species concentrations resulting from a non-equilibrium calculation for a mixture of 20% H_2O and 80% H_2 at a temperature of 4000 K and a total pressure of 1 atm.
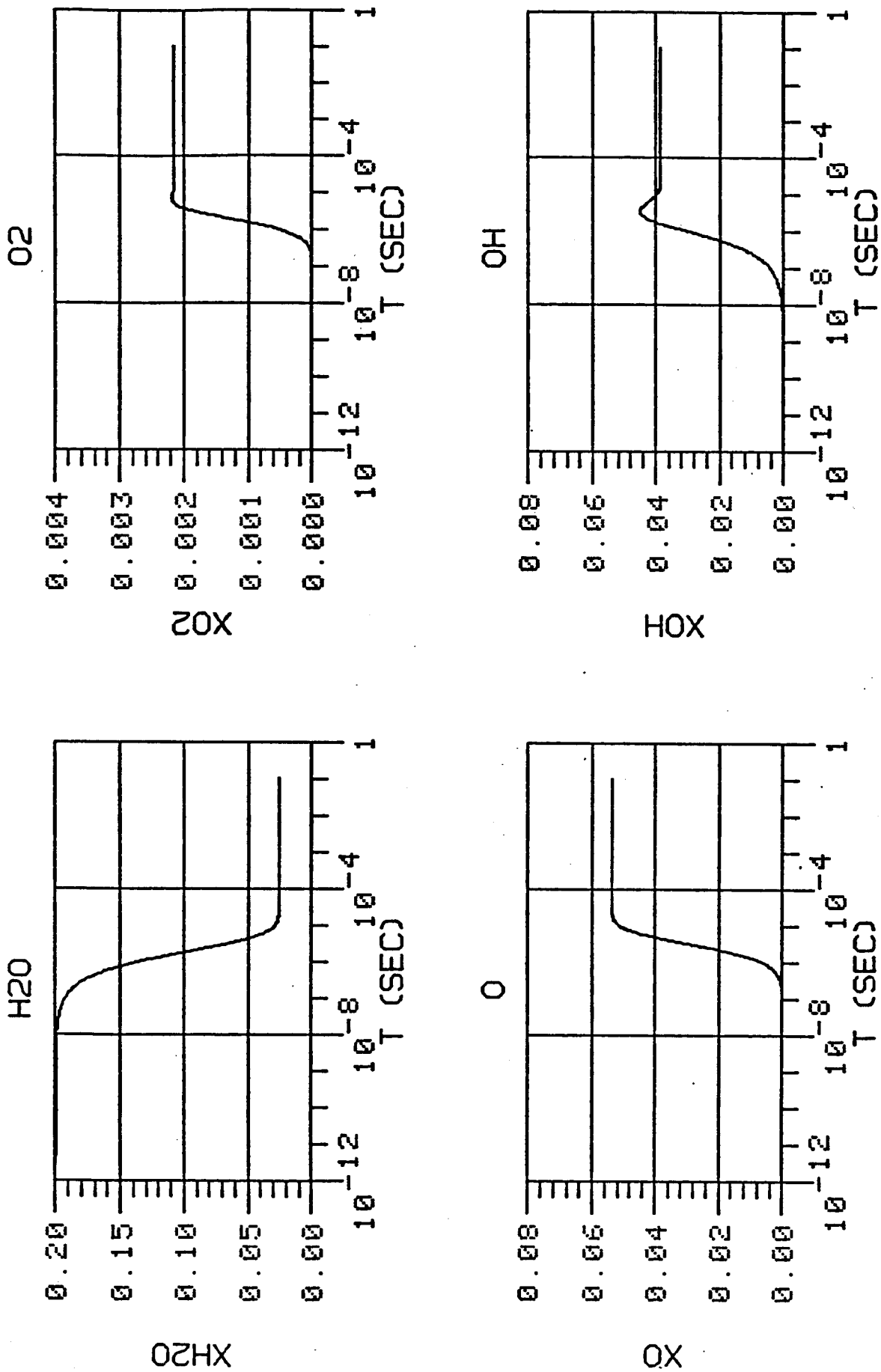
FIGURE 33 Species concentrations resulting from a non-equilibrium calculation for a mixture of 20% H_2O and 80% H_2 at a temperature of 4000 K and a total pressure of 1 *atm*.
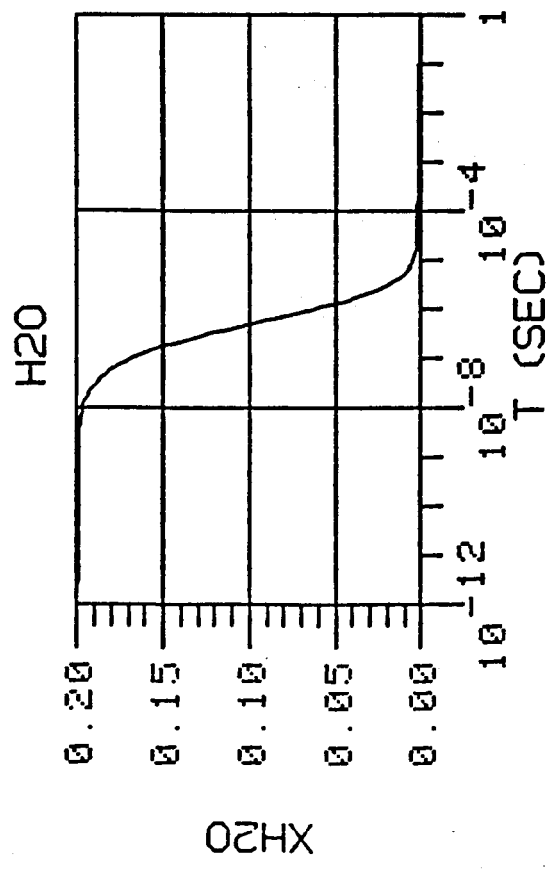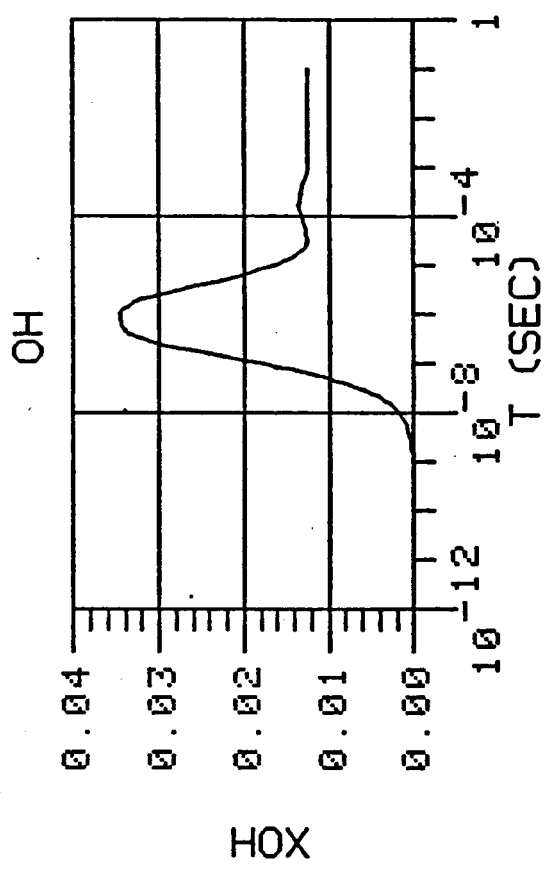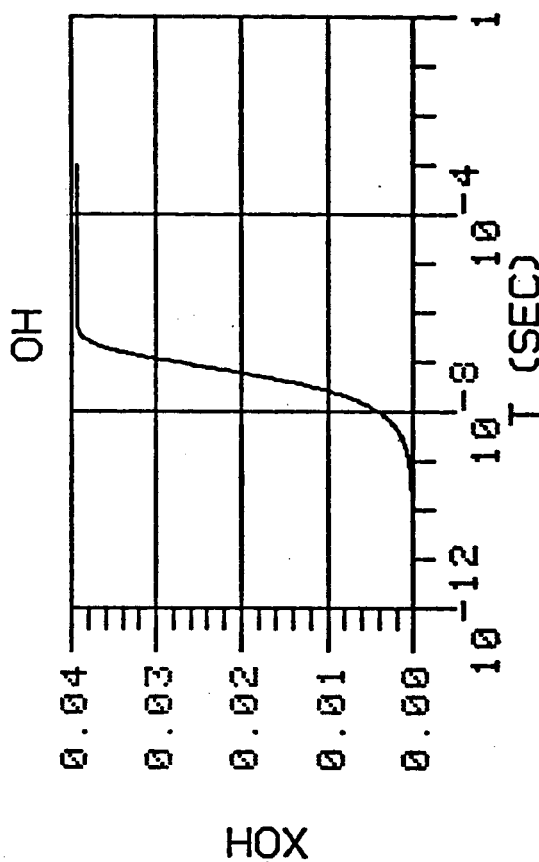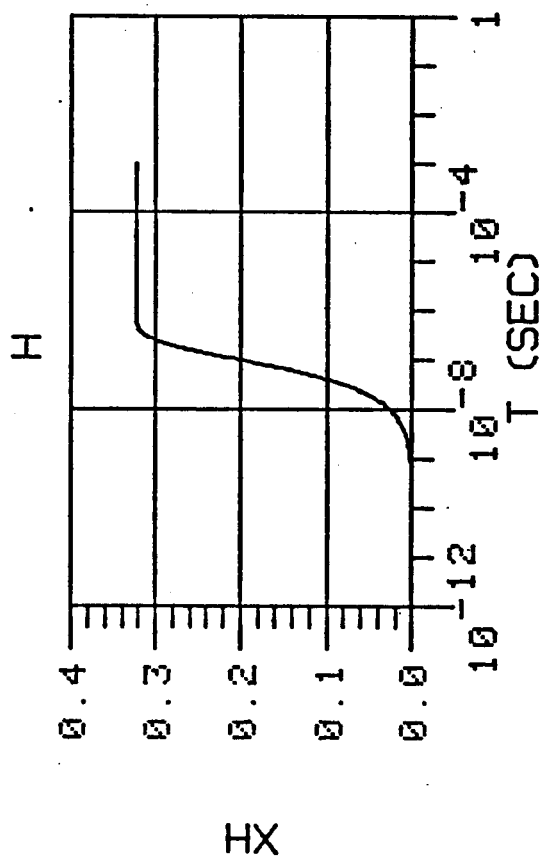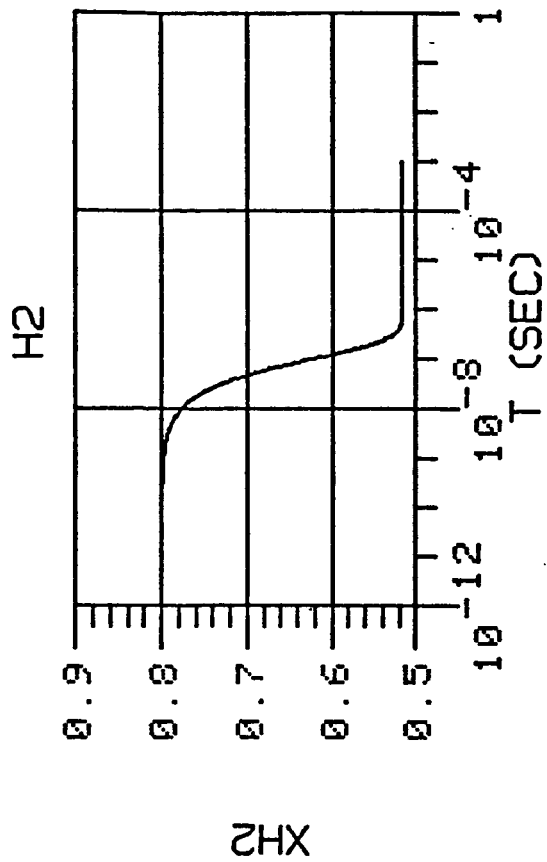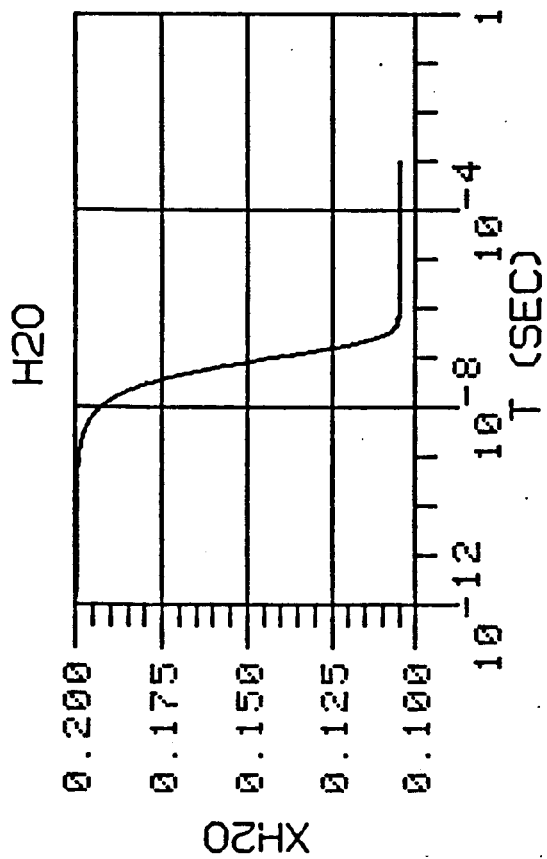
FIGURE 34 Species concentrations resulting from a non-equilibrium calculation for a mixture of 20% H_2O and 80% H_2, at a temperature of 4000 K and a total pressure of 10 atm.
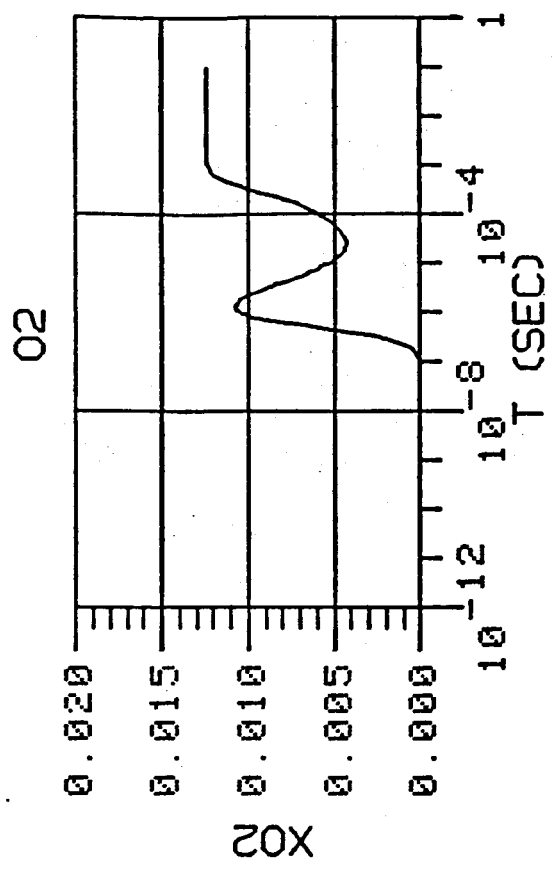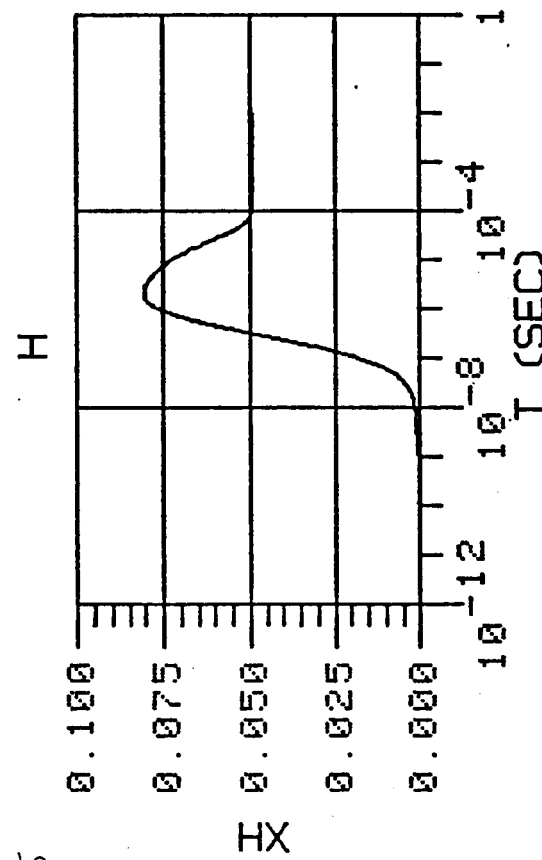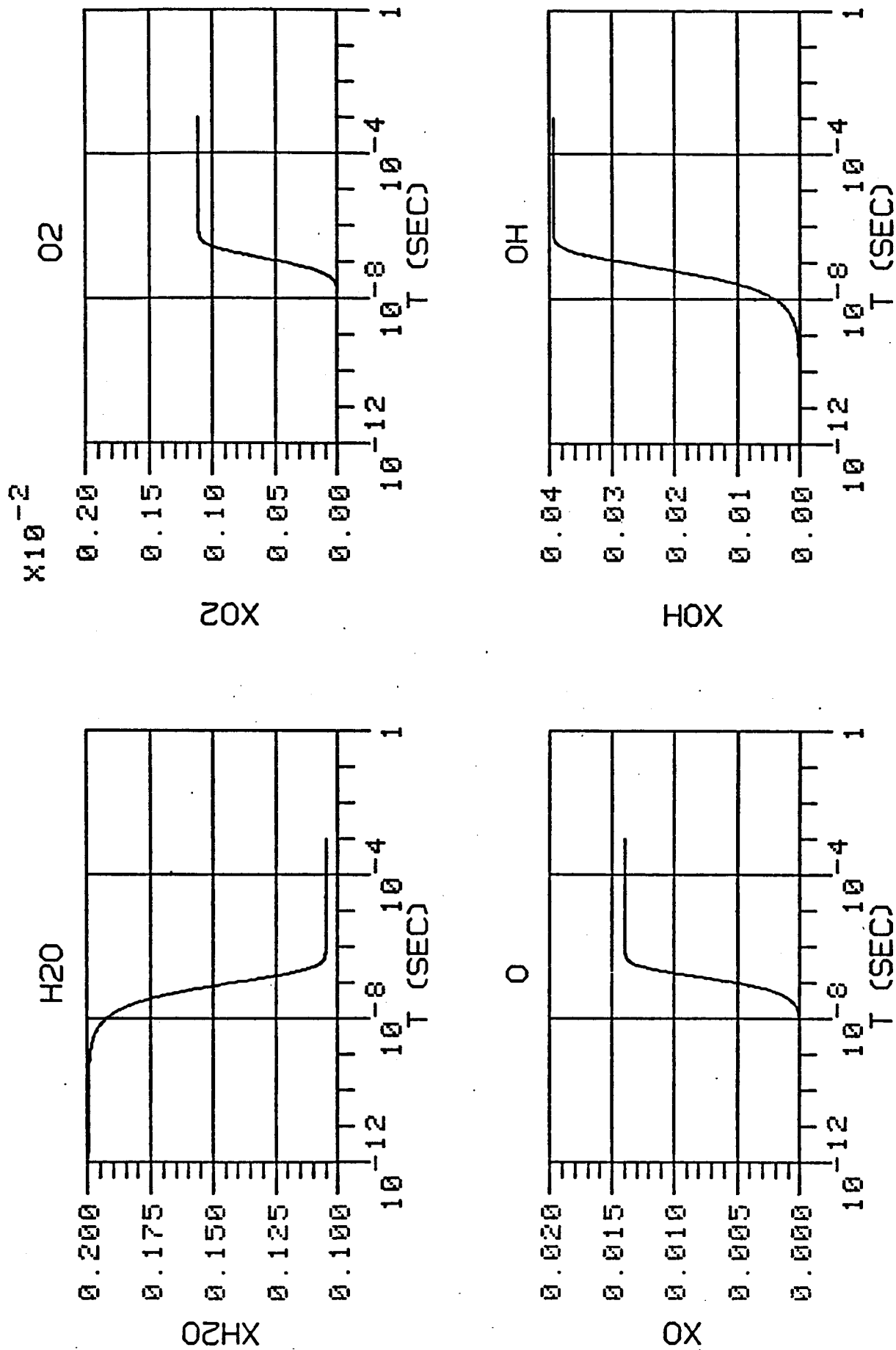
FIGURE 35 Species concentrations resulting from a non-equilibrium calculation for a mixture of 20% H_2O and 80% H_2, at a temperature of 4000 K and a total pressure of 10 atm.
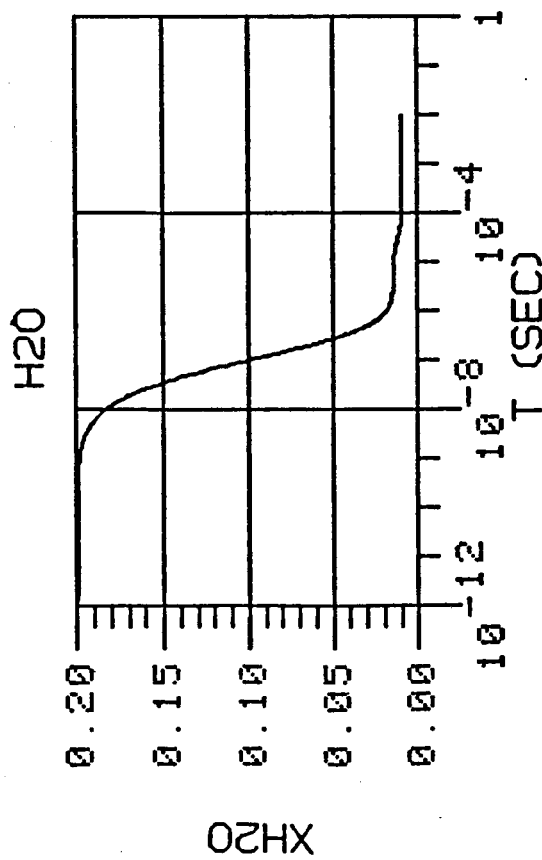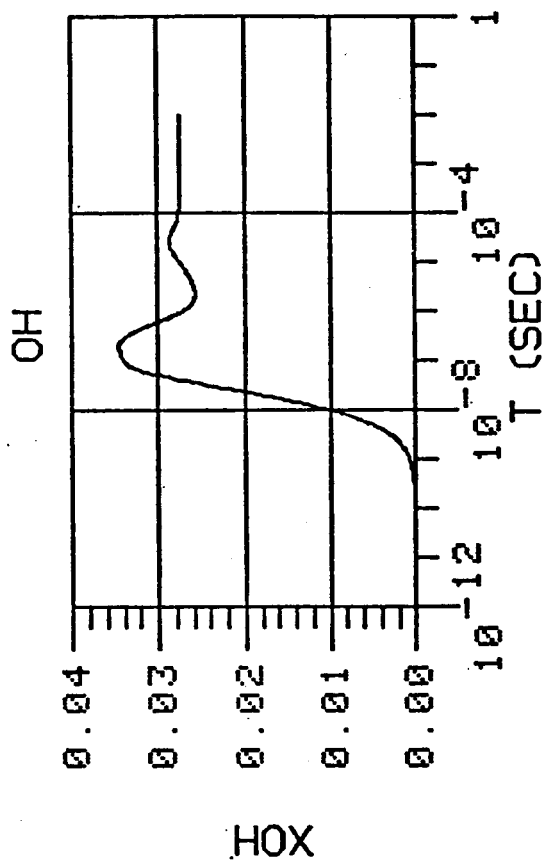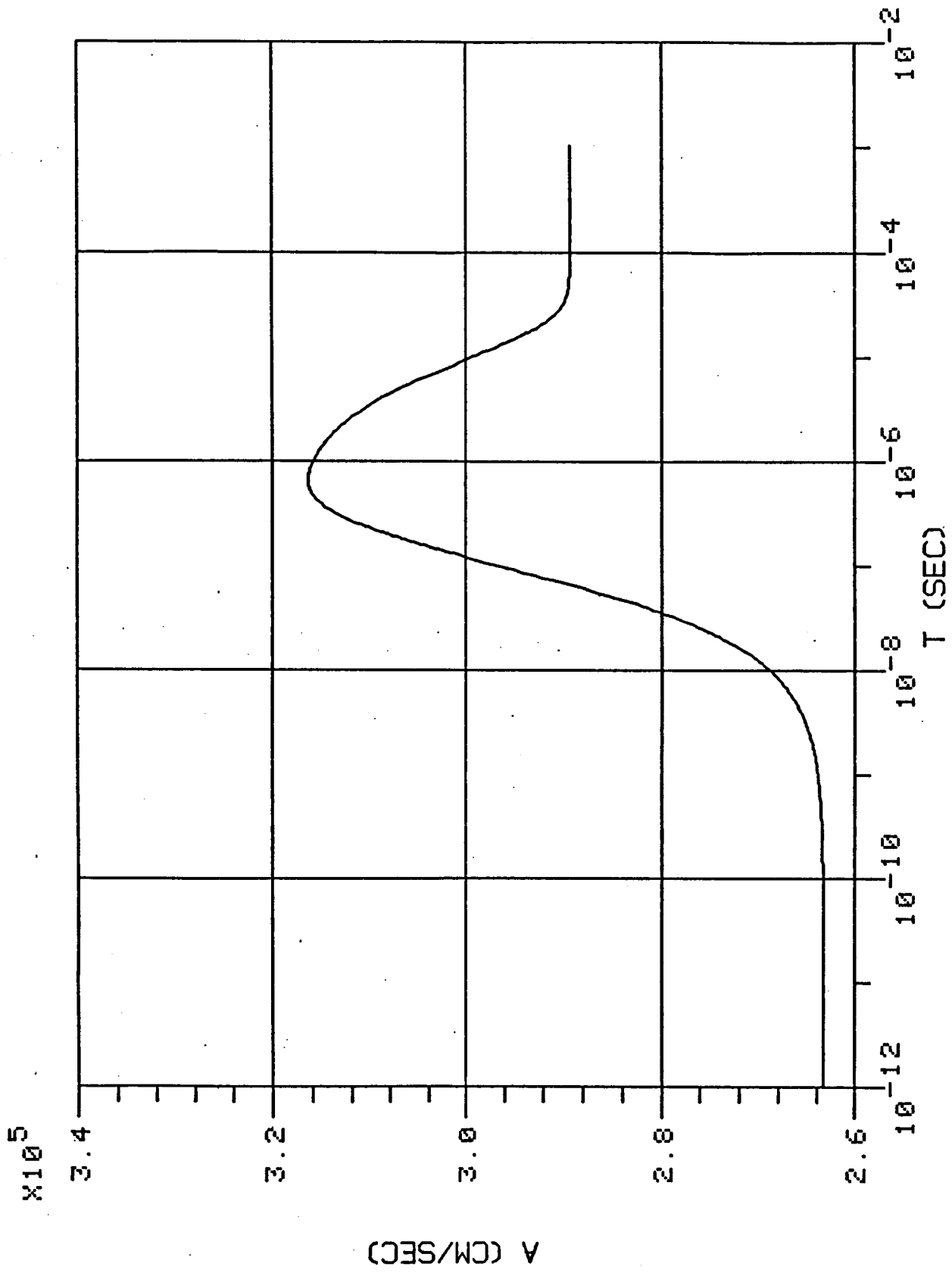
FIGURE 36 Calculated sound speed based on non-equilibrium concentrations for a mixture of 20% H_2O and 80% He at a temperature of 4000 K and a total pressure of 10 atm.
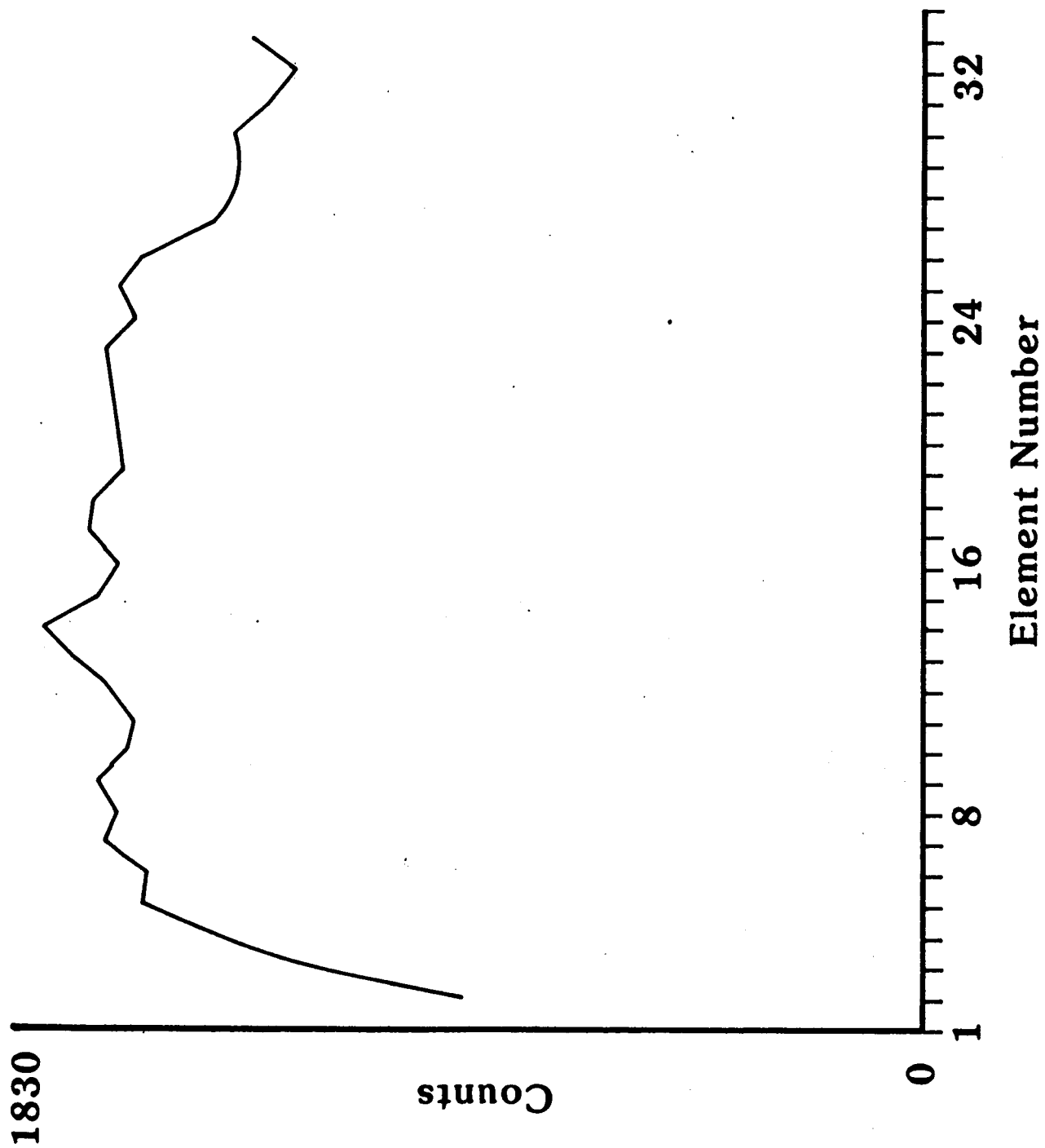
FIGURE 37 Average of 1000 scans of the array detector showing the profile of the probe laser beam prior to the beginning of heating.
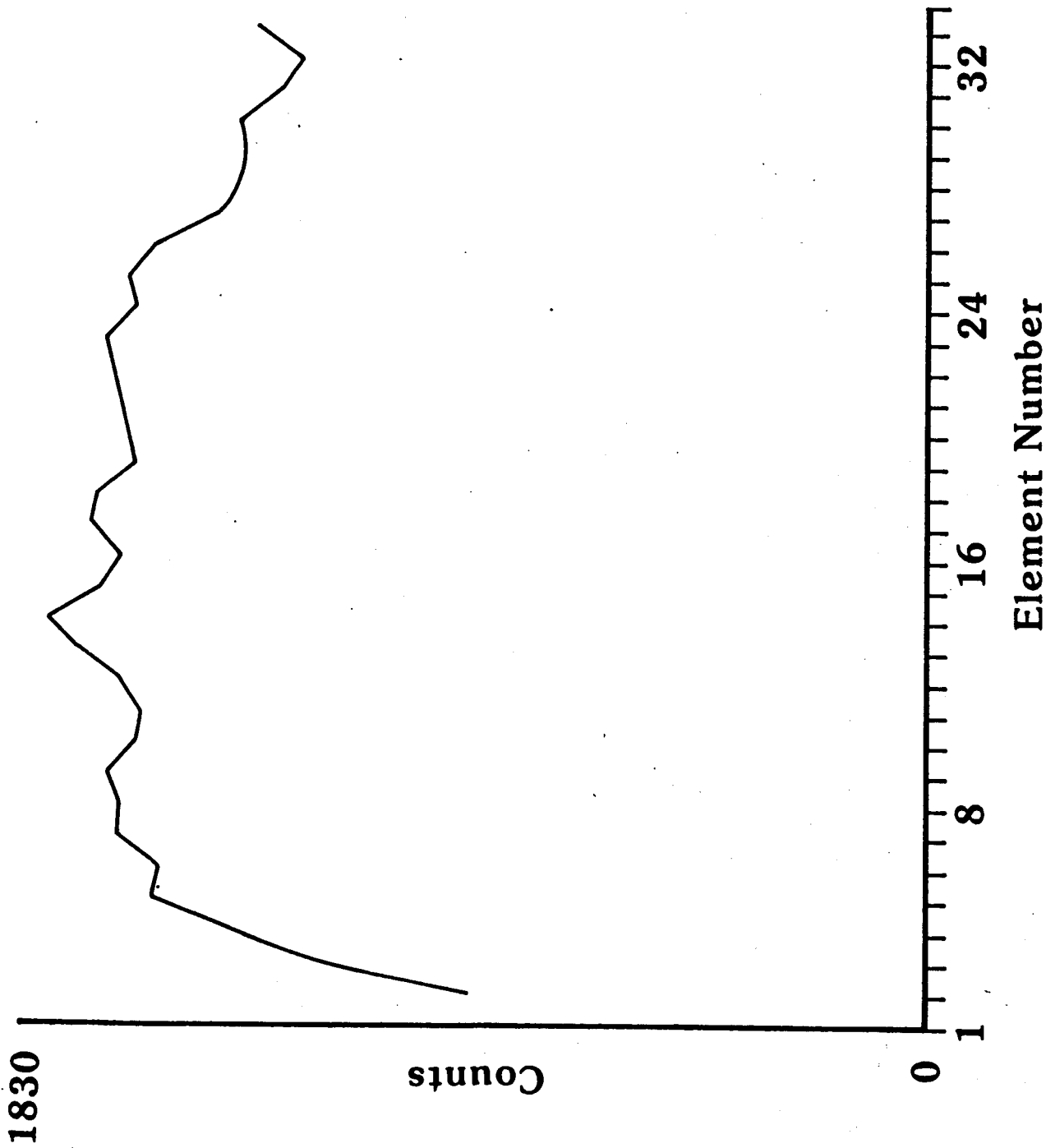
FIGURE 38 Average of 1000 scans of the array detector showing the profile of the probe laser beam during the heating experiment using 0.33 mole H_2O in argon at a total pressure of 6 *atm*.
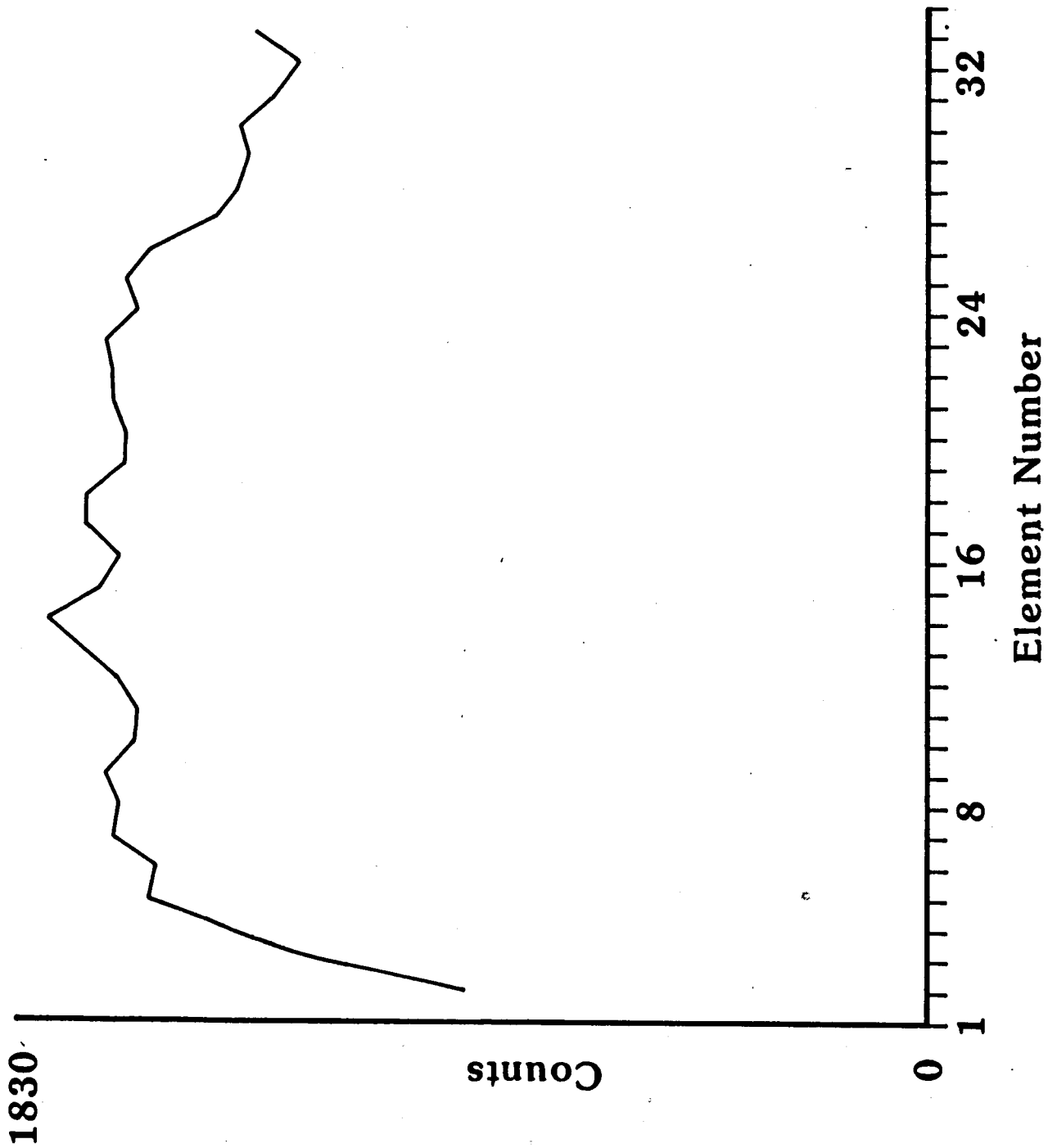
FIGURE 39 *Average of 1000 scans of the array detector showing the profile of the probe laser beam during the heating experiment using 0.33 mole H_2O in helium at a total pressure of 6 atm.*
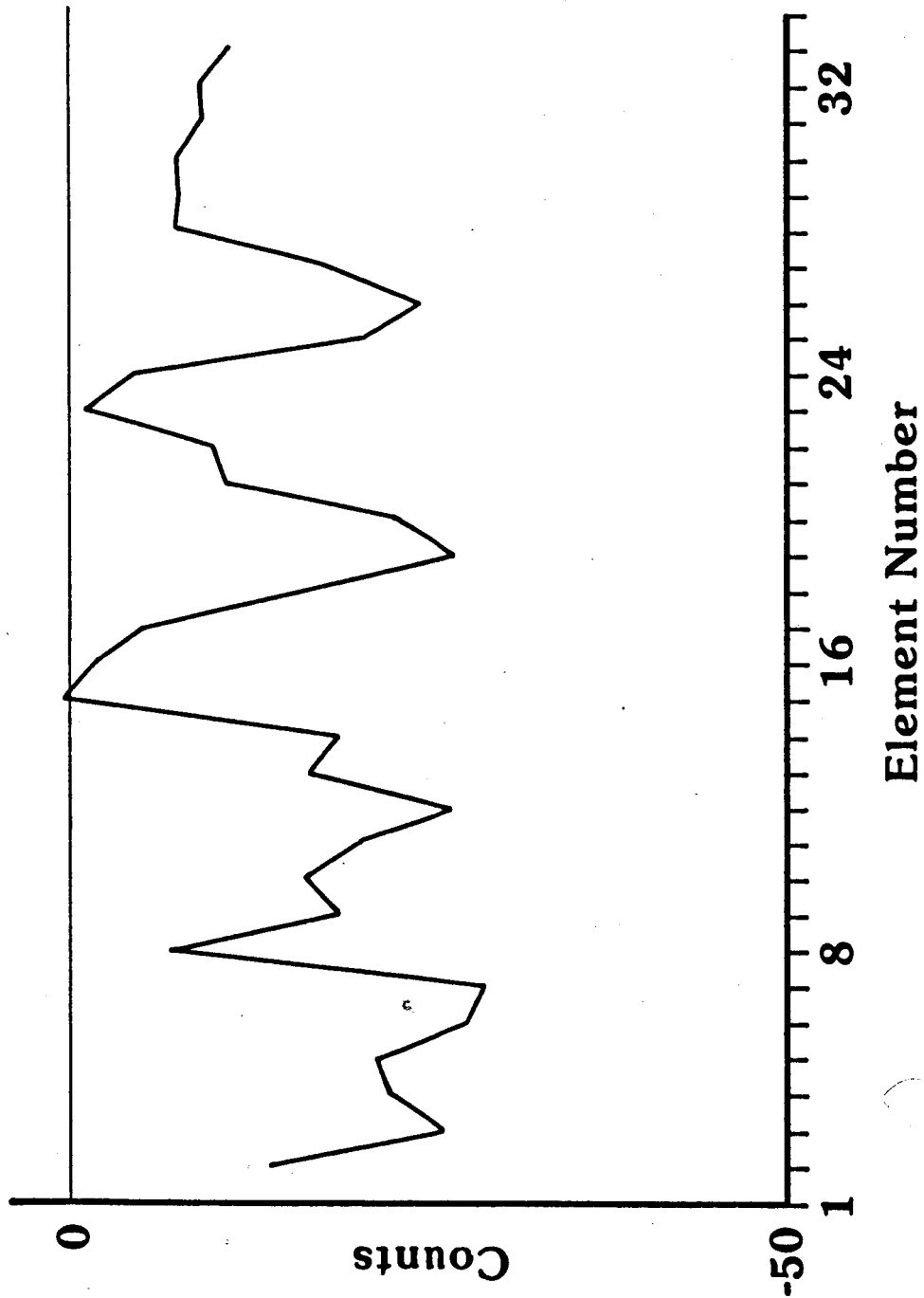
FIGURE 40   Difference between the scans of Figure 38 and Figure 37.
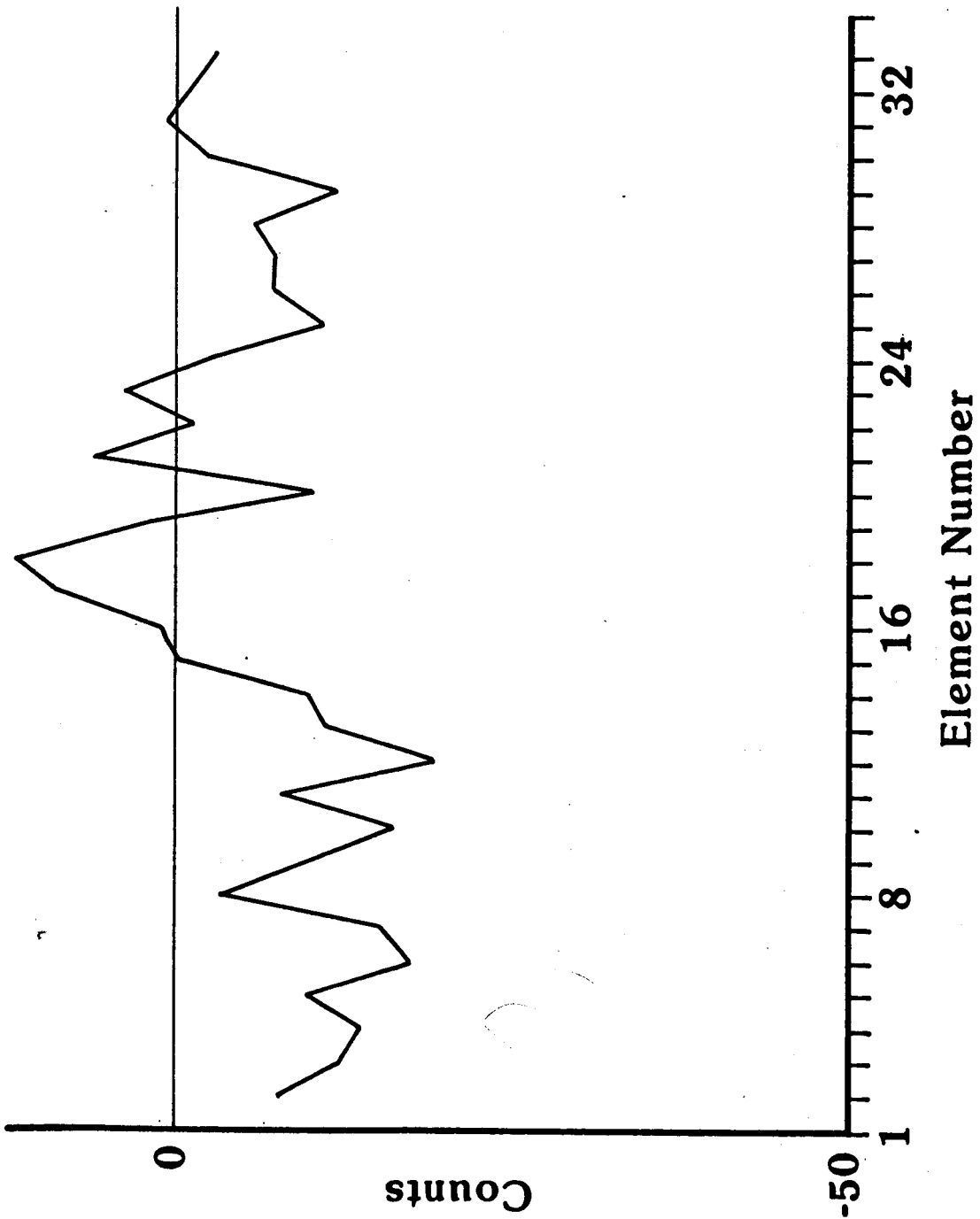
FIGURE 41 Difference between the scans of Figure 39 and Figure 37.
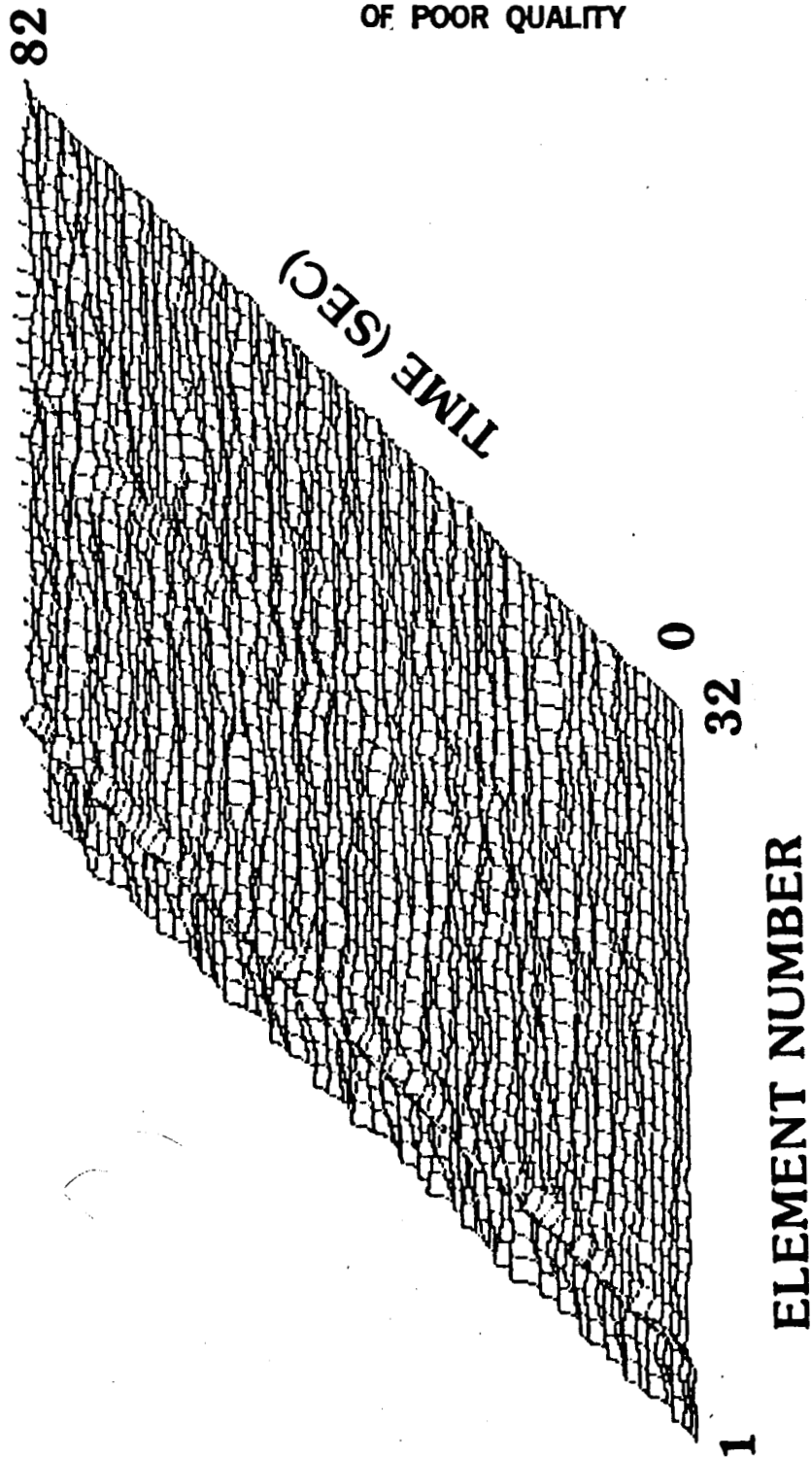
FIGURE 42 Three-dimensional representation of the difference in the array scans (proportional to absorption) for the heating experiment in 0.33 mole H_2O in argon at a total pressure of 6 atm.
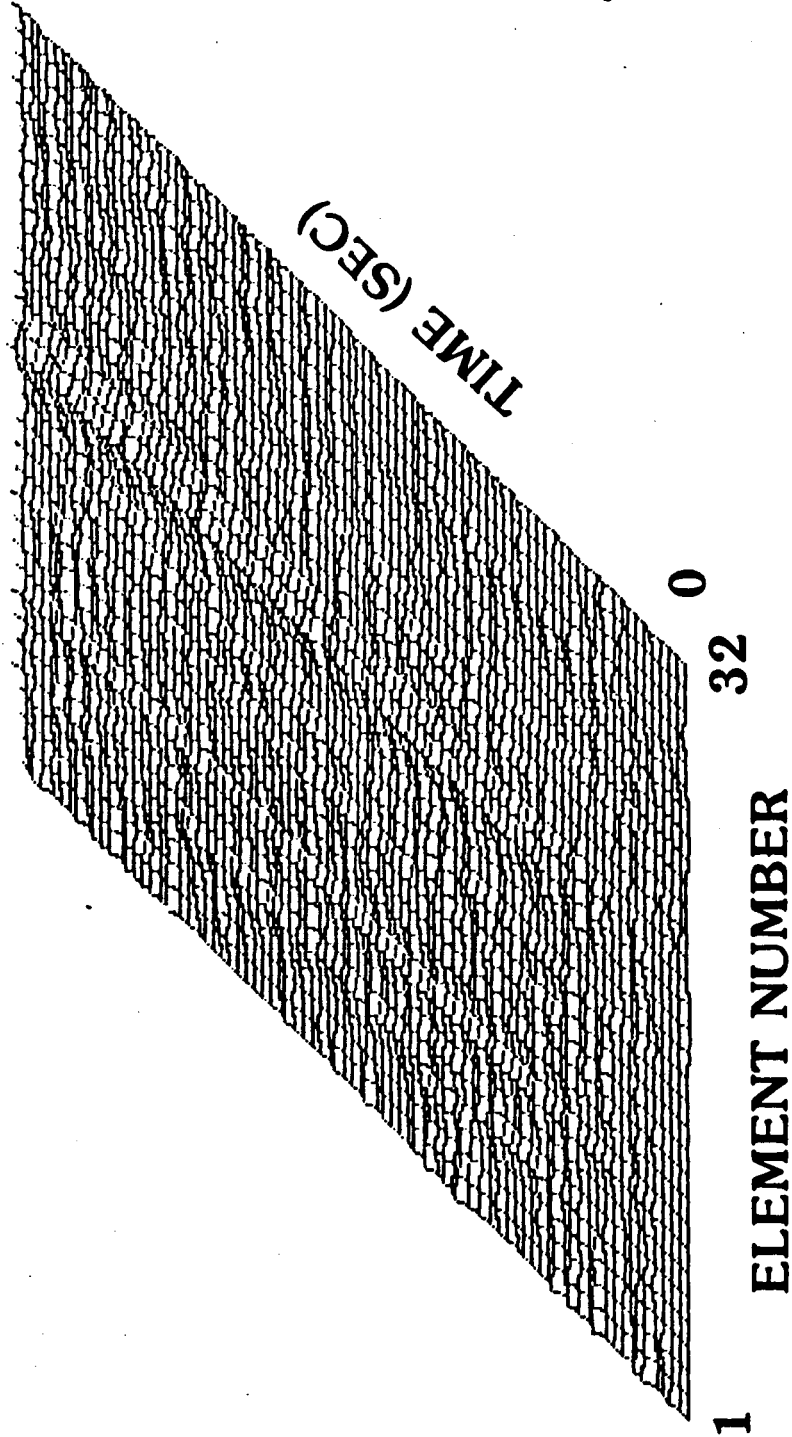
FIGURE 43 Three-dimensional representation of the difference in the array scans (proportional to absorption) for the heating experiment in 0.33 mole H_2O in helium at a total pressure of 6 atm.

APPENDIX A
FORTRAN 77 LISTING FOR LASER
ABSORPTION WAVE MODEL

```
C     ****************************************************************
C     PROGRAM TO CALCULATE UNSTEADY THERMAL WAVE IN TUBE
C         USES PATANKAR'S UNSTEADY FULLY IMPLICIT METHOD
C     ****************************************************************
C
C
      DIMENSION X(301),DELX(301),DX(301),T(301),ABSORP(301),BI(301)

      DIMENSION CP(301),S(301),TC(301),COEF(301)

      DIMENSION XCV(301),AKCELL(301)

      DIMENSION RHO(301),A1(301),A2(301),A3(301),B(301)

      DIMENSION Z(301),UD(301,2),LD(301,2)

C
C     X(N)=POSITION AT NTH GRID POINT (CM)
C     DELX(N)=X(N+1)-X(N)
C     DX(N)=DISTANCE BETWEEN CONTROL VOLUME INTERFACES AT POINT N
C     T(N)=TEMP. AT NTH GRID POINT (DEG. K)
C     RHO(N)=DENSITY OF MATERIAL (GM/CM^3)
C     BI(N)=BEAM INTENSITY AT NTH GRID LOC. (W/CM^2)
C     ABSORP(N)=ABSORPTION COEF. AT NTH GRID LOCATION
C     CP(N)=SPECIFIC HEAT AT NTH GRID LOCATION (CGS UNITS)
C     AKCELL(N)=THERMAL CONDUCTIVITY OF NTH CELL AT TEMP ,T(N)
C     S(N)=SOURCE TERM AT NTH GRID LOC. (W/CM^3)
C     TC(N)=THERMAL COND AT C.V. INTERFACE TO RIGHT OF NTH LOC
C     COEF(N)=DISCRETIZATION COEF. AT NTH GRID POINT.
C
C
C
C     ICOUNT=COUNTER FOR DATA SAVER (IE. SAVE EVERY ICOUNT PLOT)
C
C     ****************************************************************
C
C     NOTE: ALL UNITS ARE FULLY CGS UNITS!!!!!!!!!!!
C
C     ****************************************************************
C
C
C     TIME=TIME IN SECS!
      COMMON/SOLN/ T,BI,S

      COMMON/PROP/ TC,ABSORP,CP,AKCELL,RHO

      COMMON/GRID/ NPTS,X,DX,DELX,XCV,XL,NSURFACE

      COMMON/CLOCK/ TIME,DELT

      COMMON/COEF/ A1,A2,A3,B

      COMMON/TMP/ Z,UD,LD

C
C
C     OPEN INPUT UNITS
C
      OPEN(UNIT=1,NAME='GRID.DAT',TYPE='OLD')

C
C     OPEN OUTPUT UNIT
C
      OPEN(UNIT=2,NAME='TOUT.DAT',TYPE='NEW')

C
C     READ INPUT DATA
C
      READ(1,*) NPTS

      NIF=NPTS+1

      READ(1,*) NSURFACE

      READ(1,*) ICOUNT

      READ(1,*) TL,TR

C
C     TL=TEMP BC AT LEFT END,TR=TEMP. BC AT RIGHT END
C
      READ(1,*) I0
```

```
C
C   IØ=INCIDENT LASER INTENSITY ON RIGHT END OF SYSTEM
C
    BI(NIF)=IØ

C
    READ (1,*) XL

C
C   XL =LENGTH OF TUBE
C
    READ(1,*) DELT,TSTOP

C   DELT =TIME STEP (SECS)
C
C   NPTS=NO. OF GRID POINTS
C   NSURFACE = INDEX OF X LOCATION OF CERAMIC ABSORBER
C
    CALL SETGRID(NIF)

C
C   THIS ROUTINE SETS UP DX,DELX FROM X
C
    CALL IC(NPTS,T,TL,TR)

C   THIS ROUTINE SETS THE INITIAL CONDITIONS
C
    TIME=Ø

C   INITIALIZE PROPERTIES AND COEFICIENTS
    CALL UPDATE(NIF)

C
C   WRITE OUT INITIAL DISTRIBUTION
C
    CALL OUTPUT(NPTS,TIME,T,BI,S)

    NA=NINT(TSTOP/DELT)

    NARR=NPTS-2

C
C   TIME LOOP
C
C
    IPLOT=Ø

    DO 5ØØ K=1,NA

    IPLOT=IPLOT+1

    TIME=DELT*K

    CALL TDMA(A2,A1,A3,B,T,Z,UD,LD,NARR,NIF)

    IF(IPLOT.EQ.ICOUNT) IPLOT=Ø

    IF(IPLOT.EQ.Ø) CALL OUTPUT(NPTS,TIME,T,BI,S)

    CALL UPDATE(NIF)

C
C
5ØØ          CONTINUE

    CLOSE(UNIT=1)

    CLOSE(UNIT=2)

    STOP

    END
```

```fortran
      SUBROUTINE SETGRID(ISIZE)
C
C     ******************************************************
C
C     SUBROUTINE TO SET UP SPATIAL GRID FOR THE CALCULATION
C     NON-UNIFORM GRID SPACING IS ALLOWED
C     XCV=X LOC.'S OF CELL INTERFACES (CM)
C     X=X LOC. OF MAJOR GRID POINTS
C     XL =TOTAL LENGTH OF TUBE (CM)
C
C     ******************************************************
C
      DIMENSION X(301),DX(301),DELX(301)

      DIMENSION XCV(301)

      COMMON/GRID/NPTS,X,DX,DELX,XCV,XL,NSURFACE

      DO 100 NN=1,NPTS+1

      READ(1,*) XCV(NN)

100        CONTINUE

C
C     SET UP CONTROL VOLUMES OF "ZERO" THICKNESS AT BOUNDARIES
C
      XCV(1)=0.

      XCV(2)=0.

      XCV(NPTS+1)=XL

      XCV(NPTS)=XL

C
C     SET UP MAJOR GRID POINTS MIDWAY BETWEEN CELL INTERFACES
C
      DO 200 NN=1,NPTS

      X(NN)=(XCV(NN)+XCV(NN+1))/2.

200        CONTINUE

C
C     FIND SPACING BETWEEN MAJOR GRID POINTS
C
      DO 300 NN=1,NPTS-1

      DELX(NN)=X(NN+1)-X(NN)

300        CONTINUE

C
C     FIND THICKNESS OF INDIVIDUAL CONTROL VOLUMES
C
      DO 400 NN=1,NPTS

      DX(NN)=XCV(NN+1)-XCV(NN)

400        CONTINUE

      RETURN

      END
```

```fortran
      SUBROUTINE UPDATE(NIF)
C
C
C     ************************************************************
C
C     THIS SUBROUTINE UPDATES THE VALUES OF TEMPERATURE DEPENDENT
C     PROPERTIES. CALL AT THE END OF EACH TIME STEP!!!!!!!!!!!!!!!!
C
C     ************************************************************
C
      DIMENSION X(301),DELX(301),DX(301),T(301),ABSORP(301)
      DIMENSION BI(301),CP(301),S(301),TC(301),COEF(301)
      DIMENSION AKCELL(301),XCV(301),RHO(301)
      DIMENSION A1(301),A2(301),A3(301),B(301),Z(301),UD(301,2)
      DIMENSION LD(301,2)
C
C
      COMMON/SOLN/T,BI,S
      COMMON/PROP/TC,ABSORP,CP,AKCELL
      COMMON/GRID/NPTS,X,DX,DELX,XCV,XL,NSURFACE
      COMMON/CLOCK/TIME,DELT
      COMMON/COEF/ A1,A2,A3,B
      COMMON/TMP/ Z,UD,LD
C
C
C     LOOP THRU ALL CELLS AND ASSIGN NEW PROPERTIES
C
C
      DO 100 NN=1,NPTS
C
C     VARIABLE NSURFACE LOCATES THE SURFACE OF THE CERAMIC
C
      IF(NN.GT.(NSURFACE-1)) GOTO 70
C
C     COME HERE IF CURRENT POINT IS IN THE CERAMIC
C
      CALL TCSOLID(T(NN),AKCELL(NN))
      CALL CPSOLID(T(NN),CP(NN))
      CALL ASOLID(T(NN),ABSORP(NN))
      CALL RHOSOLID(T(NN),RHO(NN))
C
      GOTO 100
C
C     COME HERE IF SCANNING THRU GAS
C
70    CALL TCGAS(T(NN),AKCELL(NN))
      CALL CPGAS(T(NN),CP(NN))
      CALL AGAS(T(NN),ABSORP(NN))
      CALL RHOGAS(T(NN),RHO(NN))
C
C
100         CONTINUE
C
C     NOW FIND BEAM INTENSITY PROFILE
C
      CALL BPROFILE(NPTS,DX,ABSORP,BI)
C
C     CALCULATE SOURCE TERM USING NEW BEAM PROFILE AND PROPERTIES
C
      CALL SOURCE(NPTS+1)
```

```
C
C   FIND INTERFACE CONDUCTIVITIES
C
      DO 200 NN=2,NPTS

      T1=2*DELX(NN-1)

      T2=DX(NN-1)/AKCELL(NN-1)+DX(NN)/AKCELL(NN)

      TC(NN)=T1/T2
200            CONTINUE

      TC(1)=TC(2)

      TC(NPTS+1)=TC(NPTS)

C
C   UPDATE DISCRETIZATION COEFICIENTS FOR USE IN NEXT TIME STEP
C

      DO 300 NN=2,NPTS-1

      NM=NN-1

      A1(NM)=TC(NN)/DELX(NM)

      A3(NM)=TC(NN+1)/DELX(NN)

      AP0=RHO(NN)*CP(NN)*DX(NN)/DELT

      A2(NM)=-1*(AP0+A1(NM)+A3(NM))

      B(NM)=-1*(AP0*T(NN)+S(NN)*DX(NN))

C
C
300            CONTINUE

C
      B(1)=B(1)-A1(1)*T(1)

      B(NPTS-2)=B(NPTS-2)-A3(NPTS-2)*T(NPTS)

      RETURN

      END

      SUBROUTINE BPROFILE(NPTS,DX,ABSORP,BI)

C
C   ************************************************************
C
C   THIS SUBROUTINE INTEGRATES THE BEER'S LAW EQUATION TO
C   DETERMINE THE BEAM INTENSITY PROFILE.
C
C   ************************************************************
C
      DIMENSION DX(301),ABSORP(301),BI(301)

C
      ETA=0.

      NS=NPTS+1

C
C   BI(NPTS+1)=INCIDENT BEAM INTENSITY (W/CM^2)
C
      DO 100 NN=NPTS,1,-1

      ETA=ETA+ABSORP(NN)*DX(NN)

      IF(ETA.GT.10.) GOTO 90

      BI(NN)=BI(NS)*EXP(-ETA)

      GOTO 100

90 BI(NN)=0.
100            CONTINUE

C
C
      RETURN

      END
```

```
      SUBROUTINE SOURCE(NIF)

C
C     ***********************************************************
C
C     THIS SUBROUTINE CALCULATES THE SOURCE TERM USING THE BEAM
C     INTENSITY PROFILE,TEMPERATURE FIELD AND PROPERTIES.
C
C     ***********************************************************
C
      DIMENSION X(301),DELX(301),DX(301),T(301),ABSORP(301)

      DIMENSION BI(301),CP(301),S(301),TC(301),COEF(301)

      DIMENSION XCV(301),AKCELL(301),RHO(301)

C
C
      COMMON/SOLN/ T,BI,S

      COMMON/PROP/ TC,ABSORP,CP,AKCELL,RHO

      COMMON/GRID/ NPTS,X,DX,DELX,XCV,XL,NSURFACE

      COMMON/CLOCK/ TIME,DELT

C
C
      DO 100 NN=1,NPTS

C
C     CHECK FOR BOUNDARY POINTS (ZERO THICKNESS CELLS)
C
      IF(DX(NN).EQ.0) GOTO 90

      CALL RAD(T(NN),PHI,NSURFACE,DX(NN),NN)

C
C     PHI IS RADIATIVE LOSS FROM CONTROL VOLUME
C             ASSUME OPTICALLY THIN

C
C
C     NOW CALCULATE POWER ABSORBED FROM BEAM
C
      A=(BI(NN+1)-BI(NN))/DX(NN)

C
C
C     S=NET SOURCE TERM
C
      S(NN)=A-PHI

      GOTO 100

90    S(NN)=0.
C
C
100           CONTINUE

C
C
      RETURN

      END
```

```fortran
      SUBROUTINE OUTPUT(K,TIME,T,BI,S)

C
C     *****************************************************
C
C     THIS ROUTINE OUTPUTS THE SOLN (ARRAY T) ALONG WITH THE
C     BEAM INTENSITY (BI(NN)), AND THE SOURCE TERM (S(NN))
C     AT THE END OF EACH TIME STEP
C
C     UNITS:
C     T= DEG. KELVIN
C     S= W/CM^3
C     BI= W/CM^2
C
C
C     *****************************************************
C
C
      DIMENSION T(301),BI(301),S(301)

      DIMENSION X(301),DX(301),DELX(301),XCV(301)

      COMMON/GRID/NPTS,X,DX,DELX,XCV,XL,NSURFACE

      WRITE(2,10) TIME

10    FORMAT(1X,'TIME= ',F12.6,' SECS')
      WRITE(2,*) NPTS

      DO 100 NN=1,NPTS

      BB=(BI(NN+1)+BI(NN))/2.

      WRITE(2,20) X(NN),T(NN),BI(NN),S(NN)

20    FORMAT(1X,F12.6,3X,F12.6,3X,F12.6,3X,F13.4)
100           CONTINUE

      RETURN

      END
```

```fortran
      SUBROUTINE IC(NPTS,T,TL,TR)
C
C
C     ***********************************************************
C
C     THIS SUBROUTINE INITIALIZES THE TEMP FIELD AT TIME T=Ø
C     THE INITIAL PROFILE IS ASSUMED TO BE A LINEAR VARIATION
C     WITH X FROM T=TL TO T=TR.
C
C     ***********************************************************
C
C
      DIMENSION T(3Ø1)

      S=(TR-TL)/FLOAT(NPTS-3)

      DO 1ØØ NN=2,NPTS-1

      T(NN)=S*(NN-2)+TL

1ØØ        CONTINUE

      T(1)=TL

      T(NPTS)=TR

      RETURN

      END
```

```
      SUBROUTINE TDMA(A,AM,AP,B,X,Z,UD,LD,N,LENTH)
C***************************************************************************
C
C     THIS SUBROUTINE USES A CROUT REDUCTION ALGORITHM TO SOLVE THE
C     LINEAR SYSTEM OF EQUATIONS:
C
C     A(1)*X(1) + AP(1)*X(2) +        Ø       +       Ø       + ... +       Ø       = B(1)
C     AM(2)*X(1) +  A(2)*X(2) + AP(2)*X(3) +        Ø       + ... +       Ø       = B(2)
C        Ø        + AM(3)*X(2) +  A(3)*X(3) + AP(3)*X(4) + ... +       Ø       = B(3)
C
C          .              .             .             .                 .            .
C          .              .             .             .                 .            .
C          .              .             .             .                 .            .
C
C        Ø        +     Ø      + ... +     Ø      + AM(N)*X(N-1) +  A(N)*X(N) = B(N)
C
C     THREE WORKSPACE ARRAYS ARE REQUIRED UD, LD AND Z AS WELL AS THE
C     ARRAY X IN WHICH THE SOLUTION IS RETURNED. THE ARRAYS UD AND LD
C     MAY ALSO BE PASSED AS X AND Z FROM THE CALLING PROGRAM, IN WHICH
C     CASE THE SOLUTION OF X WILL BE PLACED IN THE FIRST COLUMN OF THE
C     ARRAY UD. IF THIS IS DONE UD MUST BE PASSED AS X AND LD AS Z OR
C     THE CORRECT SOLUTION WILL NOT BE FOUND.
C  NOTE: HERE N IS EQUAL TO NO. OF POINTS -2!!!!
C
C***************************************************************************
      REAL A,AM,AP,B,UD,LD,X,Z
      INTEGER LENTH,NPTS,I,N
      DIMENSION A(LENTH),AM(LENTH),AP(LENTH),B(LENTH),UD(LENTH,2),
     2 LD(LENTH,2),X(LENTH),Z(LENTH)
    SAVE1=X(1)

    SAVE2=X(LENTH-1)

      LD(1,1)=A(1)
      UD(1,2)=AP(1)/LD(1,1)
C
      DO 50 I=2,N-1
         LD(I,2)=AM(I)
         LD(I,1)=A(I)-LD(I,2)*UD(I-1,2)
         UD(I,2)=AP(I)/LD(I,1)
   50    CONTINUE
C
      LD(N,2)=AM(N)
      LD(N,1)=A(N)-LD(N,2)*UD(N-1,2)
C
      Z(1)=B(1)/LD(1,1)
      DO 100 I=2,N
         Z(I)=(B(I)-LD(I,2)*Z(I-1))/LD(I,1)
  100    CONTINUE
C
      X(N)=Z(N)
      DO 150 I=N-1,1,-1
         X(I)=Z(I)-UD(I,2)*X(I+1)
  150    CONTINUE
    DO 300 JJ=N,1,-1

    X(JJ+1)=X(JJ)

300          CONTINUE

    X(1)=SAVE1

    X(LENTH-1)=SAVE2

C
      RETURN
      END
```

```
      SUBROUTINE COMMENT

C     ************************************************
C     THIS SET OF SUBS GIVES PROPERTIES FOR 20%, 10 ATM
C     H2/H2O MIXTURES. TO USE: LINK AS FOLLOWS
C     $LINK TWAVE,OUTPUT,IC,TDMABV,T2010ATM
C
C     ************************************************
      RETURN

      END

      SUBROUTINE TCSOLID(T,AK)

C
C     DATA FOR 100% DENSE POLYCRYSTALLINE AL203!!!
C
C     UNITS:W/CM-K
C
      DIMENSION TDATA(6),PDATA(6)

      DATA TDATA/100.,310.8,477.4,700.,1033.,8000./

      DATA PDATA/.34,.33,.204,.130,.099,.099/

      CALL GETPROP(TDATA,PDATA,6,T,AK)

      RETURN

      END

      SUBROUTINE CPSOLID(T,C)

C
C     DATA FOR 100% DENSE POLYCRYSTALLINE AL203!!!
C     UNITS: J/G-K
C
      DIMENSION TDATA(5),PDATA(5)

      DATA TDATA/100.,366.3,700.,1644.,8000./

      DATA PDATA/.837,1.15,1.42,1.51,1.51/

      CALL GETPROP(TDATA,PDATA,5,T,C)

      RETURN

      END

      SUBROUTINE ASOLID(T,A)

      A=230.

      RETURN

      END

      SUBROUTINE RHOSOLID(T,R)

C
C     UNITS:G/CM^3
      R=3.97

      RETURN

      END
```

```
      SUBROUTINE TCGAS(T,TC)
C
C   DATA FOR H2, P=10 ATM!!!!!!!!
C
      DIMENSION TDATA(13),PDATA(13)
      DATA TDATA/100.,800.,1600.,2400.,2600.,3000.,3400.,3800.,
     1      4200.,4500.,4600.,4800.,5000./
      DATA PDATA/6.69E-04,3.35E-03,5.85E-03,8.36E-03,9.62E-03,
     1      1.67E-02,2.84E-02,4.6E-02,6.36E-02,7.03E-02,6.94E-02,
     2      6.61E-02,5.94E-02/


      CALL GETPROP(TDATA,PDATA,10,T,TC)
      RETURN
      END
      SUBROUTINE CPGAS(T,C)
C   ********************************************************
C   CP FOR H2/H20 MIX. P=10ATM. RESULTS OF NASA CODE
C   20% H2O BY VOL
C   ********************************************************
      C=59.26*EXP(-8.56E-07*(T-4500)**2)+5.74


      RETURN
      END
      SUBROUTINE AGAS(T,A)
      COMMON/SPECIES/PTOTAL,XH2O,XOH
C   *******************************
C   CALCULATES ABSORPTION FOR PTOTAL ATM,XH2O MOLE FRAC. H2O
C
C   SUB H2O CALCULATES MOLE FRAC. H2O,OH AND SETS PRESSURE, PTOTAL.
C
C   UNITS: CM^-1
C   DISSOCIATION IS TAKEN INTO ACCOUNT BY SUB H2O.
C
C   ****************************************************************
      CALL H2O(T)
      P=PTOTAL
      ETA=XH2O
      IF(T.LT.1000) GOTO 100
      AK=8.0E-8*(T-700.)**2.
      GOTO 500
100        AK=9.222E-06*(EXP(6.6615E-03*T)-1)
500        CONTINUE
C
C   AK IS ESSENTIALLY ABSORP./ AMAGAT !!!
C
      A=ETA*AK*273.*P/T
      RETURN
      END
```

```
      SUBROUTINE H2O(T)

C
C     ***************************************************
C     THIS SUB CALCULATES MOLE FRACS FOR H2O,OH AND SETS THE
C     TOTAL PRESSURE. MUST BE TAILOR MADE FOR EACH CONCENTRATION
C     YOU WISH TO RUN.
C     CURRENT CONFIGURATION IS 20%,10 ATM.!!!
C     ***************************************************
      COMMON/SPECIES/PTOTAL,XH2O,XOH

      PTOTAL=10.

C     CALCULATES MOLE FRAC H2O FOR 20%H2O, P=10 ATM.
C     ALSO CALCULATES MOLE FRC FOR OH!!!!
C     CURVE FIT USING DATA FROM NASA PRINTOUT.
C
      IF(T.LE.4250.) GOTO 100

      XH2O=.02291*EXP(-.01694*(T-4250))

      GOTO 200

100        XH2O=.2*(2.-EXP(5.839E-26*T**6.9))

200        CONTINUE

      XOH=.06*EXP(-1.28E-06*(T-4500)**2.)

C     XOH=MOLE FRAC OH,XH2O=MOLE FRAC H2O!!!
C     PTOTAL=TOTAL PRESSURE (ATM)
C
      END

      SUBROUTINE RHOGAS(T,R)

C     ***********************************
C     GIVES DENSITY FOR 20% H2O/VOL AT 10 ATM TOTAL PRESS.
C     UNITS:G/CM^3
C     CURVEFIT USING DATA FROM NASA PRINT OUT.
C
C     ***************************************************
C
C
      P=10.

C
C     HERE R IS GAS CONSTANT FOR H2O MIXTURE (ATM CM^3/(GM K))
C
      IF(T.LE.5600) R=18.25*EXP(-5.73E-07*(T-5600)**2.)+15.75

      IF(T.GT.5600) R=34.

C     BELOW HERE R IS DENSITY (GM/CM^3)
      R=P/(R*T)

      RETURN

      END
```

```
      SUBROUTINE RAD(T,RA,NS,DXX,KK)

C     ********************************************************
C     THIS SUB CHOOSES THE CORRECT RAD. TERM DEPENDING ON
C     LOCATION, IE IN CERAMIC, NOT IN CERAMIC, ETC...
C     UNITS FOR RAD ARE W/CM^3!!!!
C     ********************************************************
      IF(KK.LE.(NS-1)) GOTO 100

C
C     COME HERE IF IN GAS
C
      CALL RADH2O(T,RA)

      GOTO 1000

100         IF(KK.EQ.(NS-1)) GOTO 200

C     COME HERE IF BELOW CERAMIC SURFACE
      RA=0.

      GOTO 1000

C     COME HERE IF FIRST CELL OF CERAMIC SURFACE.
200         RA=4.56E-12*T**4./DXX

1000        CONTINUE

      RETURN

      END
```

```fortran
      SUBROUTINE GETPROP(TDATA,PDATA,NSIZE,TT,PP)

C
C     ***********************************************************
C
C     INTERPOLATION ROUTINE USING LOOK UP TABLES GIVEN BY
C     TDATA,PDATA. HERE PDATA=FUNCTION(TDATA).
C
C     ***********************************************************
C
      DIMENSION TDATA(NSIZE),PDATA(NSIZE)

      IF(TT.LT.TDATA(1)) GOTO 500

C
C     LOOKUP TABLE LOOP
C
      DO 100 NN=1,NSIZE-1

      NS=NN

      IF(TT.GT.TDATA(NN)) GOTO 50

      GOTO 100

50    IF(TT.LE.TDATA(NN+1)) GOTO 200
100             CONTINUE

      GOTO 600

C
C     VALUE IS IN TABLE, INTERPOLATE TO GET PROPERTY
C
200             CALL INTER(TDATA(NS),PDATA(NS),TDATA(NS+1),PDATA(NS+1),TT,PP)

      GOTO 1000

C
C     BACK EXTRAPOLATE
C
500             CALL INTER(TDATA(1),PDATA(1),TDATA(2),PDATA(2),TT,PP)

      GOTO 1000

C
C     FORWARD EXRAPOLATE
C
600             K1=NSIZE-1

      K2=NSIZE

      CALL INTER(TDATA(K1),PDATA(K1),TDATA(K2),PDATA(K2),TT,PP)

1000            CONTINUE

C
C     NEGATIVE PROPERTIES ARE NOT ALLOWED!!
C
      IF(PP.LT.0.) PP=1.E-12

      END

      SUBROUTINE INTER(X1,Y1,X2,Y2,X,Y)

      SLOPE=(Y2-Y1)/(X2-X1)

      Y=SLOPE*(X-X1)+Y1

      RETURN

      END
```

```fortran
      SUBROUTINE RADH2O(T,RAD)

C
C     ***********************************************************
C     THIS SUB CALCULATES RAD. FROM H2O SPECIES GIVEN THE PRESSURE,
C     FRACTION OF H2O (AT THE GIVEN TEMP). CS(N) IS CROSS SECTION
C     CALCULATED FROM KEMP'S REPORT USING THE .1 ATMFT CURVE.
C     ***********************************************************
C
      DIMENSION TDAT(14),CSOH(14)

      DIMENSION TDATA(13),CS(13)

C
C     CSOH=CROSS SECTION FOR OH RAD.,CS=CROSS SECTION FOR H2O RAD.
C
      COMMON/SPECIES/PTOTAL,XH2O,XOH

      DATA TDAT/298.,500.,1000.,1100.,1500.,2000.,2500.,3000.,
     1     3500.,4000.,4500.,5000.,5500.,6000./

      DATA CSOH/8.01E-24,4.93E-23,4.93E-22,5.92E-22,6.72E-22,6.28E-22,
     1     4.26E-22,2.69E-22,1.88E-22,1.61E-22,1.07E-22,7.17E-23,4.68E-23,
     1     2.96E-23/

      DATA TDATA/298.,500.,1000.,1500.,2000.,2500.,3000.,3500.,
     1     4000.,4500.,5000.,5500.,6000./

      DATA CS/9.32E-22,2.23E-21,3.8E-21,3.35E-21,1.97E-21,1.56E-21,
     1     1.21E-21,9.38E-22,7.15E-22,6.03E-22,4.69E-22,3.69E-22,3.22E-22/

C
C
      ANH2O=XH2O*PTOTAL/(1.362E-22*T)

      CALL GETPROP(TDATA,CS,13,T,ACS)

      RADC=ACS*ANH2O

      RAD=2.268E-11*RADC*T**4.

      CALL GETPROP(TDAT,CSOH,14,T,CST)

      ROH=1.665E11*PTOTAL*XOH*CST*T**3.

      RAD=RAD+ROH

C
C     UNITS: RAD=(W/CM^3)
C
      RETURN

      END
```

```
      SUBROUTINE TCSOLID(T,AK)

C
C     DATA FOR 100% DENSE POLYCRYSTALLINE AL2O3!!!
C
C     UNITS:W/CM-K
C
      DIMENSION TDATA(6),PDATA(6)

      DATA TDATA/100.,310.8,477.4,700.,1033.,8000./

      DATA PDATA/.34,.33,.204,.130,.099,.099/

      CALL GETPROP(TDATA,PDATA,6,T,AK)

      RETURN

      END

      SUBROUTINE CPSOLID(T,C)

C
C     DATA FOR 100% DENSE POLYCRYSTALLINE AL2O3!!!
C     UNITS: J/G-K
C
      DIMENSION TDATA(5),PDATA(5)

      DATA TDATA/100.,366.3,700.,1644.,8000./

      DATA PDATA/.837,1.15,1.42;1.51,1.51/

      CALL GETPROP(TDATA,PDATA,5,T,C)

      RETURN

      END

      SUBROUTINE ASOLID(T,A)

      A=230.

      RETURN

      END

      SUBROUTINE RHOSOLID(T,R)

C
C     UNITS:G/CM^3
      R=3.97

      RETURN

      END

      SUBROUTINE TCGAS(T,TC)

C
C     DATA FOR H2, P=1 ATM!!!!!!!!
C
      DIMENSION TDATA(12),PDATA(12)

      DATA TDATA/ 100.,400.,1700.,2200.,2500.,2800.,3500.,3700.,
     1      3900.,4700.,5000.,14500./

      DATA PDATA/67.6E-05,.00121,.0059,.0084,.013,.022,.068,.080
     1      ,.083,.033,.024,.0565/

      CALL GETPROP(TDATA,PDATA,12,T,TC)

      RETURN

      END
```

```
      SUBROUTINE CPGAS(T,C)

C     *********************************************************
C     CP FOR H2/H2Ø MIX. P=1ATM. RESULTS OF NASA CODE
C     2Ø% H2O BY VOL
C     *********************************************************
      C=82.*EXP(-1.435E-Ø6*(T-385Ø.)**2)+5.7Ø4



      RETURN

      END

      SUBROUTINE AGAS(T,A)

      COMMON/SPECIES/PTOTAL,XH2O,XOH

C     ******************************
C     CALCULATES ABSORPTION FOR PTOTAL=1 ATM,2ØXH2O BY VOL.!
C     UNITS: CM^-1
C     DISSOCIATION IS TAKEN INTO ACCOUNT BY SUB H2O.
C
C     *********************************************************
      CALL H2O(T)

      P=PTOTAL

      ETA=XH2O

      IF(T.LT.1ØØØ) GOTO 1ØØ

      AK=8.ØE-8*(T-7ØØ.)**2.

      GOTO 5ØØ

1ØØ        AK=9.222E-Ø6*(EXP(6.6615E-Ø3*T)-1)

5ØØ        CONTINUE

      A=ETA*AK*273.*P/T

      RETURN

      END

      SUBROUTINE H2O(T)

      COMMON/SPECIES/PTOTAL,XH2O,XOH

      PTOTAL=1.Ø

C     CALCULATES MOLE FRAC H2O FOR 2ØXH2O, P=1 ATM.
C     ALSO CALCULATES MOLE FRC FOR OH!!!!
C     CURVE FIT USING DATA FROM NASA PRINTOUT.
C
      IF(T.LE.395Ø.) GOTO 1ØØ

      XH2O=.Ø1533*EXP(-.Ø2Ø7*(T-395Ø.))

      GOTO 2ØØ

1ØØ        XH2O=.2*(2.-EXP(6.8Ø2E-19*T**5.))

2ØØ        CONTINUE

      XOH=.Ø4*EXP(-2.51E-Ø6*(T-366Ø)**2.)

      END
```

```fortran
      SUBROUTINE RHOGAS(T,R)

C     *********************************
C     GIVES DENSITY FOR 20% H2O/VOL AT I ATM TOTAL PRESS.
C     UNITS:G/CM^3
C     CURVEFIT USING DATA FROM NASA PRINT OUT.
C
C     *********************************************************
C
C
      P=1.0

      IF(T.LE.4000) R=15.75*EXP((T/4350.)**6.50)

      IF(T.GT. 4000) R=.0139*T-28.02

      R=P/(R*T)

      RETURN

      END

      SUBROUTINE RAD(T,RA,NS,DXX,KK)

      IF(KK.LE.(NS-1)) GOTO 100

C
C     COME HERE IF IN GAS
C
      CALL RADH2O(T,RA)

      GOTO 1000

100         IF(KK.EQ.(NS-1)) GOTO 200

C     COME HERE IF BELOW CERAMIC SURFACE
      RA=0.

      GOTO 1000

C     COME HERE IF FIRST CELL OF CERAMIC SURFACE.
200         RA=4.56E-12*T**4./DXX

1000        CONTINUE

      RETURN

      END
```

```
      SUBROUTINE GETPROP(TDATA,PDATA,NSIZE,TT,PP)
C
C     ****************************************************
C
C     INTERPOLATION ROUTINE USING LOOK UP TABLES GIVEN BY
C     TDATA,PDATA. HERE PDATA=FUNCTION(TDATA).
C
C     ****************************************************
C
      DIMENSION TDATA(NSIZE),PDATA(NSIZE)

      IF(TT.LT.TDATA(1)) GOTO 500

C
C     LOOKUP TABLE LOOP
C
      DO 100 NN=1,NSIZE-1

      NS=NN

      IF(TT.GT.TDATA(NN)) GOTO 50

      GOTO 100

50    IF(TT.LE.TDATA(NN+1)) GOTO 200
100         CONTINUE

      GOTO 600

C
C     VALUE IS IN TABLE, INTERPOLATE TO GET PROPERTY
C
200         CALL INTER(TDATA(NS),PDATA(NS),TDATA(NS+1),PDATA(NS+1),TT,PP)

      GOTO 1000

C
C     BACK EXTRAPOLATE
C
500         CALL INTER(TDATA(1),PDATA(1),TDATA(2),PDATA(2),TT,PP)

      GOTO 1000

C
C     FORWARD EXRAPOLATE
C
600         K1=NSIZE-1

      K2=NSIZE

      CALL INTER(TDATA(K1),PDATA(K1),TDATA(K2),PDATA(K2),TT,PP)

1000        CONTINUE

C
C     NEGATIVE PROPERTIES ARE NOT ALLOWED!!
C
      IF(PP.LT.0.) PP=1.E-12

      END

      SUBROUTINE INTER(X1,Y1,X2,Y2,X,Y)

      SLOPE=(Y2-Y1)/(X2-X1)

      Y=SLOPE*(X-X1)+Y1

      RETURN

      END
```

```
      SUBROUTINE RADH2O(T,RAD)

C
C     ******************************************************
C     THIS SUB CALCULATES RAD. FROM H2O SPECIES GIVEN THE PRESSURE,
C     FRACTION OF H2O (AT THE GIVEN TEMP). CS(N) IS CROSS SECTION
C     CALCULATED FROM KEMP'S REPORT USING THE .1 ATMFT CURVE.
C     ******************************************************
C
      DIMENSION TDAT(14),CSOH(14)

      DIMENSION TDATA(13),CS(13)

      COMMON/SPECIES/PTOTAL,XH2O,XOH

      DATA TDAT/298.,500.,1000.,1100.,1500.,2000.,2500.,3000.,
     1      3500.,4000.,4500.,5000.,5500.,6000./

      DATA CSOH/8.01E-24,4.93E-23,4.93E-22,5.92E-22,6.72E-22,6.28E-22,
     1      4.26E-22,2.69E-22,1.88E-22,1.61E-22,1.07E-22,7.17E-23,4.68E-23,
     1      2.96E-23/

      DATA TDATA/298.,500.,1000.,1500.,2000.,2500.,3000.,3500.,
     1      4000.,4500.,5000.,5500.,6000./

      DATA CS/9.32E-22,2.23E-21,3.8E-21,3.35E-21,1.97E-21,1.56E-21,
     1      1.21E-21,9.38E-22,7.15E-22,6.03E-22,4.69E-22,3.69E-22,3.22E-22/

C
C
      ANH2O=XH2O*PTOTAL/(1.362E-22*T)

      CALL GETPROP(TDATA,CS,13,T,ACS)

      RADC=ACS*ANH2O

      RAD=2.268E-11*RADC*T**4.

      CALL GETPROP(TDAT,CSOH,14,T,CST)

      ROH=1.665E11*PTOTAL*XOH*CST*T**3.

      RAD=RAD+ROH

C
C     UNITS: RAD=(W/CM^3)
C
      RETURN

      END
```

300
20
10
40
293   293
500.
75
.1   40

0
0
.277778
.555556
.833333
1.11111
1.38889
1.66667
1.94444
2.22222
2.5
2.77778
3.05556
3.33333
3.61111
3.950
4.300
4.7000
4.900
5
5.25
5.5
5.75
6
6.25
6.5
6.75
7
7.25
7.5
7.75
8
8.25
8.5
8.75
9
9.25
9.5
9.75
10
10.25
10.5
10.75
11
11.25
11.5
11.75
12
12.25
12.5
12.75
13
13.25
13.5
13.75
14
14.25
14.5
14.75
15
15.25
15.5
15.75
16
16.25
16.5
16.75
17
17.25
17.5
17.75
18
18.25
18.5
18.75

C-2

```
19
19.25
19.5
19.75
20
20.25
20.5
20.75
21
21.25
21.5
21.75
22
22.25
22.5
22.75
23
23.25
23.5
23.75
24
24.25
24.5
24.75
25
25.25
25.5
25.75
26
26.25
26.5
26.75
27
27.25
27.5
27.75
28
28.25
28.5
28.75
29
29.25
29.5
29.75
30
30.25
30.5
30.75
31
31.25
31.5
31.75
32
32.25
32.5
32.75
33
33.25
33.5
33.75
34
34.25
34.5
34.75
35
35.25
35.5
35.75
36
36.25
36.5
36.75
37
37.25
37.5
37.75
38
38.25
38.5
38.75
39
39.25
39.5
39.75
```

40
40.25
40.5
40.75
41
41.25
41.5
41.75
42
42.25
42.5
42.75
43
43.25
43.5
43.75
44
44.25
44.5
44.75
45
45.25
45.5
45.75
46
46.25
46.5
46.75
47
47.25
47.5
47.75
48
48.25
48.5
48.75
49
49.25
49.5
49.75
50
50.25
50.5
50.75
51
51.25
51.5
51.75
52
52.25
52.5
52.75
53
53.25
53.5
53.75
54
54.25
54.5
54.75
55
55.25
55.5
55.75
56
56.25
56.5
56.75
57
57.25
57.5
57.75
58
58.25
58.5
58.75
59
59.25
59.5
59.75

```
60
60.25
60.5
60.75
61
61.25
61.5
61.75
62
62.25
62.5
62.75
63
63.25
63.5
63.75
64
64.25
64.5
64.75
65
65.25
65.5
65.75
66
66.25
66.5
66.75
67
67.25
67.5
67.75
68
68.25
68.5
68.75
69
69.25
69.5
69.75
70
70.25
70.5
70.75
71
71.25
71.5
71.75
72
72.25
72.5
72.75
73
73.25
73.5
73.75
74
74.25
74.5
74.75
75
75
```

R. Eskridge 1 Px

REPORT DOCUMENTATION PAGE,		READ INSTRUCTIONS BEFORE COMPLETING FORM
1. REPORT NUMBER	2. GOVT ACCESSION NO.	3. RECIPIENT'S CATALOG NUMBER
4. TITLE (and Subtitle) High Temperature Measurement of Water Vapor Absorption		5. TYPE OF REPORT & PERIOD COVERED Final Report
		6. PERFORMING ORG. REPORT NUMBER
7. AUTHOR(s) Dennis Keefer, J.W.L. Lewis and Richard Eskridge		8. CONTRACT OR GRANT NUMBER(s) Contract No.: NAS8-34320
9. PERFORMING ORGANIZATION NAME AND ADDRESS The University of Tennessee Space Institute Tullahoma, TN 37388		10. PROGRAM ELEMENT, PROJECT, TASK AREA & WORK UNIT NUMBERS
11. CONTROLLING OFFICE NAME AND ADDRESS ONRRR, Georgia Institute of Technology 206 O'Keefe Building Atlanta, GA 30332		12. REPORT DATE July 31, 1985
		13. NUMBER OF PAGES
14. MONITORING AGENCY NAME & ADDRESS(if different from Controlling Office) Geo. C. Marshall Space Flight Center National Aeronautics & Space Admin. Marshall Space Flight Center, AL 35812 Procurement Office/Vickie Carft		15. SECURITY CLASS. (of this report) UNCLASSIFIED
		15a. DECLASSIFICATION/DOWNGRADING SCHEDULE

16. DISTRIBUTION STATEMENT (of this Report)

AP29-H* (Vicki Craft)   Distribution addresses same as items 11 and 14.
AS24D   5 cys   *Cy. of transmittal letter only
ONRR*   (Michael Karp)
EM12-34 1 cy
EP26   12 cys

17. DISTRIBUTION STATEMENT (of the abstract entered in Block 20, if different from Report)

18. SUPPLEMENTARY NOTES

19. KEY WORDS (Continue on reverse side if necessary and identify by block number)

20. ABSTRACT (Continue on reverse side if necessary and identify by block number)

SEE ATTACHED.

DD FORM 1473   EDITION OF 1 NOV 65 IS OBSOLETE
1 JAN 73